Universitat de Girona

ROBUST CONTROL OF SYSTEMS SUBJECTED TO UNCERTAIN DISTURBANCES AND ACTUATOR DYNAMICS

Rodolfo VILLAMIZAR MEJIA

ISBN: 84-689-2579-9
Dipòsit legal: GI-633-2005

Universitat de Girona
Departament d'Electrònica, Informàtica i Automàtica

Robust Control of Systems Subjected to Uncertain Disturbances and Actuator Dynamics

by

Rodolfo Villamizar Mejía

Advisors

Dr. Josep Vehí and Dr. Ningsu Luo

DOCTORAL THESIS
Girona, Spain
March, 2005

Universitat de Girona
Departament d'Electrònica, Informàtica i Automàtica

Robust Control of Systems Subjected to Uncertain Disturbances and Actuator Dynamics

by

Rodolfo Villamizar Mejía

A dissertation presented to the Universitat de Girona in partial fulfillment of the requirements of the degree of DOCTOR OF PHILOSOPHY

Advisors

Dr. Josep Vehí

Dr. Ningsu Luo

Girona-Spain, March, 2005

Universitat de Girona
Departament de Electrònica, Informàtica i Automàtica

Abstract

Robust Control of Systems Subjected to Uncertain Disturbances and Actuator Dynamics

by Rodolfo Villamizar Mejía

Advisors: Dr. Josep Vehí and Dr. Ningsu Luo

January, 2005
Girona, Spain

This dissertation focuses on the design and validation of robust controllers that can effectively reduce vibrations in structures due to external disturbances such as earthquakes, strong winds or heavy dynamic loads. The design of the controllers is based on control theories traditionally used in structural control: Lyapunov stability theory, Sliding Mode Control and Clipped-Optimal Control, another recently introduced: Backstepping Control and one that had not been used before in this control area: Quantitative Feedback Theory. The main advantage by using these techniques is that some open structural problems such as actuator dynamics, uncertain disturbances, uncertain parameters, measurement limitation and dynamic coupling can be treated. Numerical validation of the controllers proposed is performed on typical structural models. A 10-story base isolated structure, a truck-bridge structural platform and a two-span bridge are used. Their control scheme contains inherit one o more open structural control problems. Three experimental prototypes are used to implement the robust controllers proposed, in order to experimentally verify their viability and effectiveness. The main contribution of the present thesis is obtaining robust structural controllers, numerically and experimentally verified, that account structural control problems such as actuator dynamics, uncertain parameters, dynamic coupling, measurement limitations and unknown disturbances and based on novel control techniques.

To whom give sense to my life: my family

My parents Pedro Jesús and Ana Inés
My wife Martha Cecilia
My brothers Orlando and Jesús M
My sisters Luz Marina, Rubiela, Gloria Carmen and Floralba
All my nephews and brothers in law

Contents

List of Figures

Acknowledgments

Our life is like a long travel whose journey include special stations that after being visited, they will be recorded for ever in our minds. Today, within the journey of my travel I am arriving to a special station, my doctoral thesis. During the journey passed to arrive here a lot of people have given me an invaluable help and motivation.

First, I would like to express my gratitude to Dr. Josep Vehí for accepting me as member of the research group MICELab. He and Dr. Ningsu Luo have given me valuable advice, suggestions and researcher formation during the development of the thesis. They have been quick to help me and give me support on important decisions taken during the development of this thesis. I have learned a lot from them as advisors but also I have shared grateful moments with them as members of a work group.

I would like to express my acknowledgment to Dr. José Rodellar for his valuable suggestions and advice, during the opportunities that we had of working in joint research works.

I would like also to thank WUSCEEL research group of University of Washington in St. Louis in head of Dr. Shirley Dyke for accepting me as visitor researcher during 3 months and facilitating me the 6-story test building. I want also to than to Dr. Fabio Casciatti and Dr. Lucia Favarelli for accepting me as visitor researcher in the Department of Structural Mechanics of University of Pavia. These two stays were important for my scientific formation and the development of the thesis.

I would like to thank members of ECOLEADER-TASCB project for facilitating me the two-span bridge numerical model and the pseudo-dynamic test substructure installed at the reaction-wall building of Joint Research Center in Ispra, Italy.

I want to thank Universitat de Girona for support me economically the last four years through a research grant. I want also thank Government of Catalonia and CONVIB foundation for support economically my research stays.

Next,I want to express my gratitude to my wife Martha Cecilia for sharing wonderful days in Girona with me, but also for being unconditional during crucial moments of my thesis. At those moments she given me motivation, company and breath voice. I also want to express my gratitude to my family, who from a distant place, but with the same unconditionality and breath voice, were motivating me during this stage. This achievement pertains them.

Before starting this doctorate, Dr Gabriel Ordoñez and Dr Gilberto Carrillo motivated and encouraged me to do it, today I express them my gratitude.

I would also like to thank members of MICELab research group for their friendship and support during this time. I would also like thank Colombian people who have shared with me grateful moments in Girona during last four years.

It is difficult to remind and include every person who directly or indirectly has collaborated in the development of this thesis. I present my excuses but I will ever thank them.

Chapter 1

Introduction

1.1 Motivation

Several reasons to apply control on civil engineering structures can be found, however the most important are: i). The protection of human beings and civil engineering structures when strong external forces, such as earthquakes or heavy loads, are acting on the structures and ii). The provision of human comfort when a moderate but uncomfortable external force, such as strong winds, is acting on the structure. A meaningful reference of the practical effectiveness of a structural control system was the significant improvement of the structural performance in a real situation as like the Kobe earthquake of January 17, 1995. It caused the collapse of a vast number of buildings together with a heavy toll of human lives. There were two buildings equipped with seismic isolation systems and a certain response control effect against the major earthquake was observed on these two buildings. However, several buildings in the adjacent Osaka area equipped with active control systems, which were designed for control of wind-induced vibrations, ceased to function when the earthquake struck. This situation warns that oncoming seismic motions cannot be predicted and has demonstrated that the best way to ensure the safety of the controlled civil engineering structures is to look for the best design strategies of control systems which contemplate in all possible actions that could occur in them. However, the improving of such control systems is a joint work, where control engineers play an important role in the design of adequate control strategies and other aspects directly related with the control area. This will be an important contribution to keep the structural integrity and consequently to provide a structure protected from external excitations.

1.2 Problem Definition

Control of civil engineering structures is still an open field, and new theoretical and practical developments must be obtained. Thanks to huge technological advances in areas such as sensing, computation and control devices manufacturing, among others, important structural control problems have been solved. Thus, structural control systems are becoming implementable, mainly from the economy and reliability point of view. However, some problems still continue open and some others appear with the introduction of innovative control systems. For example the introduction of semiactive control technologies, have become in an important alternative to solve problems such as limitation of external energy, slow actuator responses and maintenance problems. Moreover, such devices include complex hysteretic dynamics, which implies that a major effort is required to design a control law.

Thus, one of the challenges in structural control is that of finding adequate control laws that

accomplish minimal design specifications such as robustness, reliability, stability, implementability, minimum control effort, but additionally taking into account some particular conditions of the structural systems, such as actuator dynamics, parametric uncertainties, resonance conditions, nonlinearities, coupling and limited measurements.

1.3 Objective of the thesis

In this thesis the problem of designing control laws for civil engineering structures are investigated. Some control methodologies that have been used in other control areas are introduced in the structural control area in conjunction with those traditionally used. Control design problems are independently studied. Then, control laws are designed for different structural control systems that contain one or more open control problems.
The main objective of the thesis is that of designing robust control laws for civil engineering structures, which are effective and contribute to solve some of the open problems existed in this kind of systems.
Control approaches are numerically and experimentally validated. Numerical models of typical structures are studied, which contain one or more open problems. Similarly, the effectiveness of the control approaches is experimentally verified by using laboratory structural prototypes, which contain some of the open control problems.
The robust structural controllers designed contribute to obtain control systems that are effective and closer to the real operation conditions. Such objective is achieved by considering control techniques that have resulted effective in other areas and that are appropriated in this kind of problems.

1.4 Structure of the thesis

The doctoral thesis is organized in six chapters. The present chapter that includes a introduction, a motivation and the main objective of the thesis. *Chapter 2* presents a brief literature review on structural control systems in order to see what has been developed until now and which are the main open problems that exist in this control area. *Chapter 3* presents the open structural control problems considered in this thesis for designing robust control approaches. The control problems studied are actuator dynamics, uncertain parameters, uncertain disturbances and uncertain temporary coupling. Each control problem is presented in someone of the structural models studied in chapter 4. In this chapter, robust controllers are designed and numerically verified. Chapter 5 is dedicated to the experimental validation of the robust control approaches. Control system configuration is such that one ore more control problems are presented. Finally, *chapter 6* presents some conclusions derived from this thesis and future work.

Chapter 2

Literature Review

2.1 Introduction

Structural control had its roots primarily in such aerospace related problems and in flexible space structures. Then, quickly it was moved into civil engineering and infrastructure-related issues, such as building and bridge protection against extreme loads such as earthquakes and providing human comfort in the structure during noncritical times [40]. The first real implementations of structural control, in the 70's, were based on base isolation, viscoelastic dampers and tuned liquid dampers. Many years later the active control concept appeared and its first real implementation was made in the 11-story Kyobashi Seiwa building in Tokyo, Japan, to reduce the vibration of the building under strong winds and moderated seismic excitations [86]. Recently, the techniques of semiactive and hybrid control were proposed for structural control and their implementations have been made successfully in Japan and USA. This chapter is devoted to present the main topics contained in a structural control system. The most relevant developments and applications on each topic and referenced in the literature are here summarized. The chapter is divided into three parts: the first part highlights the typical structural control devices, while the second part presents the most common structural control methodologies referenced in the literature and finally the main control design open problems are presented.

2.2 Structural Control Devices

Different types of structural control devices have been developed and a possible classification is done by its dissipative nature.
Passive devices: Their function is to dissipate vibratory energy by augmenting some structural parametric values (stiffness and damping) of the structure without requiring external energy.
Active devices: They deliberate energy to the structure in a opposite sense to that deliberated by the seismic force. Their nature is that of delivering energy to the system.
Semiactive devices: They dissipate energy such as a passive device, but the magnitude of the energy dissipated can be controlled on-line. Properties of the device such as stiffness or damping are controlled by means of a hydraulic, magnetic or electronic signal.

2.2.1 Passive Control Devices

Passive energy dissipation systems encompass a range of materials and devices for enhancing damping, stiffness and strength. They can be used for both natural hazard mitigation and rehabilitation of aging or deficient structures. These devices are characterized by their capability

to enhance energy dissipation in the structural systems where they are installed. Two principles are used to dissipate vibratory energy: conversion of kinetic energy to heat and transference of energy among vibration modes. The devices that pertain to the first group are those that can operate with principles such as frictional sliding, yielding of metals, phase transformation in metals, deformation of viscoelastic solids or fluids. And those of the second group are fluid orificing and supplemental oscillators, which act as dynamic vibration absorbers [10, 12, 11].

2.2.2 Active Control Devices

Active devices can provide better performance than passive strategies, by using information of the global response and determining appropriate control forces. An active control strategy can measure and estimate the response over the entire structure to determine appropriate control forces. As a result, active control strategies are more complex than passive strategies, requiring sensors and evaluator/controller equipments.

The merit of the active control systems is that they are effective for a wide-frequency range and also for the transient vibration. However they are limited by the quantity and availability of energy to develop the magnitude of forces required to control the civil infrastructure when a external forces ia acting on the structure. Other disadvantage of active control is that because external energy is introduced, probability of unstable conditions is present by unexpected dynamics changes in the structure or erroneous feedback information.

Active control strategies have been proposed and implemented in a number of civil structures [94]. There are currently nearly 40 buildings and towers implemented with active control strategies. Additionally, 15 bridge towers have been implemented with active and hybrid control devices during bridge erection. [101], provided detailed lists of these full-scale applications. Table 2.1 provided by [95]) presents a list of the active control implementations on civil engineering structures. Figure 2.1 shows one of the real structures actively controlled. The typical active control systems are active base isolation, active bracing, tuned liquid column damping, impact absorbers, multiple connected buildings and active mass driver [38, 39, 89, 76, 81, 95, 92, 74].

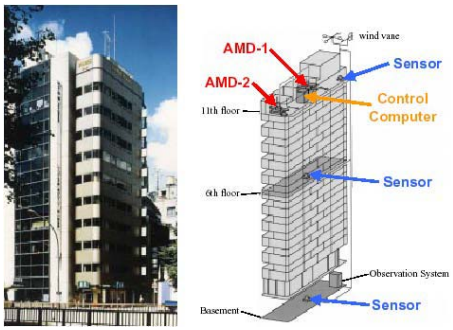

Figure 2.1: Actively controlled Kiobashi Seiwa building.

Active Mass Damper (AMD)

It consists of a mass attached to a structure such that it oscillates at the same frequency of the structure but with a phase shift. A hydraulic actuator or an electric motor is used to provide a control force u to counteract or to mitigate the motion of the structure. The Kyobashi Seiwa

Building was the first full-scale implementation of active control technology, where the active mass damper or active mass driver system was designed and installed.

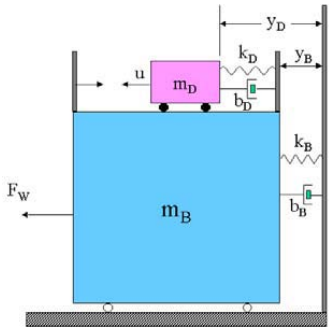

Figure 2.2: AMD control device

Active Tuned-Liquid-Column Dampers

It is composed of two vertical columns connected by a horizontal section in the bottom and they are partially filled with water or other fluid. Two propellers are installed inside and at the center of Tuned-liquid-column (see figure 2.2). These two propellers are powered by a servomotor to generate the control force. Analytical and experimental studies have been reported by [37, 87]. In hybrid systems this type of device have been used [35, 100]. In [38] the dynamic response of of high-rise buildings equipped with this type of devices is studied.

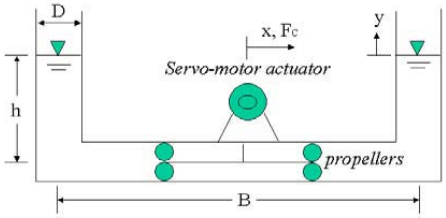

Figure 2.3: Type of Active Tuned Liquid Column Damper (ATLCD)

2.2.3 Semi-active control devices

Semi-active control devices cannot inject mechanical energy into the controlled structural system but some of its properties can be dynamically varied [94]. These devices are a promising development tool in protection of civil engineering structures. They combine the best features of both passive and active control systems and offer some adaptability, similar to active control systems, but without requiring large power sources for their control action. This advantage is fundamental in hazard situations like earthquake or strong winds, where the main power source of the structure may fail during such situation. Its stability in a bounded-input bounded-output sense is inherent, thus it is possible to implement high authority control strategies. This may result in performances that can surpass that of comparable active systems [23]. A representative full scale implementation of structural control in USA is that shown in figure 2.4. It consists of a

Table 2.1: Full Scale Implementation of Active Structural Control before year 2000

Location	Building	Year Completed	Building Use	No. of Stories	Control Device*
Japan	Kyobashi Seiwa Bldg, Tokyo	1989	Office	11	AMD
	Kajima Research Lab. # 21, Tokyo	1990	Office	3	SAVS
	Shimizu Tech. Lab., Tokyo	1991	Lab.	7	AMD
	Sendagaya INTES Bldg., Tokyo	1992	Office	11	HMD
	Elevator Tech. Lab.	1992	Lab.	(60 m)	AGS
	Hankyu Chayamachi Bldg.,Osaka	1992	Hotel	34	HMD
	Kansai Intl Airport, Osaka	1992	Control Tower	(88 m)	HMD
	Land Mark Tower, Yokohama	1993	Hotel	70	HMD
	Osaka Resort City 200, Osaka	1993	Hotel	50	HMD
	Long Term Credit Bank, Tokyo	1993	Office	21	HMD
	Ando Nishikicho Bldg., Tokyo	1993	Office	14	HMD
	NTT Kur. Mot. Bldg., Hiroshima	1993	Office	35	HMD
	Penta-Ocean Exp. Bldg., Tokyo	1994	Experimental	6	HMD
	Shinjuku Park Tower, Tokyo	1994	Office	52	HMD
	Dowa Fire Marine Ins., Osaka	1994	Office	29	HMD
	Porte Kanazawa, Kanazawa	1994	Hotel	30	AMD
	Mitsubishi Heavy Ind., Yokohama	1994	Office	34	HMD
	ACT Tower, Hamamatsu	1994	Office	(212 m)	HMD
	Riverside Sumida, Tokyo	1994	Office	33	AMD
	Hotel Ocean 45, Miyazaki	1994	Hotel	43	HMD
	RIHGA Royal Hotel, Hiroshima	1994	Hotel	35	HMD
	Hikarigaoko J City Bldg., Tokyo	1994	Office	46	HMD
	Osaka WTC Bldg., Osaka	1995	Office	52	HMD
	Dowa Kasai Phoenix Tower, Osaka	1995	Office	28	HMD
	Rinku Gate Tower Bldg., Osaka	1995	Office	56	HMD
	Hirobe Miyake Bldg., Tokyo	1995	Office	9	HMD
	Plaza Ichihara, Chiba	1995	Office	12	HMD
	Herbis Osaka, Osaka	1997	Hotel	38	AMD
	Nisseki Yokohama Bldg., Yokohama	1997	Office	30	HMD
	Itoyama Tower, Tokyo	1997	Office	18	HMD
	Otis Shibyama Test Tower, Chiba	1998	Lab.	39	HMD
	Bunka Gakuen, Tokyo	1998	School	20	HMD
	Daiichi Hotel Oasis Tower, Ohita	1998	Hotel	21	HMD
	Odakyu Southern Tower, Tokyo	1998	Office	36	HMD
	Kajima Shizuoka Bldg., Shizuoka	1998	Office	5	SAHD
	Sotetsu Kyoto Bldg., Yokohama	1998	Hotel	27	HMD
	Century Park Tower, Tokyo	1999	Resid.	54	HMD
USA	Highway I-35 Bridge, OK	1997	Highway	–	SAHD
Taiwan	TC Tower, Kaoshiung	1999	Office	85	HMD
	Shin-Jei Bldg., Taipei	1999	Office	22	HMD
China	Nanjing Communication Tower,	1999	Comm.	(310 m)	AMD

bridge controlled by means of a semiactive variable-orifice damper installed at a frame subjected to the deck. Some important survey on semiactive control systems found in the literature are [99, 68, 40, 13].

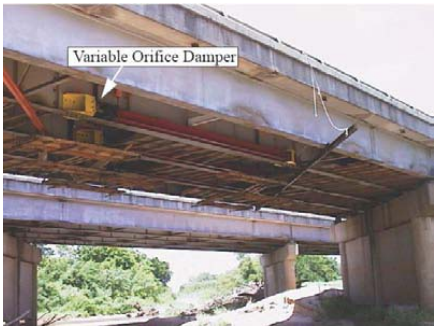

Figure 2.4: Full-Scale Implementation of Structural Control in USA

The most common semiactive control devices are: variable-orifice fluid dampers, controllable friction devices and controllable-fluid dampers.

Variable-orifice fluid dampers

It behaves as linear viscous dampers with adjustable damping coefficient [98]. Its operation principle consists of controlling the damping coefficient by adjusting the opening of a valve in order to alter the resistance to flow of a conventional hydraulic fluid damper. Thus, large forces can be controlled with a low external power, (semiactive principle).

In [56] this type of devices have been implemented using different control strategies. In [55] by using a semiactive oil damper it has been proved that this device can dissipate energy twice more than a passive damper. Real implementations on high-rise buildings have been accomplished. The most important ones are:
∗ [54] implemented this device on a 11-story building and the damping augmentation capacity was ensured.
∗Real implementation made on the Shiodome Kejima Tower in Tokyo, recently finished.
∗Full-scale experiment with variable-orifice damper implemented by [48] at the Kobori research complex.
∗Implementation made by [53] on the Kajima Shizuoka Building in Japan. ∗Experiments conducted by [84] on a single-lane model bridge. ∗Full-scale experiment on a bridge on interstate highway I-35 conducted by [78, 79, 51]. This experiment corresponds to the first full-scale implementation in USA (see figure 2.4).

Controllable fluid dampers

In these devices some properties of their internal fluid can be modified by means of an electrical/magnetic field, resulting a modification in the quantity of force absorbed. The principal advantage of this type of devices is that the piston is the only moving part. Consequently, it can change rapidly from a state to another (linear viscous fluid to a semi-solid in milliseconds) when exposed to an electric/magnetic field. Two types of semiactive controllable fluid dampers

are found: Electrorheological (ER) and Magnetorheological (MR) damper. Their difference is the type of fluid used: Magnetorheological or Electrorheological fluid.

Several ER dampers have been developed and adapted to civil engineering structures. The most important developments have been obtained by [31, 32, 30, 26, 69, 58, 59] among others.

The MR damper has become an alternative of ER damper. Its operation principle is similar to ER damper, except that the external signal applied is a magnetic field, which becomes the inside fluid from semisolid to viscous state and it exhibits a viscoplastic behavior similar to that of an ER fluid. MR devices with a high bandwidth can be constructed and controlled with low voltage (i.e. 12-24V) and low electrical currents about 1-2 amps. Batteries can supply this level of power.

MR devices can operate at temperatures from -40C to 150C and slight variations occur in the yield stress. The transition velocity of both MR and ER devices is too fast (a few of miliseconds).

A MR damper model was developed in [21], where a simple mechanical model is used to describe its behavior. Numerical examples and implementations to demonstrate the effectiveness of MR devices have been developed in [20, 23]. These developments have demonstrated that MR dampers may be closed to the linear active control performance, while only a power fraction of that required by the active controller is enough. Lord Corporation designed and built a full-scale, 20-t MR damper, which could be the more biggest MR damper in structural control implementations [96, 22]. A schematic diagram of this device is shown in figure 2.5.

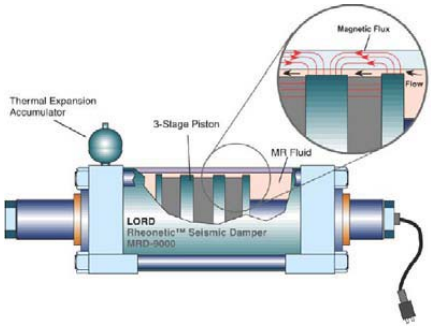

Figure 2.5: Full-scale 20T MR Fluid Damper

Variable-Friction Damper

Its functioning principle consists in utilizing forces generated by surface friction to dissipate vibratory energy. These forces can be varied by means of an electrical signal or a gas pressure, which varies the friction coefficient of the device. In [15] the ability of these devices to reduce the inter-story of a seismically excited structure was investigated. In [27, 28] these devices have been used in parallel with a seismic isolation system. At the University of British Columbia a friction device was developed, where the frictional interface is adjusted by allowing slippage in controlled amounts, similar to the device proposed in [2, 77].

2.3 Structural Control Algorithms

During the last two decades, various types of structural control strategies have been applied to the control of civil engineering structures. Depending on the available information for each

controlled structure, mathematical model associated, types of measurements, actuators and disturbances, each control solution can be suitable only for one specific type of structure and not for all kinds. In this section, the most used structural control algorithms are grouped in 3 kinds and their more representative applications in civil engineering structures are presented

2.3.1 Optimal Control

The general optimal control problem may be stated as follows: given a system subjected to external inputs, find the control which minimizes a certain measure of the performance of the system [112]. Optimal control algorithms are based on the minimization of a performance index that depends on the system variables, while maintain a desired system state and minimize the control effort. According to classical performance criterion, the active control force u is found by minimizing the performance index subject to a second order system. The performance index can include a measure of operating error, a measure of control or any other variable which is important for the user of the control system. There are two control design objectives: Regulator problem, which consists in stabilizing the system so that its states and/or outputs remain small, and Tracker or servomechanism problem which controls the system so certain prescribed outputs follow the desired trajectories and all states remain bounded. The main optimal control techniques derived are the Linear Quadratic Regulator (LQR), Linear Quadratic Gaussian (LQG), Clipped Optimal Control and Bang-Bang Control.

LQR Control Algorithm

This technique is characterized by requiring that all the state variables are available. This algorithm is the classical one used for active and semiactive control of structures. However it is not always possible to use it for structural control due to the limitations such are number of sensors that could be installed in the large structures or nonlinearities present in the structure or actuator. The control input takes the form $u = -\mathbf{K}x$, where $\mathbf{K}$ is a $n \times n$ feedback matrix. Then, the control design problem is to choose the m entries of the feedback matrix $\mathbf{K}$ to yield a guaranteed desired behavior of the closed-loop system. The selection of such entries is made by minimizing a linear quadratic index.

Several semiactive structural applications using LQR control technique have been achieved in [52, 85, 28, 75, 1]. In [98] this algorithm was applied on a small scaled model with a semiactive control system, where a fluid damper is used. A variation of LQR control is the Instantaneous Optimal Control, which uses a performance index as control objective similar to LQR control algorithm, but this does not need to solve the Riccatti equation.

LQG Control Algorithm

The LQG method for structural control was examined by Yang and Yao in 1974. It is based on calculating the control gain k that minimizes the performance index with the difference that an observer (i.e Kalman filter) is included in the design equations, such as:

$$\hat{\dot{x}} = A\hat{x} + Bu + L(y - C\hat{x}); \qquad u = -K\hat{x} + y \tag{2.1}$$

Then the design problem here is to select K and L, to obtain good robustness and high performance. Several applications of this theory have been made in civil engineering structures both active and semiactive control [110, 111, 106, 4, 5].

Clipped-Optimal Control

Clipped-control technique consists on designing a linear optimal controller K that calculates a desired control forces vector $f = [f1, f2, f3, .., fn]$. The computation of this force is based on the measured structural responses. The clipped optimal control can be considered as a practical approximation of the LQR or LQG (depending which technique is used to compute the desired force) controller when it is impossible to obtain the optimal control force value from the LQR or LQG design. Thus, the control objective in clipped-optimal control is to keep the available force f, that can be delivered by the device, as closed as possible to the optimal force f_d.

This algorithm has been used in structural control problems, mainly in [20, 22, 23, 18, 19, 112, 46, 47, 107, 108, 24, 21, 17], where its efficiency has been demonstrated.

Bang-Bang Control

This strategy is useful in the case where the performance index is the pure minimum-time objective of the form $J(t_0) = \int_{t_0}^{t_f} 1dt = t_f - t_0$. Then, the solution is to apply infinite control energy over an infinitesimal time period. A Lyapunov function is established, (i.e. vibrational energy of the structure) and a possible objective of the control strategy may be to reduce the rate in which energy is transmitted to the structure. The control objective can be satisfied by minimizing $\dot{V}$.

ER and MR dampers are well suited to bang-bang control applications due to their fast response times and main applications can be found in [70, 17, 18, 46, 47, 36].

2.3.2 Robust Control

The principal objective of robust control is to develop feedback control laws that are robust against plant model uncertainties and changes in dynamic conditions. A system is robustly stable when the closed-loop is stable for any chosen plant within the specified uncertainty set and a system has robust performance if the closed-loop system satisfies performance specifications for any plant model within the specified uncertainty description.

The need of using robust control in structural control is because that the structure models contain appreciable uncertainty. This uncertainty may be expressed as bounds on the variation in frequency response or parametric variations of the plant. The mostly used robust control approaches in control of structures are H_∞ control theory, Lyapunov theory based control and Sliding Mode Control.

H_∞ Control

H_∞ control algorithm is a design method, where the transfer function from excitation (u) to controlled output (y)is designed to be lower than a prescribed small value. The goal is to find a constant state-feedback matrix F to stabilize a matrix P, which is a combination of state matrix, and to satisfy a given ∞-norm bound $||F_1(P, F)||_\infty < \gamma$ on the closed-loop response. Because H_∞ control algorithm designs the controller in frequency domain, the frequency shape function can be used easily, it makes the control of specified frequency rang possible and the spillover can be avoided. It is suitable for system subject to unmodelled dynamics or unknown disturbances.

In [104] this method is used in seismically excited buildings. In [105] two H_∞ controllers with peak response constraints and energy-bounded or peak-bounded excitations are proposed. A long-span cable-stayed benchmark bridge subject to earthquakes is used to illustrate the appli-

cability of such controllers to practical problems and control performances. Others applications of this method on civil structures have been developed by [3, 88, 45, 110, 111, 103, 50].

Control Based on Lyapunov Stability Theory

Control based on Lyapunov stability theory consists in selecting a positive definite function denominated Lyapunov function. According to Lyapunov stability theory, if the rate of change of the Lyapunov function is negative semi-definite, the closed-loop system is asymptotically stable (in the sense of Lyapunov). The objective of the law is to select control inputs, which make the derivative Lyapunov function as negative as be possible. The importance of this function is that it may contain the any variable that interests to be minimized (i.e. system states, control law error, control force, etc).

Lyapunov theory based control is one of the most commonly techniques used in the control of structures. Several developments are found in [18, 46, 108, 30, 62, 47, 16, 36, 70, 73, 58, 83, 61, 57].

In [80] a control input function is assumed to be continuous in state variables and linear in control action, but additionally admissible uncertainty is considered. Then, a practical stability, the ultimate boundedness, of the system is demonstrated.

In [70] a Lyapunov function is used to represent the total vibratory energy in the structure (kinetic plus potential energy). This approach is a decentralized control because only local measurements of the absolute velocities are required.

Sliding Mode Control

The sliding model control was introduced by Utkin in 1977 to the Western world. Sliding mode control is characterized by being a nonlinear (discontinuous) control, which restricts the state of a system to a sliding surface by switching the control structure on both sides of a stable hyperplane in the state-space. The method requires to design first a sliding surface that is defined by $\sigma = \mathbf{Sx} = 0$ and represents the closed-loop control performance. Then, the control gain is calculated to make the state trajectory to reach the sliding surface and to maintain in it afterwards until sliding to the origin. This technique can achieve excellent robustness of the control system. In the sliding mode the system satisfies $\sigma = 0$ and $\dot{\sigma} = 0$. In order to find the control law, a Lyapunov function is defined as $V = \frac{1}{2}\sigma^2$. Then, time derivative is given by $\dot{V} = \sigma\dot{\sigma} = \sigma S\dot{x} = \sigma S(\mathbf{Ax}+\mathbf{Bu})$ whose negativeness is achieved by using some discontinuous control law which can use only the information on the bounds of uncertain variables.

[61, 65, 63] use this control method on different structures, such as buildings and bridges. In [49], this technique is used to control a seismic excited tall building, where dynamic interaction between the structural components is taken into account and springs are installed between them to produce appropriate control forces by utilizing the variable stiffness.

2.3.3 Predictive Control

The methodology of predictive control was introduced in 1974 by J.M Martin S. This principle can be defined as: Based on a model of the process, predictive control is the one that makes the predicted process dynamic output equal to a desired dynamic output conveniently predefined. The predictive control strategy may be generalized and implemented through a predictive model and a driver block (see figure 2.6). The predictive control generates, from the previous input and output process variables, the control signal that makes the predicted process output equal to the desired output. In fact, predictive control results in a simple computational scheme with parameters, having clear physical meaning and handling of time delays related to the actuators

in the control system. Predictive control has been shown to be an effective strategy for structural control [67, 61]

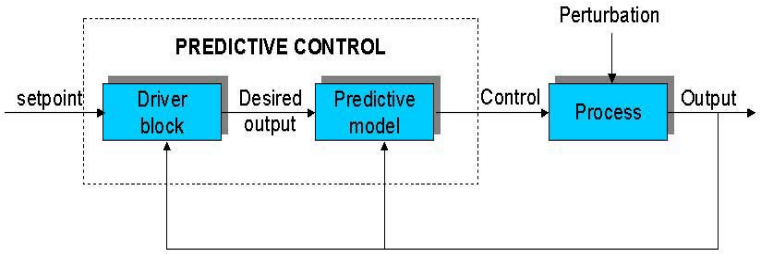

Figure 2.6: Basic block diagram for predictive control system (PCS)

Model Based Predictive Control

The performance of this technique depends significantly on the prediction made by the model. The basic strategy of predictive control implies the direct application of the control action in a single-step prediction, thus the predictive control must be formulated in discrete time. At each sampling instant k, the desired output for the next instant $k+1$ is calculated, which is denoted by $y_d(k+1|k)$. The basic predictive control strategy can be summarized by the condition $\hat{y}(k+1|k) = y_d(k+1|k)$, whit $\hat{y}(k+1|k)$ the output predicted at instant k for the next instant $k+1$ and the control $u(k)$ to be applied at instant k must ensure the above condition. An essential feature of the model based predictive control is that the prediction for instant $k+1$, necessary to establish the control action $u(k+1)$, is made based on the information of the outputs $y(\cdot)$ and the inputs $u(\cdot)$ known at the instant k and at preceding instants. However, such prediction may differ from the real output, which will be measured at instant $k+1$, thus the real measurement at $k+1$ is used as the initial condition instead of the output that was predicted for this instant, which is essential for the effectiveness of the predictive control.

At the NatHaz Modelling Laboratory at the University of Notre Dame researchers are studying the design and development of the Model Predictive Control. It has been effectively shown to be feasible for structural control applications in [72]. In [82] a predictive control in civil engineering was employed. In [60] the predictive control was used to control individually the first few shape modes to reduce the overall structural response. In [102] The Rodellar's predictive control method in a hybrid control system was used.

Adaptive Predictive Control

An adaptive predictive control system, consists in the combination of a predictive control system and an adaptive system, such as is shown in the figure 2.7 [67]. In an adaptive system, the predictive model gives an estimation of the process output at instant $k+1$ using the model parameters estimated at instant k, the control signals and the process outputs already applied or measured at previous instants. The predictive model calculates the control action $u(k)$ in order to make the predicted output at instant $k+d$ equal to the driving desired output at the same instant. After a certain time for adaptation, the process output should follow a driving desired trajectory (DDT) with a tracking error that is always bounded in the real case or is zero at the limit in the ideal case and the (DDT) should be physically realizable and bounded.

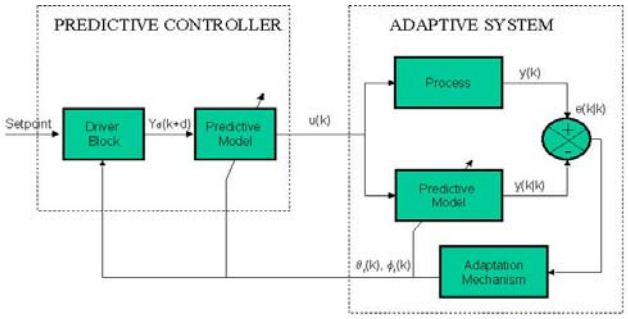

Figure 2.7: Overall block diagram of an adaptive predictive control system

2.3.4 Conclusions

It is difficult to develop a control strategy which can include all the aspects that affect the control system performance. The principal problem is that there is not any existing control theory that takes into account all the aspects related to structural control. However, it seems possible to find some new strategies for structural control design including every one of these aspects and to obtain some reasonable theoretical and implementable solutions.

Chapter 3

Open Problems in Structural Control

3.1 Introduction

In structural control, similar to other application fields, the main objective is to develop integrated control methodologies that are robust, effective, implementable, reliable and with the minimum control effort. However, sometimes it is difficult due to some problems such like nonlinearities, uncertainties, dynamic coupling and measurement limitation. During years researchers have been working in the obtention of control laws that consider one o more of such problems, however this is still an open research field and new control methodologies must be investigated. This chapter is devoted to present some of the main structural control design problems and different control laws approaches. The methodology followed in this thesis consists in using numerical and experimental structural models, that contain one o more control problems and designing and validating the controllers proposed. The control laws are designed using control techniques traditionally applied: Lyapunov stability theory, Sliding Mode Control and Clipped-Optimal control, one recently introduced: Backstepping Control and one considered new in this control area : Quantitative Feedback Theory.

3.2 Unknown Disturbances

Structural disturbances, such as earthquake accelerations, heavy loads, strong winds, crossing vehicles, are of unknown and unpredictable nature. It is not possible to know exactly when a disturbance is going to occur and which is its dynamic behaviour. This unpredictable and unknown nature, is a big limitation for designing effective control systems. If a variable associated with the disturbance (i.e. acceleration or force) would be available online or at least its dynamic behaviour would be predicted, such information could be included in the control law and computation of the control action would be closer to the real requirements to reduce vibrations in the structure. A first approximation in order to consider the disturbance in the control law is by assuming that a bounded value (based on historic records and knowledge of experts) of its magnitude can be assigned. Concretely, the unknown disturbance force $f(t)$ is bounded by $|f(t)| \leq F_0$ for all $t \geq 0$, with F_0 being some known positive constant.

This problem will be considered for all the structural systems in chapter 4 and for all the experimental prototypes in chapter 5.

3.3 Measurements Limitations

When a real time feedback control is used but the state variable measured does not take the real value, the effectiveness of control strategy may be reduced and the stability guaranty may also be failed in practice. Depending on the accuracy of the measurement devices there is always uncertainty concerning the measured variables, thus this condition must be considered at the moment of using the measurements as feedback variables [80]. An additional limitation in civil engineering structures is that not all the state variables can be directly measured and normally only a few of sensors are installed in the structure because of space limitations or implementation problems. Thus the on-line knowledge of all state variables at any place of the structure most of times is not possible. On other hand if state variables could be measured at any place of the structure, measurements far away from the place where the control device is installed are not always reliable when structure is being excited. Thus, the control strategy should be focused on only using the on-line measurements at points closer to the installed control device.

This challenge will be considered in the design of the control laws for the structural systems A and C in chapter 4 and for experimental prototypes B and C in chapter 5. Lyapunov stability theory, Sliding Mode Control, Backstepping Control and Quantitative Feedback Theory techniques are used to design the control laws.

3.4 Dynamic Coupling

There is a class of structures where the excitation is induced by the coupling with another dynamic system during a time period. Normally, the dynamics of exciting system are of unknown nature and normally online measurements are not available. This type of systems can be modelled by means of two or more coupled subsystems, where one of them contains all the measurable dynamics. So, the open problem here is to consider such unknown dynamics in the controller design, ensuring at least the global boundedness of the controlled system.

This challenge will be considered in the design of the control laws for the structural system B in the chapter 4. Lyapunov stability theory and Sliding Mode Control techniques were used to design the control laws.

3.5 Actuator Dynamics

From the control design point of view, an ideal control device is that which can deliver exactly the desired command force. However, in real conditions it is not possible since actuator dynamics are inherent in the device. The most significant dynamics presented in active control devices correspond to saturation, time delays and friction forces, while for semiactive control devices the most significant are the hysteresis phenomenon and state variables dependence. This last dynamics is related with the dissipative nature of the semiactive device, whose force delivered depends on structural variables such as velocities or displacements. Thus, these devices are commanded by means of voltage signal in place of a force signal.
In structural control, unpredictable events such as earthquakes occurred in very short time period a fast and effective control action is required. Thus, actuator dynamics are an important aspect to take into account in order to achieve an adequate control action. This is a challenge presented in this type of systems.

3.5.1 Hysteretic Dynamics

The hysteresis phenomenon is an important dynamics in semiactive and passive structural control devices. In this thesis the semiactive device studied corresponds to the Magnetorheological MR damper. The reason to study this kind of device is because its promising future and real applications that have been already initiated. Two challenges are contained in this problem: The first one is to consider the hysteretic behaviour in the controller design and the second one to find a commanding voltage signal in place of a commanding force signal.
The first challenge has not been sufficiently studied in structural control. A solution to this problem is based on the controller design by using Backstepping Control Algorithm. This control approach has been recently introduced in structural control ([41]-[44],[66]. The control approach consists in obtaining a desired commanding force and then computing an equivalent commanding voltage by estimating the nonlinear variable z contained in the dynamics equation of the MR damper. The Backstepping technique consists in the step-by-step construction of a transformed system with state $e_i = y_i - \alpha_{i-1}$, $i = 1, \ldots, n$, where α_i is the so-called *virtual control signal* at the design step i. It is computed at step $i+1$ to drive $e = [e_1, \ldots, e_n]^T$ to the equilibrium state $[0, \ldots, 0]^T$, which can be verified through a standard analysis (i.e. Lyapunov analysis). The Lyapunov functions computed at each step are used to determine the most suitable α_i. The last *stabilizing* signal (α_n) is the true control $u(t)$, which is applied directly to the original system. Some authors have utilized these strategies to solve specific problems [90, 9, 71].

For the second challenge a solution has been stated by using the Clipped-Optimal control [21, 19, 107]. The control algorithm consists in appending m force feedback loops to induce each MR damper to produce approximately a desired control force by applying an equivalent commanding voltage signal.

In the design of a structural control law, the new states $e_i = y_i - y_{ri}$ correspond to the error between the states to be controlled y_i and the desired output y_{ri} (normally set to zero or a minimum vibration value). The total candidate Lyapunov function includes the energy of each new state variable e_i^2, an error energy $\tilde{z}^2$, in order to verify that stability of the system is kept in spite of estimating z. The error $\tilde{z} = z - \hat{z}$ corresponds to the difference between the real value of z and the estimated value $\hat{z}$.

The two control challenges derived from this problem, will be considered in the design of control laws for the structural systems A and C in chapter 4, and for the experimental prototype A. Backstepping control technique is used to design the controllers and additionally for the experimental model the clipped-optimal technique is used in combination with Quantitative Feedback Theory and Backstepping control technique

3.5.2 Actuator Time Delay and Friction Force

Control devices with a considerable time delay is a factor to take into account in the control law design, since one of requirements in control of structures is that its control action must be fast. That is because disturbances, such as seismic forces, occur in short time periods with a big destruction action. In this thesis a time delay will be included in the actuator dynamics in the form of a first order time lag. Friction force is also considered in active hydraulic actuators. For the case of some semiactive devices the time delay (>10ms) is considerable and it must be taken into account in the control law design. For control design purposes the time delay τ is approximated by a first order time lag. By using a direct Lyapunov function or Sliding

Mode Control theory, a desired command force v is obtained and then an equivalent control command is derived by using the actuator dynamics equation. Thus, the force command tracks asymptotically the real force. A new Lyapunov function that includes the error between the desired and real force is defined and then negativity of its derivative is demonstrated.

This control challenge is studied in the design of control laws for the structural systems A, B and C in chapter 4. Implementation of the control approaches is made on the experimental prototype C in chapter 5. The control techniques used are Lyapunov stability theory and Sliding Mode Control.

3.6 Uncertain Structural Parameters

Most of structural control system designs are based on mathematical model. This is because structural models are easily derivable by using control oriented models such as the Finite Element Model (FEM). However, in the construction of such mathematical models there are inherent uncertainties, which produces that response of the real system can not be exactly reproduced. For example to obtain a FEM model, it is necessary to concentrate parameters in a finite number of nodes. It implies that parametric values of nodes are approximated values and uncertainties are presented. Uncertainties are among others reasons, because unconsidered parametric nonlinearities, parameters variation by excitation or aging (structured uncertainties), neglected dynamics (unstructured uncertainties) or may result from non-deterministic features of the structure. Materials properties in structures, such as stiffness or damping, cannot be estimated exactly and strong assumptions must be done. For example, concrete contains different phases during its drying, thus different values of stiffness and damping are presented. Only after having got dried a stable value of its properties may be obtained. However, in that state there does not exist an adequate measurement equipment that estimates such properties. Then, only theoretical approximations can be applied, through coefficients established such as young modulus. On other hand a source of uncertainty is by considering that stiffness and damping are linear parameters under dynamics conditions of structure, however a time variation is presented.

The uncertain problem becomes more complicated when it is tried to design a controller that reduce the vibration modes of the structure, which are directly related with the excitation frequencies. An uncertain external disturbance could excite the structure at the natural frequencies which can produce such undesirable vibration modes. An example of such shape modes for a cable-stayed bridge are presented in figure 3.1 [25].

Thus, the challenge consists in considering such uncertainties, but also taking into account the behaviour of the controlled structure in the frequency domain. The problem of controlling uncertain structures has gained the attention of an increasing number of researchers during last years [64, 63, 105, 103, 29], most of them design in the time domain.

An interesting control technique studied here and that results useful and adequate for this kind of systems is the Quantitative Feedback Theory (QFT). Today, it is one of well known effective frequencial techniques for controlling different types of practical processes. The main properties of QFT are: i). the controller design procedure is rigorous, transparent and systematic, and ii). inclusion of plant uncertainties and formulation performance's specifications is relatively easy. In this sense, the quantitative formulation of plant uncertainty and different performance specifications are essential for the feedback control.

Structural systems A and C in chapter 4 have been used to design and numerically verify QFT controllers, while experimental prototypes A and C in chapter 5 were used for their implementation. A brief explanation of the QFT technique is included in the following section.

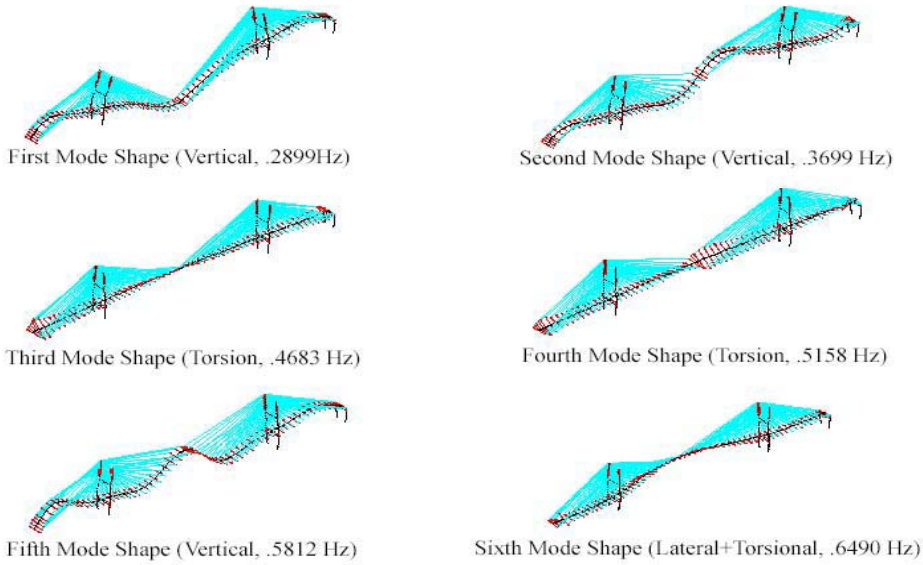

Figure 3.1: Representative Mode Shapes of the Bridge Evaluation Model

3.6.1 QFT LTI design

The basic developments with QFT theory are focused on the control design problem for uncertain Linear Time Invariant (LTI) systems. Consider the system of the figure 3.2 as the basic structure. R represents the command input set, P the LTI plant set and T the OK transfer function set. For each $R \in \boldsymbol{R}$, P in $\boldsymbol{P}$, the closed-loop output will be $Y(s) = T(s)R(s)$ for some T in $\boldsymbol{T}$. For a large class of LTI problems, QFT based design is executable; i.e., a pair of controllers $F(s)$ and $G(s)$ can be found to guarantee that $Y(s) = T(s)R(s)$.

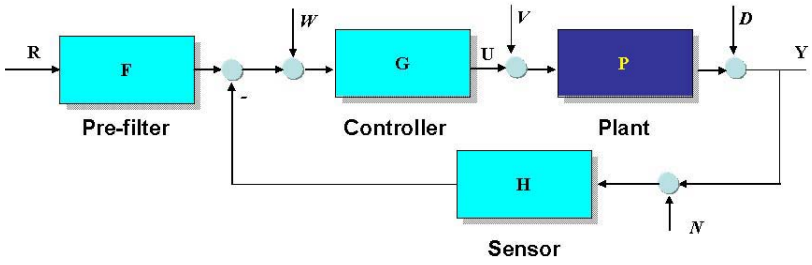

Figure 3.2: LTI structure

Suppose that the LTI plant P is an uncertain but known member of the set $\boldsymbol{P}$. The designer is free to choose the LTI prefilter F and the loop compensator G in order to ensure that the system transfer function $T = \dfrac{FPG}{1+PG}$ satisfies the assigned specifications. This gives an OK set $\boldsymbol{M}$ for $|T(j)|$, to be achieved for all $P \in \boldsymbol{P}$, with $y_u(t)$ and $y_L(t)$ or $B_U(j\omega)$ and $B_L(j\omega)$ being the upper or lower bounds on M (see figure 3.3).

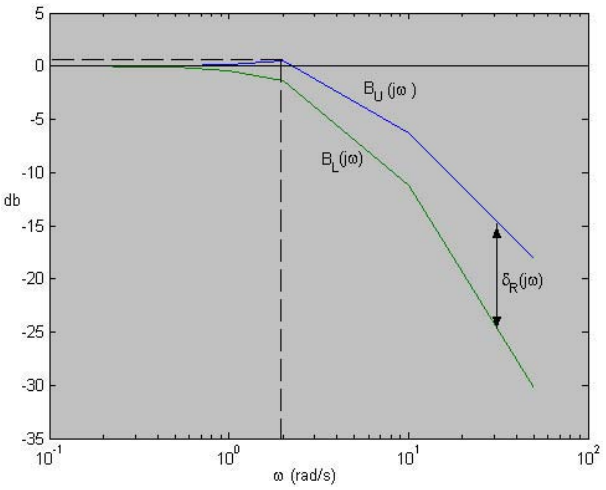

Figure 3.3: Bounds allowed for M

It is highly desirable to have the possibility of designing either F or G simultaneously. This can be easily done by considering the variation in $log_{10}|T|$.

$$\Delta log|T(j\omega)| = \Delta \left| \frac{L(j\omega)}{1 + L(j\omega)} \right| \tag{3.1}$$

By eliminating F, the purpose of G in $L = PG$ is to ensure that the variation $R(j\omega) = B_U(j\omega) - B_L(j\omega)$ allowed in $M(\omega) = |T(j\omega)|$, in figure 3.3, is not exceeded at each ω.

The Logarithmic Complex Plane (Nichols Chart) is a highly transparent medium for visualizing the design procedure for the above purpose. It consists of locking constant $M = |T|$, and $Arg(T)$ in the logarithmic L plane: $Angle(L)$ in degrees, $Magnitude(L)$ in db ($20log_{10}|L|$). $Arg(T)$ is not needed.

Four steps must be followed to obtain G and F.

Step 1. Plant Templates (P) and Loop Templates ($L = PG$). In this step, it is tried to display on the Nichols Chart the existent plant uncertainty. At each frequency, $P(j\omega)$ will be a complex number. Because of plant uncertainty, the plant template $P(j\omega)$ is a set of complex numbers corresponding to a set of uncertain plants at each frequency ω . For example, for the plant $P(s) = k/s(s + a)$ with parametric uncertainties $k \in [1\,5]$ and $a \in [4\,8]$, the plant templates at ω=5,10 rad/s are given by the set of complex numbers shown in figure 3.4: $P(j[5, 10]) = k/[5, 10]/(j[5, 10] + a)$, $k \in [1\,5]$, $a \in [4\,8]$. According to figure 3.3 a variation $\delta(5)$ of 5.3db for $M(5) = |T(j5)|$ and $\delta(10)$ of 4.9 db for $M(10) = |T(j10)|$ are allowed. Here, the idea is to find the bounds on $L(j5)$, for example to assure the last condition. Since $L = PG$ varies with P, it is convenient to choose a nominal P_N giving a nominal $L_N = P_N G$, for this purpose. Values used for nominal plant are: $k = 1$, $a = 4$, so $1/P_N = s^2 + 5s$. The nominal plant P_N (which corresponds to the nominal loop template $L_N = P_N G$ value) is marked 1 in figure 3.4. Note that the template of $L = PG$, is isometric to the template of P. The template $L(j\omega)$ is obtained by shifting the plant template $P(j\omega)$, by $Angle(G(\omega))$ horizontally, by $|G(j\omega)|$ vertically. Its shape and size is the same as the template P.

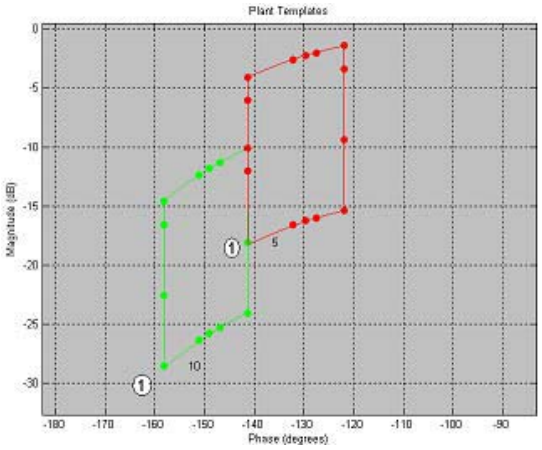

Figure 3.4: Plant templates at ω=10,30

Step 2. Bounds on the nominal $L_N(j\omega)$. In this step, the design tool is the nominal loop template $L_N(j\omega)$. By making it the smallest possible, specifications can be satisfied and economic (quantitative) control is obtained. Simply manipulate the *plant = loop template* on the Nichols chart, until (at any fixed angle), the minimum $|L_N|$ is found, then specifications are satisfied. It is seen that this $|L_N|_{min}$ is a function of $Angle(L_N)$. The resulting curve is called the bound $B(j\omega)$ on $L_N(j\omega)$. One systematized procedure to find each bound on $B(j\omega_i)$ is presented in [6].

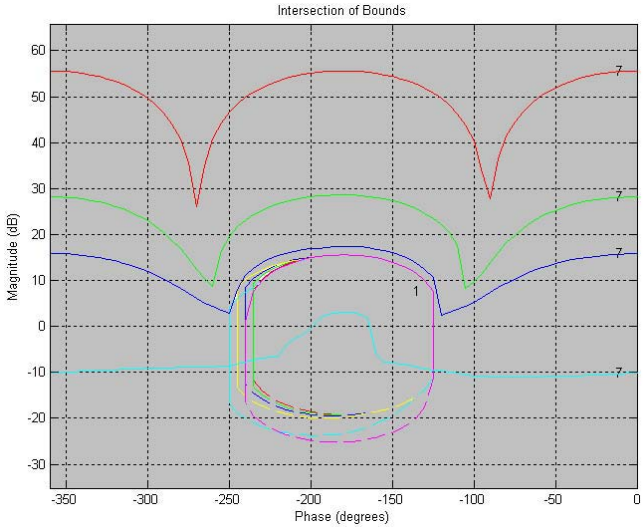

Figure 3.5: All bounds in the Nichols Chart

Step 3. The Universal High-Frequency Bound UH(B). For $\omega >> 1$, the templates $P(j\omega)$ are almost vertical lines, because $P(s)$ is close to k/s^2 at such large s. So, uncertainty of P is approximately the k uncertainty. In this frequency range the allowed M variation is larger than the plant uncertainty. This means that while the sensitivity reduction is obtained in one

frequency range, in other range this may be worse than an open loop system (no feedback control). However, sensitivity to the plant is not the only matter of concern, there is also the effect of disturbances (W, V and D). An additional constraint γ in this "higher" frequency range must be added. It can be recognized by the specifications, allowing L_N to trend increasingly to -1, where the sensitivity becomes very large. This constraint determines the nominal bound L_N at high frequencies. The fact that in the higher frequency the plat template is a fixed vertical line, leads to universal high frequency bound (UHωB). To find γ in the Nichols Chart (i.e., locus for which $|L/(1+L)| = \gamma$) the exclusion zone is projected downward by the amount of the k uncertainty ($V = Log(k_{max}) - Log(k_{min})$. This gives the entire UHωB.

Step 4. Find $L_N(j\omega)$ which satisfies its bounds $B(\omega)$. The idea is to design a controller $G(s)$, which allows the function $L(s) = G(s)P(s)$ to accomplish the specifications defined by means of the bounds (see figure 3.5). By considering the most restrictive conditions from this set of bounds, the resulting bound is found by intersecting the constrained bounds (figure 3.6).

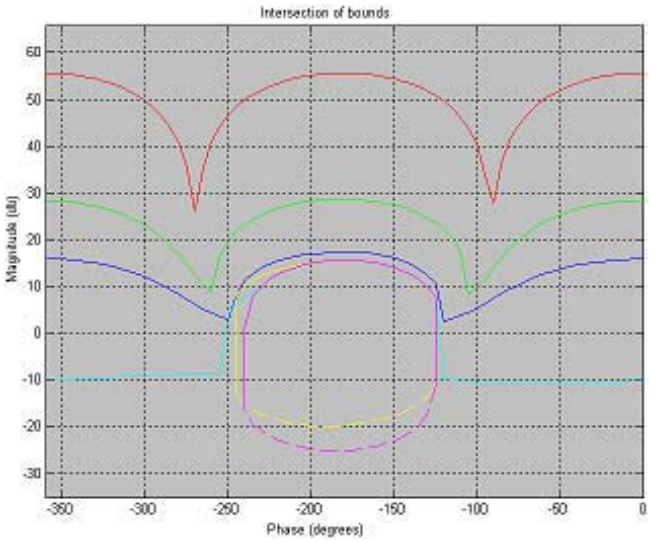

Figure 3.6: Intersection of bounds

By taking into account such bound, the optimal design is ensured if for each ω_i, $L_N(j\omega_i)$ is in its corresponding bound. In a practical way, $L_N(j\omega)$ is designed to be as near as possible to $B(j\omega)$, in order to keep minimum the bound width of $T(j\omega)$. A basic controller k_c/s is used as initial, and poles or zeros are added according to the needs to accomplish the specifications. One possible loop L_N that accomplishes the specifications of the example is shown in figure 3.7. There exists a MATLAB toolbox, which contains some functions that have been written for this purpose.

Step 5. Design of Feedback Controller and Prefilter $F(s)$. The controller $G(s)$ is available from $L_N(G(s) = L_N(s)/P_N(s))$. Under design conditions L_N may result with excess of pole over zeros, however since the design has 2 DOFs ($G(s)$ and $L(s)$), the excess of poles is not a problem. G has been computed to assure that the allowed variation in $|T(j\omega)|$, $M_max - M_min = \delta(\omega)$ be satisfied for all ω. But, suppose for example that at some $\delta(\omega_1)$, the specification dictates $M_{max} = 8db$, $M_{min} = 1db$, then $\delta(\omega_1) = 7db$, at this frequency $M_{max} = -2db$, $M_{min} = -8db$, with variation of 6<7. Although of the accomplishment of variation specification, the

M specification has not been satisfied. Since $|T| = |F|M$, the function of F is to maintain the actual OK variation inside the M specification. This is achieved by assigning bounds on $|F(j\omega)| : Log\{Fmin(j\omega)\} < Log\{F(j\omega)\} < Log\{Fmax(j\omega)\}$ and additionally to ensure that $lim_{s\to 0}F(s) = 1$. For the example $Log\{F_{min}(j\omega)\} = 1 - (-8) = 9$db and $Log\{Fmax(j\omega)\} = 8 - (-2) = 10$db. The free range of $|F| = 10 - 9 = 1$db is precisely the amount of overdesign of $G(j\omega)$, which gives a variation of 6 db, while a variation of 7 db is allowed by the specifications. The results of including F are graphically shown in figure 3.8.

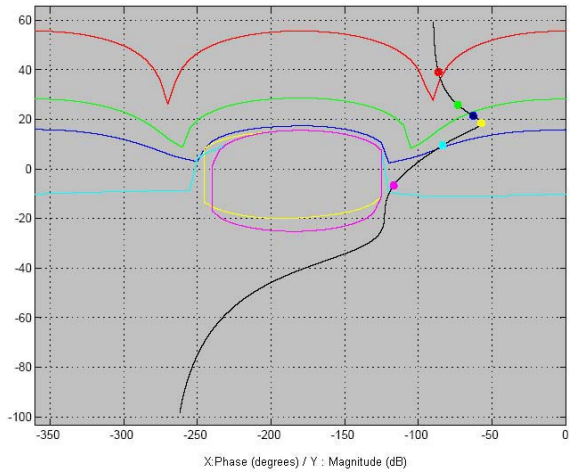

Figure 3.7: A possible final loop L_N

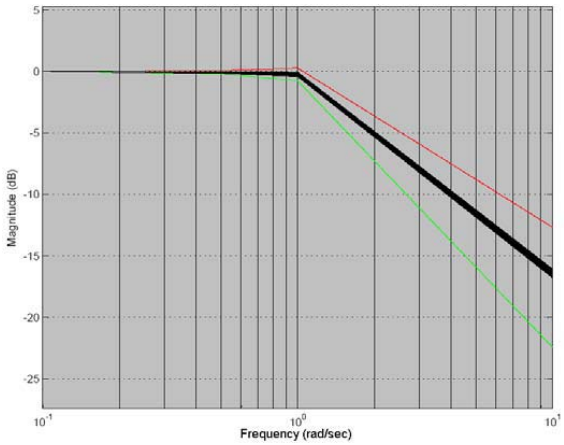

Figure 3.8: Effect of including $F(j\omega)$

3.6.2 QFT controller for uncertain structures

Taking into account that in structural control the main control objective is to reduce vibrations to zero if it is possible, the reference point r cab ne set to zero all time and a prefilter does not have sense in this kind of problems. Therefore, the structural control scheme is that shown in

figure 3.9. In which V represents the external disturbance of the structure plus other possible terms that cannot be included in the plant but a bounded value can be assigned. The output Y corresponds to the state variable to be controlled and U represents the force developed by the control devices at the point where the output Y is measured. The plant P contains the structural parameters directly related with the variable to be controlled, while the other nonmeasurable states are not included or included as a bounded value. Terms related with other measurable states are added to input U, and then the force f that the control device must develop is obtained by doing the respective difference of U minus the other added terms. An equivalent plant is found from the motion equation of the structure and for the node where the control device is installed. If more than one device is present in the structure, the respective plants are obtained and in some cases the input U can be combination of forces from different actuators.

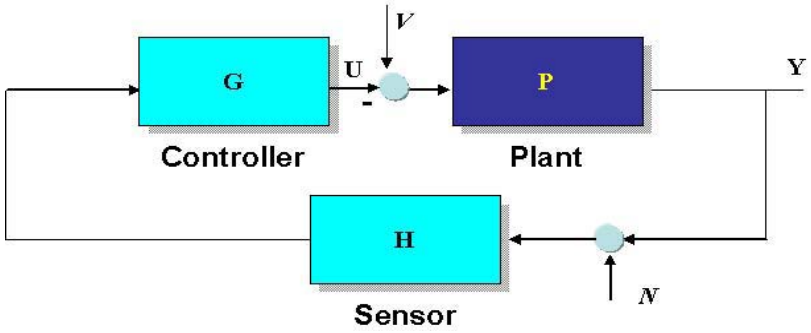

Figure 3.9: LTI structure for structural control

Chapter 4

Structural Control Approaches

This chapter present the design and numerical verification of control law approaches for structural systems that contain one or more structural control problems. The methodology followed in this chapter is: first the structural system and its control problems are stated, then numerical results of the controlled and uncontrolled structural system are presented. Three structural systems are studied, whose control configurations present one or more problems presented in chapter 3.

4.1 Structural System A: 10-story Base Isolated Structure

Consider a nonlinear base isolated building structure as shown in Figure 4.1, whose dynamic behavior can be described by means of a model composed of two coupled subsystems, namely, the main structure (S_r) and the base isolation (S_c):

$$\begin{aligned} &S_r : \boldsymbol{M}\ddot{\boldsymbol{q}}_r + \boldsymbol{C}\dot{\boldsymbol{q}}_r + \boldsymbol{K}\boldsymbol{q}_r = [c_1, 0, ..., 0]^T \dot{q}_c + [k_1, 0, ..., 0]^T q_c \,. \\ &S_c : m_0\ddot{q}_c + (c_0 + c_1)\dot{q}_c + (k_0 + k_1)q_c - c_1\dot{q}_{r1} - k_1 q_{r1} = -c_0\dot{d} - k_0 d + f_N \,. \\ &f_N = -sgn(\dot{q}_c - \dot{d})[\mu_{max} - \Delta\mu e^{-\nu|\dot{q}_c - \dot{d}|}]G \end{aligned} \tag{4.1}$$

This model assumes that the structure has a linear behavior due to the effect of the base isolation. This behavior is represented by the positive definite mass, damping and stiffness matrices $\boldsymbol{M}$, $\boldsymbol{C}$ and $\boldsymbol{K} \in I\!R^{n\times n}$ respectively.

$$\boldsymbol{M} = diag([m_1\, m_2 \ldots m_n]) \quad ; \quad (i = 1, 2, ..., n) \tag{4.2}$$

$$\boldsymbol{C} = \begin{bmatrix} c_1 + c_2 & -c_2 & 0 & \cdots & 0 \\ -c_2 & c_2 + c_3 & -c_3 & \cdots & 0 \\ \vdots & \vdots & \vdots & \cdots & \vdots \\ 0 & 0 & 0 & \cdots & c_n \end{bmatrix} \quad \boldsymbol{K} = \begin{bmatrix} k_1 + k_2 & -k_2 & 0 & \cdots & 0 \\ -k_2 & k_2 + k_3 & -k_3 & \cdots & 0 \\ \vdots & \vdots & \vdots & \cdots & \vdots \\ 0 & 0 & 0 & \cdots & k_n \end{bmatrix}$$

$\boldsymbol{q}_r = [\, q_{r1}\,, q_{r2}\,, \cdots, q_{rn}\,]^T \in I\!R^n$ represents the horizontal displacements of each floor with respect to an inertial frame. The base isolation is described as a single degree of freedom with horizontal displacement $q_c \in I\!R$. It is assumed to exhibit a linear behavior characterized by mass, damping and stiffness m_0, c_0 and k_0, respectively, plus a nonlinear behavior represented by a force f_N supplied by a frictional isolator with G being the force normal to the friction surface, μ the friction coefficient, ν a constant, μ_{max} the coefficient for high sliding velocity and

$\Delta\mu$ the difference between μ_{max} and the friction coefficient for low sliding velocity. The term $-c_0\dot{d}-k_0 d$ is a dynamic excitation force acting on the base due to the horizontal seismic ground motion represented by inertial displacement $d(t)$ and velocity $\dot{d}(t)$ at each time instant t.

In general, the base isolator (passive control device) can achieve satisfactory performance if its resonance frequency is well tuned. However, it is very difficult to make such tuning in practice due to the lack of information on the forthcoming earthquake [91, 8]. Another serious problem is that sometimes the peak response of absolute base displacement is so large as to exceed the elastic limit of the base isolator. The main purpose for the use of active and semiactive controllers in combination with the passive controller (base isolator) is to reduce the peak response of the absolute base displacement so that the base isolator works always in the elastic region and also to attenuate the dependence of structural performance on the resonance frequency of the base isolator.

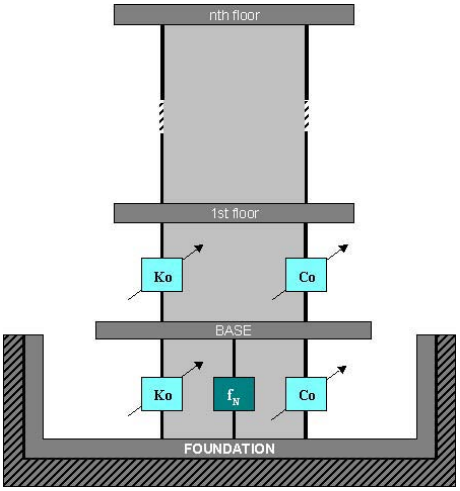

Figure 4.1: A 10-story base isolated building

4.1.1 Control Configuration 1

Usually, the semiactive control devices have to be installed in all stories of the building to guarantee the global stability of the whole base-structure system. In the present control configuration, we only use semiactive controllers at the base and the first floor to adjust the stiffness $k_i(t)$ and the damping $c_i(t)$ $(i = 0, 1)$, as illustrated in Figure 4.1. In this way, the number of semiactive control devices is significantly reduced. The following equations of motion of the base and the first floor will be used in the controller design:

$$S_{r1} \;:\; m_1\ddot{q}_{r1} + c_1\dot{q}_{r1} + k_1 q_{r1} = \alpha + \beta\,. \tag{4.3}$$

$$S_c \;:\; m_0\ddot{q}_c + [c_0 + c_1]\dot{q}_c + [k_0 + k_1]q_c = c_1\dot{q}_{r1} + k_1 q_{r1} - c_0\dot{d} - k_0 d + f_N\,. \tag{4.4}$$

where

$$\alpha =: c_1\dot{q}_c + k_1 q_c \quad \text{and} \quad \beta =: c_2[\dot{q}_{r2} - \dot{q}_{r1}] + k_2[q_{r2} - q_{r1}] \tag{4.5}$$

It is well accepted that the movement of the building S_r is very close to the movement of a rigid body due to the base isolation [91]. Then it is reasonably to assume that the inter-story motion of the building will be much smaller than the absolute motion of the base. Hence, the right-hand terms of the equation (4.3) can be simplified as: $\alpha + \beta \approx \alpha = c_1\dot{q}_c + k_1(t)q_c$. A numerical verification of the above assumption can be found in Figure 2. Consequently, the following simplified equation of motion of the first floor can be used in the subsequent controller design:

$$S_{r1}: \qquad m_1\ddot{q}_{r1} + c_1\dot{q}_{r1} + k_1 q_{r1} = c_1(t)\dot{q}_c + k_1(t)q_c\,. \tag{4.6}$$

The semiactive controller is designed to provide adaptive damping and stiffness as being functions of the absolute motion. Concretely, the operation of control system is based on the on-line modification of the stiffness and the damping parameters of both the base $(k_0(t); c_0(t))$ and the first floor $(k_1(t); c_1(t))$. It is assumed that these parameters can take any value within prescribed bounds. That is,

$$k_i(t) = k_i^* + \Delta_i^k(t); \qquad c_i(t) = c_i^* + \Delta_i^c(t); \qquad i = 0, 1 \tag{4.7}$$

where k_i^* and c_i^* are considered generally as the nominal values of $k_i(t)$ and $c_i(t)$. Suppose that $\Delta_i^k(t)$ and $\Delta_i^c(t)$ can be adjusted by control signals $u_i^k(t)$ and $u_i^c(t)$ $(i = 0, 1)$. For instance, without loss of generality, let

$$\Delta_i^k(t) = \delta_i^k u_i^k(t); \qquad \Delta_i^c(t) = \delta_i^c u_i^c(t); \qquad u_i^{k,c}(t) \in [-1, 1] \tag{4.8}$$

where

$$k_i^* = \frac{1}{2}(k_i^+ + k_i^-); \quad c_i^* = \frac{1}{2}(c_i^+ + c_i^-); \quad \delta_i^k = \frac{1}{2}(k_i^+ - k_i^-); \quad \delta_i^c = \frac{1}{2}(c_i^+ - c_i^-) \tag{4.9}$$

By taking into account the actuator dynamics, such as time delay and frictional force, the real control forces $v_i^k(t)$ and $v_i^c(t)$ generated by the semiactive controllers to the structure are given as follows

$$\begin{array}{ll} v_0^k = \Delta_0^k q_c + P_{a_0}^k \dot{q}_c; & v_0^c = \Delta_0^c \dot{q}_c + P_{a_0}^c \dot{q}_c \\ v_1^k = \Delta_1^k (q_c - q_{r1}) + P_{a_1}^k (\dot{q}_c - \dot{q}_{r1}) & v_1^c = \Delta_1^c (\dot{q}_c - \dot{q}_{r1}) + P_{a_1}^c (\dot{q}_c - \dot{q}_{r1}) \end{array} \tag{4.10}$$

with

$$\Delta_i^k = \delta_i^k u_i^k - \tau_i^k \dot{\Delta}_i^k; \qquad \Delta_i^c = \delta_i^c u_i^c - \tau_i^c \dot{\Delta}_i^c \tag{4.11}$$

i.e.

$$u_i^k = \frac{1}{\delta_i^k}\left[\Delta_i^k - \tau_i^k \dot{\Delta}_i^k\right]; \quad u_i^c = \frac{1}{\delta_i^c}\left[\Delta_i^c - \tau_i^c \dot{\Delta}_i^c\right] \tag{4.12}$$

where τ_i^k and τ_i^c are time constants of the actuator dynamics for the stiffness and damping changing, $P_{a_i}^k$ and $P_{a_i}^c$ are the parameters related to the frictional forces existed in the actuator.

Concretely, the control forces generated by the semiactive control device are formulated as:

$$\begin{array}{ll} v_0^k = (\delta_0^k u_0^k - \tau_0^k \dot{\Delta}_0^k) q_c + P_{a_0}^k \dot{q}_c & v_0^c = (\delta_0^c u_0^c - \tau_0^c \dot{\Delta}_0^c) \dot{q}_c + P_{a_0}^c \dot{q}_c \\ v_1^k = (\delta_1^k u_1^k - \tau_1^k \dot{\Delta}_1^k)(q_c - q_{r1}) + P_{a_1}^k (\dot{q}_c - \dot{q}_{r1}) & v_1^c = (\delta_1^c u_1^c - \tau_1^c \dot{\Delta}_1^c)(\dot{q}_c - \dot{q}_{r1}) + P_{a_1}^c (\dot{q}_c - \dot{q}_{r1}) \end{array} \tag{4.13}$$

By substituting the above control laws into the dynamic equations of the base(equation (4.4)) and the first floor (equation (4.6)), we obtain

$$\begin{aligned}\ddot{q}_c &= \frac{1}{m_0}\Big[-(c_0^* + c_1^* + P_{a_0}^k + P_{a_0}^c + P_{a_1}^k + P_{a_1}^c)\dot{q}_c - (k_0^* + k_1^*)q_c + (c_1^* + P_{a_1}^k + P_{a_1}^c)\dot{q}_{r_1} + k_1^* q_{r_1} + f \\ &\quad -u_0^k\delta_0^k q_c + \tau_0^k\dot{\Delta}_0^k q_c - u_0^c\delta_0^c\dot{q}_c + \tau_0^c\dot{\Delta}_0^c\dot{q}_c - \delta_1^k u_1^k(q_c - q_{r1}) + \tau_1^k\dot{\Delta}_1^k(q_c - q_{r1}) - \delta_1^c u_1^c(\dot{q}_c - \dot{q}_{r1}) \\ &\quad +\tau_1^c\dot{\Delta}_1^c(\dot{q}_c - \dot{q}_{r1})\Big] \qquad (4.14)\\ \ddot{q}_{r_1} &= \frac{1}{m_1}\Big[-(c_1^* + P_{a_1}^k + P_{a_1}^c)\dot{q}_{r_1} - k_1^* q_{r_1} + (c_1^* + P_{a_1}^k + P_{a_1}^c)\dot{q}_c + k_1^* q_c\delta_1^k u_1^k(q_c - q_{r1}) - \tau_1^k\dot{\Delta}_1^k(q_c - \\ &\quad q_{r1}) + \delta_1^c u_1^c(\dot{q}_c - \dot{q}_{r1}) - \tau_1^c\dot{\Delta}_1^c(\dot{q}_c - \dot{q}_{r1})\Big] \qquad (4.15)\end{aligned}$$

Controllers Design

Two controllers are designed for this configuration. Controller 1 is based on the Lyapunov stability theory, while contoller 2 is based on the Sliding Mode Control (SMC) technique.
Controller 1.

Define the Lyapunov function candidate as

$$V(\boldsymbol{x}, t) = \frac{1}{2}\boldsymbol{x}^T(t)\boldsymbol{P}\boldsymbol{x}(t) \qquad (4.16)$$

where $\boldsymbol{P} =\in R^{4\times 4}$ is the positive definite solution of the Lyapunov equation

$$\boldsymbol{P}\boldsymbol{A} + \boldsymbol{A}^T\boldsymbol{P} + \boldsymbol{Q} = 0 \qquad (4.17)$$

for a given symmetric positive definite matrix $\boldsymbol{Q}$.

Now, define $\boldsymbol{x} = [q_{r_1}, \dot{q}_{r_1}, q_c, \dot{q}_c]^T$, $\boldsymbol{u} = [u_1^k, u_1^c, u_0^k, u_0^c]^T$ and $z = [\dot{\Delta}_1^k, \dot{\Delta}_1^c, \dot{\Delta}_0^k, \dot{\Delta}_0^c]^T$. Then, the following state equation is obtained

$$\dot{\boldsymbol{x}}(t) = \boldsymbol{A}\boldsymbol{x}(t) + \boldsymbol{B}(\boldsymbol{x}, t)\boldsymbol{u}(t) + C(\boldsymbol{x}, t)\boldsymbol{z}(t) + \boldsymbol{F}(\boldsymbol{x}, t) \qquad (4.18)$$

where

$$\boldsymbol{A} = \begin{pmatrix} 0 & 1 & 0 & 0 \\ \frac{-k_1^*}{m_1} & -\frac{c_1^* + P_{a1}^k + P_{a1}^c}{m_1} & \frac{k_1^*}{m_1} & \frac{c_1^* + P_{a1}^k + P_{a1}^c}{m_1} \\ 0 & 0 & 0 & 1 \\ \frac{k_1^*}{m_0} & \frac{c_1^* + P_{a1}^k + P_{a1}^c}{m_0} & -\frac{k_0^* + k_1^*}{m_0} & -\frac{c_0^* + c_1^* + P_{a0}^k + P_{a0}^c + P_{a1}^k + P_{a1}^c}{m_0} \end{pmatrix}$$

$$\boldsymbol{B}(\boldsymbol{x}, t) = \begin{pmatrix} 0 & 0 & 0 & 0 \\ \frac{\delta_1^k(q_c - q_{r_1})}{m_1} & \frac{\delta_1^c(\dot{q}_c - \dot{q}_{r_1})}{m_1} & 0 & 0 \\ 0 & 0 & 0 & 0 \\ -\frac{\delta_1^k(q_c - q_{r1})}{m_0} & -\frac{\delta_1^c(\dot{q}_c - \dot{q}_{r1})}{m_0} & -\frac{\delta_0^k q_c}{m_0} & -\frac{\delta_0^c\dot{q}_c}{m_0} \end{pmatrix}$$

$$\boldsymbol{C}(\boldsymbol{x}, t) = \begin{pmatrix} 0 & 0 & 0 & 0 \\ -\frac{\tau_1^k(q_c - q_{r1})}{m_1} & -\frac{\tau_1^c(\dot{q}_c - \dot{q}_{r1})}{m_1} & 0 & 0 \\ 0 & 0 & 0 & 0 \\ \frac{\tau_1^k(q_c - q_{r1})}{m_0} & \frac{\tau_1^k(\dot{q}_c - \dot{q}_{r1})}{m_0} & \frac{\tau_0^k q_c}{m_0} & \frac{\tau_0^c\dot{q}_c}{m_0} \end{pmatrix}$$

$$\boldsymbol{F}(\boldsymbol{x},t) = \begin{bmatrix} 0 \\ 0 \\ 0 \\ 0 \\ \dfrac{1}{m_0} \end{bmatrix} f[q_c(t), \dot{q}_c(t), d(t), \dot{d}(t)] \tag{4.19}$$

Suppose that the seismic excitation $(d, \dot{d})$ is unknown but bounded,

$$\|f[q_c(t), \dot{q}_c(t), d(t), \dot{d}(t)]\| \leq \phi_0\,, \tag{4.20}$$

where ϕ_0 is a known constant. Then

$$\|\boldsymbol{F}(\boldsymbol{x},t)\| \leq \frac{1}{m_0}\|f[q_c(t), \dot{q}_c(t), d(t), \dot{d}(t)]\| \leq F_0 \tag{4.21}$$

consequently $F_0 = \phi_0/m_0$ is a known constant.

By using eqns. 4.16-4.21, the derivative of $V(\boldsymbol{x},t)$ is obtained

$$\begin{aligned} \dot{V}(\boldsymbol{x},t) &= -\frac{1}{2}\boldsymbol{x}^T\boldsymbol{Q}\boldsymbol{x} + \boldsymbol{x}^T\boldsymbol{P}\boldsymbol{b}_0^k u_0^k + \boldsymbol{x}^T\boldsymbol{P}\boldsymbol{b}_0^c u_0^c + \boldsymbol{x}^T\boldsymbol{P}\boldsymbol{b}_1^k u_1^k + \boldsymbol{x}^T\boldsymbol{P}\boldsymbol{b}_1^c u_1^c + \boldsymbol{x}^T\boldsymbol{P}\boldsymbol{c}_0^k\dot{\Delta}_0^k + \boldsymbol{x}^T\boldsymbol{P}\boldsymbol{c}_0^c\dot{\Delta}_0^c \\ &\quad + \boldsymbol{x}^T\boldsymbol{P}\boldsymbol{c}_1^k\dot{\Delta}_1^k + \boldsymbol{x}^T\boldsymbol{P}\boldsymbol{c}_1^c\dot{\Delta}_1^c + \boldsymbol{x}^T\boldsymbol{P}\boldsymbol{F} \end{aligned} \tag{4.22}$$

where

$$\boldsymbol{b}_0^k = \begin{pmatrix} 0 \\ 0 \\ 0 \\ \dfrac{-\delta_0^k q_c}{m_0} \end{pmatrix} \quad \boldsymbol{b}_1^k = \begin{pmatrix} 0 \\ \dfrac{\delta_1^k(q_c - q_{r_1})}{m_1} \\ 0 \\ \dfrac{-\delta_1^k(q_c - q_{r1})}{m_0} \end{pmatrix} \quad \boldsymbol{b}_0^c = \begin{pmatrix} 0 \\ 0 \\ 0 \\ \dfrac{-\delta_0^c \dot{q}_c}{m_0} \end{pmatrix} \quad \boldsymbol{b}_1^c = \begin{pmatrix} 0 \\ \dfrac{\delta_1^c(\dot{q}_c - \dot{q}_{r_1})}{m_1} \\ 0 \\ \dfrac{-\delta_1^c(\dot{q}_c - \dot{q}_{r1})}{m_0} \end{pmatrix}$$

$$\boldsymbol{c}_0^k = \begin{pmatrix} 0 \\ 0 \\ 0 \\ \tau_0^k q_c m_0 \end{pmatrix} \quad \boldsymbol{c}_1^k = \begin{pmatrix} 0 \\ \dfrac{-\tau_1^k(q_c - q_{r1})}{m_1} \\ 0 \\ \dfrac{-\tau_1^k(q_{r1} - q_c)}{m_0} \end{pmatrix} \quad \boldsymbol{c}_0^c = \begin{pmatrix} 0 \\ 0 \\ 0 \\ \dfrac{\tau_0^c \dot{q}_c}{m_0} \end{pmatrix} \quad \boldsymbol{c}_1^c = \begin{pmatrix} 0 \\ \dfrac{-\tau_1^c(\dot{q}_c - \dot{q}_{r_1})}{m_1} \\ 0 \\ \dfrac{-\tau_1^c(\dot{q}_{r1} - \dot{q}_c)}{m_0} \end{pmatrix}$$

It can be verified from the above relations that

$$\boldsymbol{c}_i^k = -\frac{\tau_i^k}{\delta_i^k}\boldsymbol{b}_i^k; \qquad \boldsymbol{c}_i^c = -\frac{\tau_i^c}{\delta_i^c}\boldsymbol{b}_i^c; \qquad (i = 0, 1) \tag{4.23}$$

The control objective is to minimize $\dot{V}(\boldsymbol{x},t)$ for every $(\boldsymbol{x},t)$. The semiactive control signals that result in the minimum of $\dot{V}(\boldsymbol{x},t)$ for $u_i^k(t) \in [-1,1]$ and $u_i^c(t) \in [-1,1]$ are

$$u_i^{k,c} = -sgn(\boldsymbol{x}^T\boldsymbol{P}\boldsymbol{b}_i^{k,c}); \qquad i = 1, 2 \tag{4.24}$$

Now, rewrite the expression of $\dot{V}(\boldsymbol{x},t)$ into the following form

$$\begin{aligned} \dot{V} &= -\frac{1}{2}\boldsymbol{x}^T\boldsymbol{Q}\boldsymbol{x} + \boldsymbol{x}^T\boldsymbol{P}\boldsymbol{b}_0^k(\delta_0^k u_0^k - \tau_0^k\dot{\Delta}_0^k) + \boldsymbol{x}^T\boldsymbol{P}\boldsymbol{b}_0^c(\delta_0^c u_0^c - \tau_0^c\dot{\Delta}_0^c) + \boldsymbol{x}^T\boldsymbol{P}\boldsymbol{b}_1^k(\delta_1^k u_1^k - \tau_1^k\dot{\Delta}_1^k) + \\ &\quad + \boldsymbol{x}^T\boldsymbol{P}\boldsymbol{b}_1^c(\delta_1^c u_1^c - \tau_1^c\dot{\Delta}_1^c) + \boldsymbol{x}^T\boldsymbol{P}\boldsymbol{F} \end{aligned} \tag{4.25}$$

By applying the semiactive control laws in eqn.(4.24), we can show that

$$\boldsymbol{x}^T \boldsymbol{P}\boldsymbol{b}_i^k(\delta_i^k u_i^k - \tau_i^k \dot{\Delta}_i^k) < 0; \qquad \boldsymbol{x}^T \boldsymbol{P}\boldsymbol{b}_i^c(\delta_i^c u_i^c - \tau_i^c \dot{\Delta}_i^c) < 0; \qquad i = 1, 2 \tag{4.26}$$

In fact, if $\boldsymbol{x}^T(t)\boldsymbol{P}\boldsymbol{b}_0^k(\boldsymbol{x}, t) > 0$ for $t \geq t_s$ then $u_0^k(t) = -1$. In this case, we get from eqn.(4.11) that

$$\Delta_0^k(t) = -\delta_0^k \left(1 - e^{-(t-t_s)/\tau_0^k}\right); \qquad \dot{\Delta}_0^k(t) = -\frac{\delta_0^k}{\tau_0^k} e^{-(t-t_s)/\tau_0^k} \geq -\frac{\delta_0^k}{\tau_0^k} \tag{4.27}$$

thus the first relation in eqn.(4.26) for i=1 is accomplished. If $\boldsymbol{x}^T(t)\boldsymbol{P}\boldsymbol{b}_0^k(t) < 0$ that implies $u_0^k(t) = -1$, then we obtain that $k_0(t) \leq \delta_0^k/\tau_0^k$. Therefore, the first relation in eqn.(4.26) for i=1 is also accomplished. The remaining relations derived form eqn.(4.26) can be proved in a similar way.

Denote that

$$\theta(\boldsymbol{x}) = \boldsymbol{x}^T \boldsymbol{P}\boldsymbol{b}_0^k(\delta_0^k u_0^k - \tau_0^k \dot{\Delta}_0^k) + \boldsymbol{x}^T \boldsymbol{P}\boldsymbol{b}_0^c(\delta_0^c u_0^c - \tau_0^c \dot{\Delta}_0^c) + \boldsymbol{x}^T \boldsymbol{P}\boldsymbol{b}_1^k(\delta_1^k u_1^k - \tau_1^k \dot{\Delta}_1^k) + \boldsymbol{x}^T \boldsymbol{P}\boldsymbol{b}_1^c(\delta_1^c u_1^c - \tau_1^c \dot{\Delta}_1^c)$$

then, $\theta(\boldsymbol{x}) < 0$ and the equation (4.25) can be rewritten as

$$\dot{V} = -\frac{1}{2}\boldsymbol{x}^T \boldsymbol{Q}\boldsymbol{x} + \theta(\boldsymbol{x}) + \boldsymbol{x}^T \boldsymbol{P}\boldsymbol{F} \tag{4.28}$$

Since $\boldsymbol{Q}$ and $\boldsymbol{P}$ are positive definite matrices, using (4.21) we may write

$$\dot{V} \leq -\frac{1}{2}\lambda_{min}(\boldsymbol{Q})||\boldsymbol{x}(t)||^2 + \theta[\boldsymbol{x}(t)] + \lambda_{max}(\boldsymbol{P})F_0||\boldsymbol{x}(t)|| \tag{4.29}$$

where λ_{min} and λ_{max} represent the minimum and maximum eigenvalue, respectively.

The compact set $\mathcal{K} = \{\boldsymbol{x} \in I\!R^4 \,|\, V(\boldsymbol{x}) \leq \gamma\}$ is a global uniform attractor for the semiactively controlled system (4.29), where

$$\gamma = \max\{V(\boldsymbol{x}) | \boldsymbol{x} \in I\!R^4, \psi(\boldsymbol{x}) \leq 0\},$$

with

$$\psi(\boldsymbol{x}) = \frac{1}{2}\lambda_{min}(\boldsymbol{Q})\|\boldsymbol{x}\|^2 - \theta(\boldsymbol{x}) - \lambda_{max}(\boldsymbol{P})F_0\|\boldsymbol{x}\| \tag{4.30}$$

By using the property that

$$\frac{\lambda_{min}(\boldsymbol{P})}{2}\|\boldsymbol{x}\|^2 \leq V(\boldsymbol{x}, t) \leq \frac{\lambda_{max}(\boldsymbol{P})}{2}\|\boldsymbol{x}\|^2 \tag{4.31}$$

it is easy to find that the set $\mathcal{B} = \{\boldsymbol{x} \in I\!R^4 \,|\, \|\boldsymbol{x}\| \leq \rho\}$, with

$$\rho = \sqrt{\frac{2\gamma}{\lambda_{min}(\boldsymbol{P})}}, \tag{4.32}$$

is the smallest ball that contains the attractor $\mathcal{K}$. This is called the *ball of ultimate boundedness* in the literature[9]. In control practical terms, this is a ball such that any trajectory entering at certain time T remains there for all $t > T$.

Controller 2

The sliding function $\boldsymbol{\sigma}(t) = [\sigma_0(t),\, \sigma_1(t)]^T \in I\!R^2$ is defined with:

$$\sigma_0(t) = \dot{q}_c(t) + \lambda_0 q_c(t); \qquad \sigma_1(t) = \dot{q}_{r1}(t) + \lambda_1 q_{r1}(t) \tag{4.33}$$

where λ_0 and λ_1 are scalars to be chosen to guarantee the closed–loop stability of the base isolated structure. By following the SMC theory, a Lyapunov function is defined as $V = \frac{1}{2}\boldsymbol{\sigma}^T(t)\boldsymbol{\sigma}(t)$ and sliding motion will be generated if $\dot{V} < 0$ for $t \geq 0$. Then by deriving σ and replacing $\ddot{q}_{r1}$ and $\ddot{q}_c$ from (4.15), the derivative of V is expressed as:

$$\dot{V} = S_1 + S_2 + S_3 \tag{4.34}$$

with

$$S_1 = S_0^k + S_0^c + S_1^k + S_1^c \qquad S_2 = S_{0_d}^k + S_{0_d}^c + S_{1_d}^k + S_{1_d}^c \tag{4.35}$$

$$\begin{aligned} S_3 = {} & -m_1^{-1}\sigma_1[c_1^*(\dot{q}_{r1} - \dot{q}_c) + k_1^*(q_{r1} - q_c) + c_2^*(\dot{q}_{r1} - \dot{q}_{r2}) + k_2^*(q_{r1} - q_{r2})] - m_0^{-1}\sigma_0[c_0^*\dot{q}_c \\ & + k_0^* q_c + c_1^*(\dot{q}_c - \dot{q}_{r1}) + k_1^*(q_c - q_{r1}) + f(q_c, \dot{q}_c, d, \dot{d})] + \lambda_0\sigma_0\dot{q}_c + \lambda_1\sigma_1\dot{q}_{r1} \end{aligned} \tag{4.36}$$

where S_1 contains all terms which can be controlled, S_2 contains the terms related with actuator time delay effects and S_3 contains the rest uncontrollable and unmeasurable terms with, i.e.

$$\begin{array}{ll} S_0^k = -m_0^{-1}\sigma_0\dot{q}_c\dot{\delta}_0^k u_0^k; & S_{0_d}^k = -m_0^{-1}\sigma_0 q_c \tau_0^k \dot{\Delta}_0^k \\ S_0^c = -m_0^{-1}\sigma_0\dot{q}_c\dot{\delta}_0^c u_0^c; & S_{0_d}^c = -m_0^{-1}\sigma_0\dot{q}_c\tau_0^c\dot{\Delta}_0^c \\ S_1^k = -[m_1^{-1}\sigma_1 - m_0^{-1}\sigma_0](q_{r1} - q_c)\dot{\delta}_1^k u_1^k & S_{1_d}^k = -[m_1^{-1}\sigma_1 - m_0^{-1}\sigma_0](q_{r1} - q_c)\tau_1^k\dot{\Delta}_1^k \\ S_1^c = -[m_1^{-1}\sigma_1 - m_0^{-1}\sigma_0](\dot{q}_{r_1} - \dot{q}_c)\dot{\delta}_1^c u_1^c & S_{1_d}^c = -[m_1^{-1}\sigma_1 - m_0^{-1}\sigma_0](\dot{q}_{r_1} - \dot{q}_c)\tau_1^c\dot{\Delta}_1^c \end{array}$$

By individually minimizing the functions S_0^c, S_0^k, S_1^c, S_1^c the following semiactive control laws are found:

$$\begin{array}{ll} u_0^k = sgn(\sigma_0 q_c) & u_1^k = sgn[(m_1^{-1}\sigma_1 - m_0^{-1}\sigma_0)(q_{r_1} - q_c)] \\ u_0^c = sgn(\sigma_0\dot{q}_c) & u_1^c = sgn[(m_1^{-1}\sigma_1 - m_0^{-1}\sigma_0)(\dot{q}_{r_1} - \dot{q}_c)] \end{array} \tag{4.37}$$

The above semiactive control laws ensure negativity of S_1, moreover negativity of $S_1 + S_2$ can also be demonstrated. By adding the first terms of S_1 and S_2 we have:

$$S_0^k + S_{0_d}^k = -m_0^{-1}\sigma_0 q_c(\delta_0^k u_0^k - \tau_0^k\dot{\delta}_0^k) < 0. \tag{4.38}$$

In fact, if $\sigma_0 q_c > 0$ for $t \geq t_s$ then $u_0^k = 1$ and $(\delta_0^k(1) - \tau_0^k\dot{\Delta}_0^k) > 0$ or equivalently $\dot{\Delta}_0^k < \delta_0^k\tau_0^k$ must be accomplished. In this case we get from (4.11) that:

$$\Delta_0^k = \delta_0^k(1 - e^{-(t-t_s)/\tau_0^k}); \qquad \dot{\Delta}_0^k = \frac{\delta_0^k}{\tau_0^k}e^{-(t-t_s)/\tau_0^k} \leq \frac{\delta_0^k}{\tau_0^k} \tag{4.39}$$

If $\sigma_0 q_c < 0$ that implies $u_0^k = -1$, then we obtain $\Delta_0^k \geq -\delta_0^k/\tau_0^k$. Therefore, the negativity of $S_o^k + S_{0_d}^k$ is ensured. In a similar way additions of terms in S_1 and S_2 are demonstrated to be negative and consequently $S_1 + S_2$ results to be negative for all $t \geq t_s$. Therefore, it is demonstrated that $S_1 + S_2$ keeps its negativity in spite of actuator dynamics.

Numerical Results

As an application example, a 10-story base isolated building structure is considered in the numerical simulation. The mass of each floor, including that of the base, is 6×10^5 kg. The stiffness of the base is $1.184 \times 10^7 N/m$ and its damping ratio is 0.1. The stiffness of the structure

varies in $5 \times 10^7 N/m$ between floors, from $9 \times 10^8 N/m$ the first one to $4.5 \times 10^8 N/m$ the top one with damping ratio 0.05. A frictional device is used for the base isolation, where the nonlinear force f_N is described by the next equation

$$f_N(q_c, \dot{q}_c, d, \dot{d}) = -sgn(\dot{q}_c - \dot{d})[\mu_{max} - \Delta\mu e^{-\nu|\dot{q}_c - \dot{d}|}]G \tag{4.40}$$

with $G = \sum_{i=1}^{10} m_i$, $\mu = 0.1$, $\nu = 2.0$, $\mu_{max} = 0.185$ and $\Delta\mu = 0.09$. In the simulation, the seismic excitation has been that of the El Centro (1940) earthquake as shown in Figure 3.

The semiactive device is used with $\tau_i^k = \tau_i^c = 1\,ms$, $\delta_0^k = 1.184 \times 10^7\,N/mV$, $\delta_0^c = 2.176 \times 10^5\,Ns/mV$, $\delta_1^c = 9.487 \times 10^5\,Ns/mV$, $\delta_1^k = 9.0 \times 10^8\,N/mV$, $P_{a_0}^c = P_{a_0}^k = 2.176 \times 10^4\,m^2$, $P_{a_1}^c = P_{a_1}^k = 9.487 \times 10^4\,m^2$.

Both passive case (pure base isolation) and hybrid case (base isolation plus semi-active control) are studied. The semiactive sliding mode control law in equation (4.37) is used with $\lambda_0 = 1.0$, $\lambda_1 = 3.0$, while the semiactive Lyapunov stability theory based control law in equations (4.17) and (4.51) is used with

$$\boldsymbol{P} = \begin{bmatrix} 116120000 & -194.07 & -103520000 & -194.07 \\ -194.07 & 0.69176 & 196.67 & 0.56275 \\ -103520000 & 196.67 & 104270000 & 194.12 \\ -194.07 & 562.75 & 194.12 & 0.56282 \end{bmatrix}$$

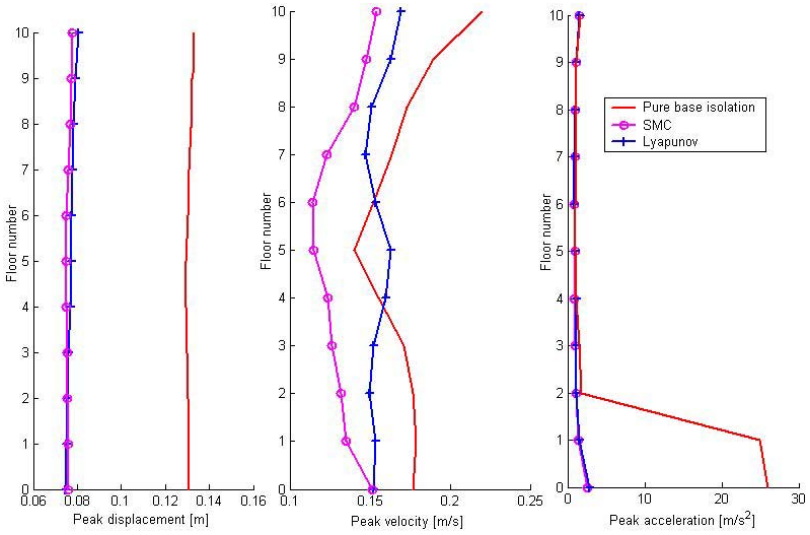

Figure 4.2: Absolute peak values a). Displacement, b). Velocity c). Acceleration

It is observed that semiactive controller reduces the peak response of absolute displacements of the base from a margin of $\pm 5.5cm$ (a reduction about 42.7%). and the 10th floor from a margin of $\pm 5cm$ (a reduction about 38.8%). See figures 4.3 and 4.4. It was also observed in the figure 4.2 that the semiactive controllers reduce the peak response of the base on a margin

of $\pm 5.6cm$ (43.08%) and of the others floors from 5.5 cm (42.31%) to $5.6cm$ (42.42%). The reduction of the peak inter-story displacement was from $5.65 \times 10^{-3}cm$ (3.6%) to 0.19 (45.65%). It was seen a reduction of the peak inter-story displacement in the upper floors, for example for the top floor is about $0.5597[m/s^2]$ (38.55%). The reduction of the peak velocity in the base is of $0.012m/s$ (6.85%) and for the floors is from $0.035m/s$ (29.12%) to $0.075m/s$ (32.85%). Both controllers perform well, however SMC controller is more effective than Lyapunov controller, in reducing velocity at the half level of the structure.

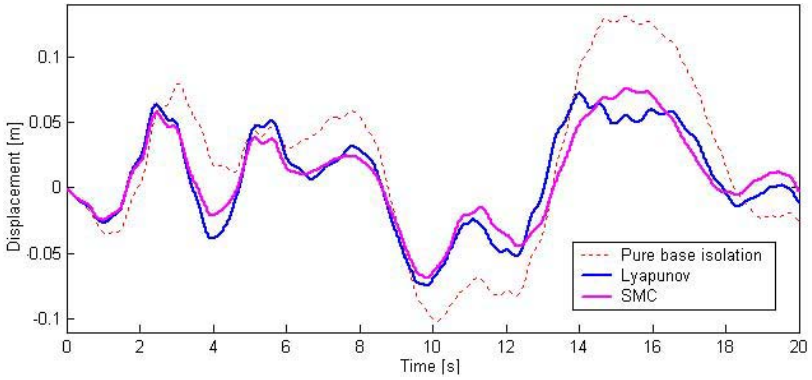

Figure 4.3: Absolute 1st floor displacement

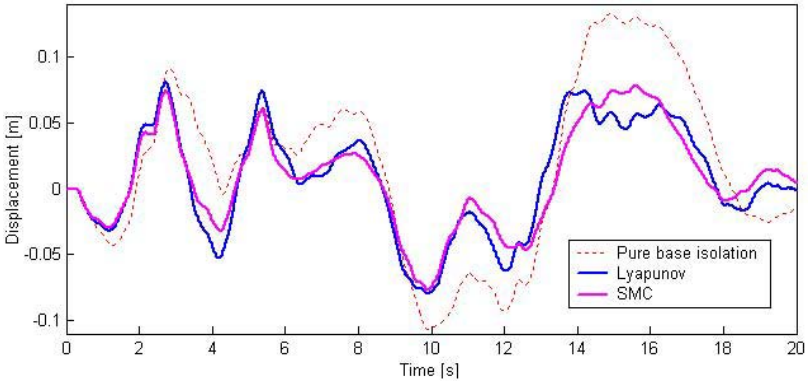

Figure 4.4: Absolute 10th floor displacement

4.1.2 Control Configuration 2

Consider the same nonlinear base isolated building structure of figure 4.1, but in this case only one MR damper is installed at the base in parallel with a nonlinear passive isolator. The dynamic behavior at the base level is expressed as:

$$m\ddot{y} + c\dot{y} + ky + f_{bf} = \Phi(\dot{y}, \dot{d}) + f_g + f_c \tag{4.41}$$

with

$$\Phi(\dot{y},\dot{d}) = -sgn(\dot{y}-\dot{d})[\mu_{max} - \Delta\mu e^{-\nu|\dot{y}-\dot{d}|}]Q \tag{4.42}$$

$$f_g = -c\dot{d} - kd \qquad and \qquad f_{bf} = c_{bf}(\dot{y}-\dot{y}_f) + k_{bf}(y-y_f) \tag{4.43}$$

where $y, y_f \in I\!R$ represent the horizontal displacements of the base and the first floor. A semiactive control force f_c is applied by means of a MR damper.

The hysteretic behavior of the MR damper is described by using the so-called Bouc-Wen model. The MR damper force is represented by a linear part related to the transversal velocity $\dot{x}$ plus a nonlinear part related to a nonlinear and nonphysical variable z, given by:

$$f = f_l + f_{nl} = -\delta\dot{y} - \alpha z \tag{4.44}$$

where δ is a damping parameter and α is a positive value that relates the hysteretic behavior of the MR damper force to the evolutionary variable z. z is governed by

$$\dot{z} = -\gamma|\dot{x}|z|z|^{n-1} - \beta\dot{x}|z|^n + A\dot{x} \tag{4.45}$$

where the parameters γ, β, n and A are of constant values and are previously adjusted by using parameter identification in order to control the linearity under the unloading condition and to obtain the smoothness of the transition from the pre-yielded to the post-yielded region.

For control purposes, the parameters δ and α are made to be dependent on the commanding voltage signal v, according to what have been proposed by [21, 107]

$$\alpha = \alpha(v) = \alpha_a + \alpha_b v \qquad and \qquad \delta = \delta(v) = \delta_a + \delta_b v \tag{4.46}$$

The following assumptions complete the description of semi-actively controlled base isolated structure.

Assumption 1. The displacements and velocities of the base and the first floor are measurable.

Assumption 2. The unknown seismic excitation $d(t)$ and $\dot{d}(t)$ are bounded by $|d(t)| \leq D_d$ and $|\dot{d}(t)| \leq D_v$ for all $t \geq 0$ where D_d and D_v are known positive constants.Under this assumption, it is easy to verify that the unknown disturbance force $f_g(t)$ is bounded by $|f_g(t)| \leq F$ for all $t \geq 0$, with F being some known positive constant.

Controller Design

For the present configuration, a controller based on the Backstepping technique is designed. The control objective is to design a backstepping controller such that the closed-loop system is globally stable and consequently the structural vibration is attenuated.

First, rewrite the dynamic equation (4.41) into the following state equation:

$$\dot{y}_1 = y_2 \tag{4.47}$$

$$\dot{y}_2 = -\frac{1}{m}\left[cy_2 + ky_1 + f_{bf}(y_1, y_2, \dot{y}_f, y_f) - \Phi(y_2,\dot{d}) - f_g(d,\dot{d}) - f_c(y_2, z, v)\right] \tag{4.48}$$

where $y_1 =: y$ and $y_2 =: \dot{y}$.

The following standard variables, typically adopted in the literatures of backstepping control, are used for controller design:

$$\begin{array}{lll} e_1 = y_1; & \dot{e}_1 = y_2; & e_1\dot{e}_1 = e_1y_2; \\ \alpha_1 = -h_1e_1; & \dot{\alpha}_1 = -h_1y_2; & \\ e_2 = y_2 - \alpha_1; & \dot{e}_2 = \dot{y}_2 + h_1y_2; & e_2\dot{e}_2 = e_2(\dot{y}_2 + h_1y_2); \end{array} \tag{4.49}$$

By using equations (4.47) to (4.49), it is obtained:

$$e_2\dot{e}_2 = -\frac{e_2}{m}\left[cy_2 + ky_1 + f_{bf} - \Phi - f_g + \alpha_a z + \delta_a y_2 + (\alpha_b z + \delta_b y_2)v - mh_1 y_2\right] \tag{4.50}$$

In order to achieve the asymptotic error suppression, the following control law is derived for giving the commanding voltage signal to the MR damper:

$$v = \frac{-(c + \delta_a - mh_1)y_2 - ky_1 - f_{bf} + \Phi + f_g - \alpha_a z + me_1 + h_2 e_2}{\alpha_b z + \delta_b y_2} \tag{4.51}$$

However, since Φ, f_g and z contain unmeasurable variables, the control law (4.51) is not implementable in practice. In order to overcome the measurement limitation problem, some approximation and estimation are made below.

Approximation and bounding of the restoring force Φ

The objective of making the approximation of the restoring force is to find a linear part of Φ associated with measurable variables so as to reduce the computing effort. When a base isolator is well tuned for incoming seismic excitation, very small relative movement is achieved such that $\nu|y_2 - \dot{d}| < 1$ during a time period T_0. This fact can be verified for some standard (El Centro, Taft) earthquake records as shown in Figure 1. In this case, Euler approximation approach can be employed in the following way:

$$e^{-\nu|y_2-\dot{d}|} \simeq \frac{1}{1 + \nu|y_2 - \dot{d}| + \frac{\nu^2}{2}|y_2 - \dot{d}|^2 + \frac{\nu^3}{6}|y_2 - \dot{d}|^3} \tag{4.52}$$

Thus, the approximated restoring force $\bar{\Phi}$ is obtained

$$\bar{\Phi} \;=\; -sgn(y_2 - \dot{d})\left[\mu_{max} - \Delta\mu\left(\frac{1}{1 + \nu|y_2 - \dot{d}| + \frac{\nu^2}{2}|y_2 - \dot{d}|^2 + \frac{\nu^3}{6}|y_2 - \dot{d}|^3}\right)\right] Q \tag{4.53}$$

Denote $|y_2 - \dot{d}|_0$ as the maximum value of $|y_2 - \dot{d}|$. It is known from equation (4.42) that the maximum restoring force, $\bar{\Phi}_{max}$ is obtained with $|y_2 - \dot{d}|_0$. By replacing this value in equation (4.53), the next consideration can be made:

$$\bar{\Phi} \;\leq\; \Delta_0 + \Delta_1 D_v - \Delta_1 y_2 \tag{4.54}$$

where

$$\Delta_0 = \left(\frac{\mu_{max} - \Delta\mu}{1 + \nu|y_2 - \dot{d}|_0 + \frac{\nu^2}{2}|y_2 - \dot{d}|_0^2 + \frac{\nu^3}{6}|y_2 - \dot{d}|_0^3}\right) Q \tag{4.55}$$

$$\Delta_1 = \left(\frac{\mu_{max}\left[\nu + \frac{\nu^2}{2}|y_2 - \dot{d}|_0 + \frac{\nu^3}{6}|y_2 - \dot{d}|_0^2\right]}{1 + \nu|y_2 - \dot{d}|_0 + \frac{\nu^2}{2}|y_2 - \dot{d}|_0^2 + \frac{\nu^3}{6}|y_2 - \dot{d}|_0^3}\right) Q \tag{4.56}$$

by taking into account the result of base isolation $\left|y_2 - \dot{d}\right|_0 < \frac{1}{\nu}$.

Estimation of the evolutionary variable $\mathbf{z}$

Since the variable z cannot be directly measured, an estimated value $\hat{z}$ is obtained:

$$\dot{\hat{z}} = -\gamma|y_2|\hat{z}|\hat{z}|^{n-1} - \beta y_2|\hat{z}|^n + Ay_2 \tag{4.57}$$

Define $\tilde{z} = z - \hat{z}$ as the estimation error between the real value z and the estimated value $\hat{z}$, then

$$z = \tilde{z} + \hat{z}; \qquad \dot{\tilde{z}} = \dot{z} - \dot{\hat{z}} \tag{4.58}$$

By taking $\tilde{z} = e_2$, the denominator of the commanding voltage signal v can be replaced by $\delta_b y_2 + \alpha_b \hat{z} + \alpha_b \tilde{z} = \delta_b y_2 + \alpha_b \hat{z} + \alpha_b e_2$.

Now, an implementable law, based upon the bounded values of f_g and Φ and the estimated value of z, is adopted for the backstepping control:

$$v = \frac{-(c + \Delta_1 + \delta_a - mh_1)y_2 - ky_1 - f_{bf} + (\Delta_0 + \Delta_1 D_v + F)sgn(e_2) - \alpha_a \hat{z} + me_1}{\alpha_b \hat{z} + \delta_b y_2 + \alpha_b e_2} \tag{4.59}$$

for all $\alpha_b \hat{z} + \delta_b x_2 + \alpha_b e_2 \neq 0$ and otherwise $v = 0$. Moreover, for some types of MR dampers (Spencer et al, 1997; Yi et al, 1998), the constraints $\gamma \geq |\beta| \geq 0$ and $n = 1$ must be satisfied by the control law.

Stability Analysis

In order to verify the closed-loop stability, the following Lyapunov function candidate is defined:

$$V = \frac{1}{2}e_1^2 + \frac{1}{2}e_2^2 + \frac{1}{2}\tilde{z}^2 \tag{4.60}$$

$$\dot{V} = e_1\dot{e}_1 + e_2\dot{e}_2 + \tilde{z}\dot{\tilde{z}} \tag{4.61}$$

From equations (4.49), (4.50) and (4.59), one obtains:

$$e_1\dot{e}_1 = e_1 y_2 \tag{4.62}$$

$$\begin{aligned} e_2\dot{e}_2 &= -\frac{e_2}{m}\left[-\Phi - \Delta_1 y_2 - f_g + \alpha_a \tilde{z} + (\Delta_0 + \Delta_1 D_v + F)sgn(e_2) + me_1\right] \\ &= -\frac{1}{m}[(\Delta_0 + \Delta_1 D_v)|e_2| - (\Phi + \Delta_1 y_2)e_2 + F|e_2| - f_g e_2] - e_1 e_2 - h_2 e_2^2 \end{aligned} \tag{4.63}$$

with $h_2 = \dfrac{\alpha_a}{m}$.

From equations (5.19) and (5.20), one gets:

$$\tilde{z}\dot{\tilde{z}} = \tilde{z}(\dot{z} - \dot{\hat{z}}) = -\tilde{z}\left[\gamma\,|y_2|\,(z\,|z|^{n-1} - \hat{z}\,|\hat{z}|^{n-1}) - \beta y_2(\,|z|^n - |\hat{z}|^n)\right] \tag{4.64}$$

For $n = 1$,

$$\tilde{z}\dot{\tilde{z}} = -\gamma\,|y_2|\,\tilde{z}^2 - \beta y_2 \tilde{z}\,(\,|z| - |\hat{z}|\,) \leq -(\,\gamma - |\beta|\,)\,|y_2|\,\tilde{z}^2 \leq 0 \tag{4.65}$$

Finally, the derivative Lyapunov function becomes:

$$\begin{aligned} \dot{V} &= e_1\dot{e}_1 + e_2\dot{e}_2 + \tilde{z}\dot{\tilde{z}} \\ &= -\frac{1}{m}[(\bar{\Phi} + \Delta_1 y_2)|e_2| - (\Phi + \Delta_1 y_2)e_2 + F|e_2| - f_g e_2] - h_1 e_1^2 - h_2 e_2^2 - (\,\gamma - |\beta|\,)\,|y_2|\,\tilde{z}^2 \;\leq\; 0 \end{aligned}$$

Therefore, stability of the closed-loop system is ensured.

Numerical Results

From equation (4.59) the following control law is employed:

$$v = \frac{-(c+\delta_a+\Delta_1-mh_1)y_2 - ky_1 - f_{bf} + (\Delta_0+\Delta_1 D_v+F)sgn(e_2) - \alpha_a\hat{z} + me_1}{\alpha_b\hat{z}+\delta_b y_2+\alpha_b e_2} \tag{4.66}$$

with $\gamma=\beta=3\times10^2\,m^{-1}$, $A=120$, $\alpha_a=4.5\times10^4$, $\alpha_b=3.6\times10^4$, $\delta_a=3\times10^2\,kNs/m$, $\delta_b=1.8\times10^2\,kNs/m$, $\Delta_0=2.87\times10^2\,kN$, $\Delta_1=1.63\times10^3\,kNs/m$, $D_v=0.32$, $F=1.45\times10^3\,kN$, $h_1=1.5$ and $h_2=86.3$.

Both passive (pure base isolation) and hybrid case (base isolation plus semiactive control) are studied in the presence of the Taft earthquake. From figure 4.5 it is seen that by using the backstepping controller, peak vibrations are more reduced than with the MR damper in *on* state (passive on). It is also seen that the absolute displacement of the base has been significant reduced by using the semiactive controller such that the base isolator can work safely within its elastic region and the structural acceleration has been kept small so that the human comfort is guaranteed. On other hand figure 4.8(a) gives the control force supplied by the MR damper during the seismic excitation, while figure 4.8(b) shows the hysteretic behavior of MR damper.

A semiactive backstepping control scheme has been proposed for the vibration attenuation of civil engineering structures. In the control design, frictional nonlinearity of the base isolator and hysteretic dynamics of the semiactive MR damper have been taken into account. In this way, the control system has a better performance in real operation conditions. The peak response of the absolute movements of the base and main structure has been significantly reduced by using the hybrid control scheme as compared with the purely passive controlled case.

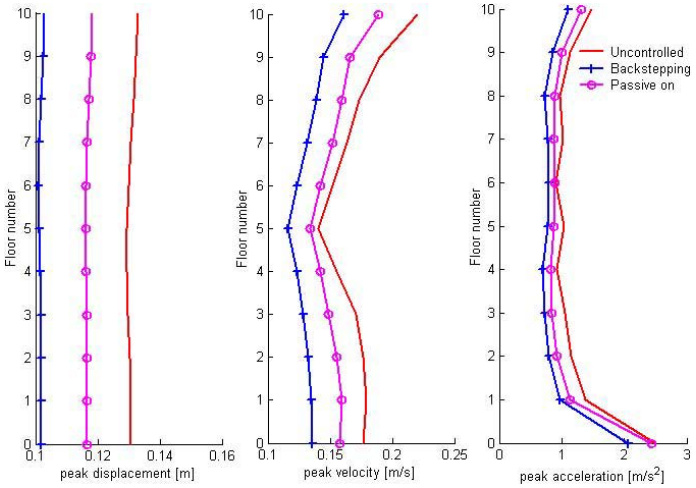

Figure 4.5: Peak Vibrations Profiles a). Displacement b). Velocity c).Acceleration

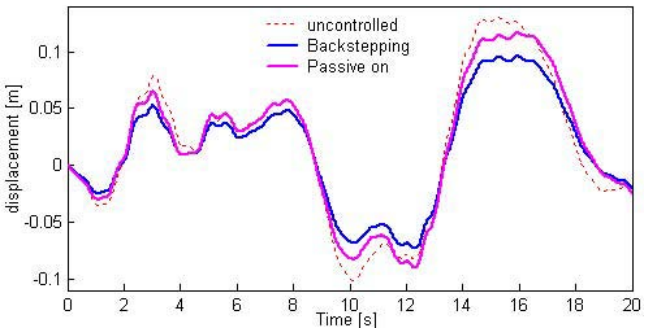

Figure 4.6: Absolute displacement of the 1st floor

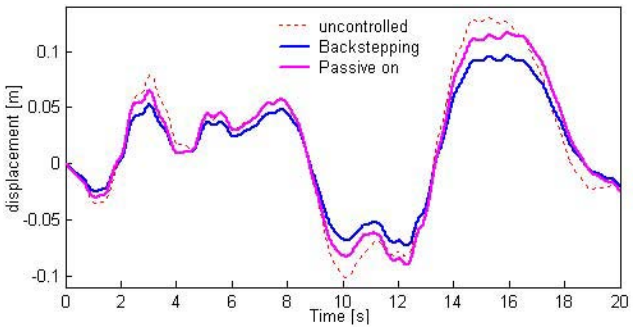

Figure 4.7: Absolute displacement of the 10th floor

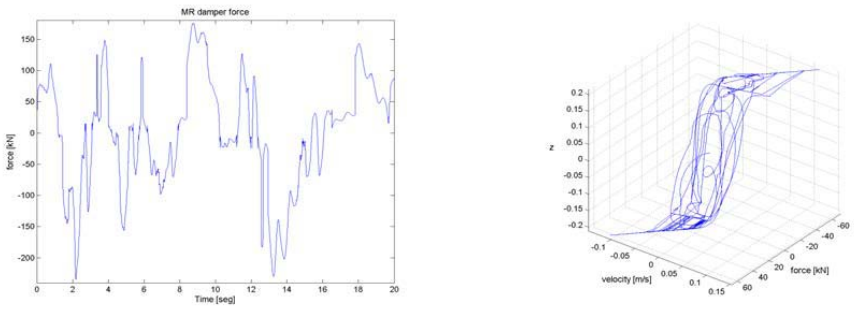

(a) Force (b) Hysteretic behaviour

Figure 4.8: MR damper dynamics

4.1.3 Control Configuration 3

Consider the same 10-story base isolated building of figure 4.1, but now actively controlled at the base level. The main purpose of using an active controller is to reduce the peak response of the absolute base displacement and to attenuate the dependence of structural performance on the resonance frequency of the base isolator.

QFT Controller Design

The QFT controller design is made by doing the next considerations. i) The stiffness at the base is an uncertain parameter and its value varies between [0.97 1.03]*k_{0_N}, where k_{0_N} is the nominal value of k_0. Consequently, c_0 is also uncertain and takes the value of $c_0 = 2\xi\sqrt{k_0 m}$. ii). The earthquake acceleration is considered as uncertain but bounded; i.e., $|f(t)| \leq F$ for all $t \geq 0$. iii). Only local measurements of displacement and velocity are available, which contain a noise percentage of 5%. The design conditions for the QFT controller are: i) The displacement at the base be less than 0.03 m for the uncertain but bounded disturbance and ii) The displacement be less than 0.01 m for a measurement with 5% of white noise. For design purposes the motion equation of the base is represented in the following Laplace form:

$$q_c(s) = \frac{1}{m_0 s^2 + c_0 s + k_0}\left[-(sc_1 + k_1)(q_c(s) - q_{r_1}(s)) + f(s) - u(s)\right] \tag{4.67}$$

Since the relative movement between the base and the first floor is very small with respect to the absolute movement of the base, the term is neglected to simplify the design procedure. According to the LTI structure presented in figure 3.9, the plant is described by:

$$P(s) = \frac{1}{m_0 s^2 + c_0 s + k_0} \tag{4.68}$$

The problem is reduced to design a QFT controller G for a SISO LTI system, in the presence of uncertain parameters k_0 and c_0 in the plant, disturbance f at the input of the plant and noise N in the measurement. Then, the equation of the system in close loop is expressed as:

$$q_r = \frac{P}{1+PG} f - \frac{PG}{1+PG} N \tag{4.69}$$

And the frequencial specifications are formulated as:

$$\underbrace{\left|\frac{P}{1+PG}\right| = \left|\frac{q_r(j\omega)}{f(j\omega)}\right| \leq W_{s_3}}_{\textit{Disturbance Rejection}} \quad \underbrace{\left|\frac{PG}{1+PG}\right| = \left|\frac{q_r(j\omega)}{N(j\omega)}\right| \leq W_{s_1}}_{\textit{Robust Stability}} \tag{4.70}$$

The mass of each floor, including that of the base m_0, is 6×10^5 kg. The stiffness of the base is 1.184×10^7 N/m and its damping ratio is 0.1. The stiffness of the structure varies in 5×10^7 N/m between floors, from 9×10^8 N/m the first one to 4.5×10^8 N/m the top one with damping ratio 0.05. In the simulation, the seismic excitation has been that of the El Centro (1940) earthquake. For the QFT design the bounds are $W_{s_1} = 4$ and $W_{s_3} = 3.4 \times 10^{-3}$ for all the working frequencies. Concretely, the frequencies studied are [1.31 5.49 9.55 15.21 18.56 24.74 27.23 33.63 37.04 41.63 43.84] (rad/s), where resonance frequencies of the structure are included. QFT controller design is done by using the MATLAB QFT toolbox. For the Loop Shaping step the final loop for L_N obtained on the Nichols chart is that shown in figure 4.9(a), while figure 4.9(b) presents the frequency analysis for the specification W_{s_1}. The transfer function G for the controller resulting from L_N is:

$$G(s) = 0.0882\frac{1467s^2 + 636.84s + 1}{0.0352s^2 + 2.167s + 1} \tag{4.71}$$

El Centro earthquake acceleration was applied to validate the QFT controller. Figure 4.10 shows that the absolute displacement, velocity and acceleration have been attenuated at the base and all floors, with respect to the purely passive case.

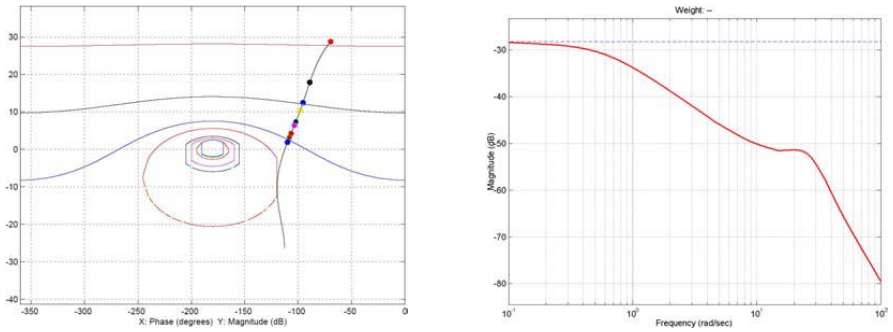

(a) Final loop L_N (b) Analysis of W_{s_1}

Figure 4.9: QFT controller design

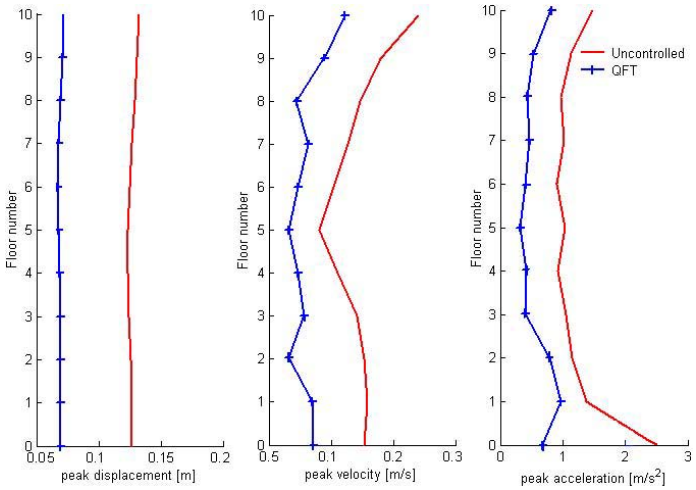

Figure 4.10: Absolute peak values profiles of a). displacement b). Velocity c). Acceleration

4.2 Structural System B: Structure Uncertainly Excited by Temporary Coupling

Consider the problem of active control of an elastically suspended bridge with crossing vehicles as shown in Figure 4.11. The bridge section consists of a rigid platform with elastic mounts on the left-hand and right-hand sides. The main variables to be measured are the vertical deviation z of the center of mass of the bridge and the inclination Θ with respect to the horizon of the bridge platform. Vibration of the bridge is produced when a truck crosses the bridge with velocity $v(t)$ within a time interval $[t_0, t_f]$. Without the loss of generality, t_0 is set to zero

and t_f denotes the final time of interaction between the structure and the truck. The truck is modelled by a mass m with an elastic suspension of damping c and stiffness k. Additional variables ξ, η and ζ are chosen according to Figure 4.11. The mass of the platform is given by M, and the moment of inertia with respect to C by the parameter J. The active control is implemented by two actuators located between the ground and the bridge at the left and the right ends respectively. The actuators A_1 and A_2 supply vertical control forces Mu_1 and Mu_2 which complement the resistant passive forces F_1 and F_2 given by the elastic supports. u_1 and u_2 are the control variables. The objective is to attenuate the vibration of the bridge induced by the crossing vehicle by using active forces Mu_1 and Mu_2.

When the truck is not in the bridge (for $t < 0$ and $t > t_f$), the equation of motion of the truck is $m\,\ddot{\eta} = k\,\eta_0 - m\,g$, where η_0 is the position of relaxed suspension. When $t \in [0, t_f]$, the truck is crossing the bridge. Assume that the declination angle Θ is small, then the dynamic motion of the truck is described by the following equation

$$\left\{\begin{array}{lcl} m\ddot{\eta} & = & F - mg \\ F: & = & k[\eta_0 - (\eta + \zeta)] - c(\dot{\eta} + \dot{\zeta}) \\ \zeta: & = & z + (\xi - a)\Theta \end{array}\right. \tag{4.72}$$

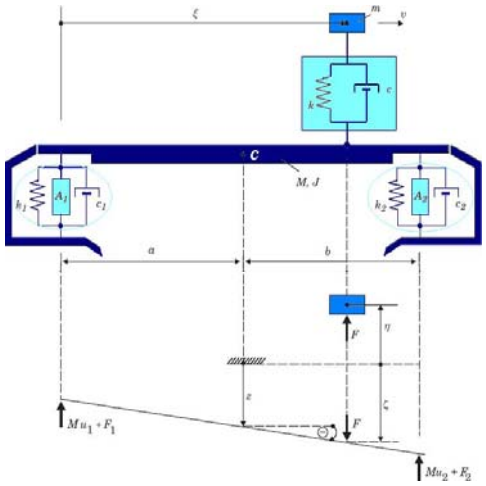

Figure 4.11: Actively controlled bridge platform with crossing vehicle

For $t < 0$ the bridge is in a steady state. For $t \in [0, t_f]$, the dynamic behavior of the bridge is described by the following equations of motion:

$$\left\{\begin{array}{rcl} M\ddot{z} & := & M\,g + F - F_1 - F_2 - Mu_1 - Mu_2 \\ J\ddot{\Theta} & := & (\xi - a)F + aF_1 - bF_2 + aMu_1 - bMu_2 \\ F & := & k[\eta_0 - (\eta + \zeta)] - c(\dot{\eta} + \dot{\zeta}) \\ F_1 & := & k_1(-z_{1,0} + z - a\Theta) + c_1(\dot{z} - a\dot{\Theta}) \\ F_2 & := & k_2(-z_{2,0} + z + b\Theta) + c_2(\dot{z} + b\dot{\Theta}) \end{array}\right. \tag{4.73}$$

where $z_{1,0}$ and $z_{2,0}$ represent the vertical positions of relaxed left-hand and right-hand suspension, respectively.

We consider the bridge as the main system and the truck as the attached uncertain subsystem. The space state variables are split into the measurable ones, $\mathbf{x} := (z, \Theta, \dot{z}, \dot{\Theta})^T$, and the unmeasurable ones $\mathbf{y} := (\eta, \dot{\eta})^T$. $\mathbf{u} := (u_1, u_2)^T$ are control signals. The uncertain coupling between the bridge and the truck is due to the scalar force F. When the truck has left the bridge for $t > t_f$, the two systems are obviously decoupled with $F = 0$ and then the equations of motion of the bridge are

$$\left\{ \begin{array}{rcl} M\,\ddot{z} & = & M\,g - F_1 - F_2 - Mu_1 - Mu_2, \\ J\,\ddot{\Theta} & = & aF_1 - bF_2 + aMu_1 - bMu_2. \end{array} \right. \tag{4.74}$$

In the above models, consider that the structural parameters of the bridge (M, J, c_1, c_2, k_1, k_2) are known, while the parameters related to the truck (m, c, k, η_0, ξ, v) are assumed to be uncertain but bounded; i.e.,

$$\begin{array}{llll} \dfrac{k}{m} = \omega_0 + \Delta\omega \quad \text{with} \quad |\Delta\omega| \le \bar{\omega} & \dfrac{c}{m} = \sigma_0 + \Delta\sigma \quad \text{with} \quad |\Delta\sigma| \le \bar{\sigma} & |v(t)| \le \bar{v} \\ \dfrac{k}{M} = \Omega \quad \text{with} \quad \Omega \le \bar{\Omega} & \dfrac{c}{M} = \Upsilon \quad \text{with} \Upsilon \le \bar{\Upsilon} & |\eta_0| \le \bar{\eta}_0 \end{array}$$

where ω_0 and σ_0 are known nominal values and $\bar{\omega}$, $\bar{\sigma}$, $\bar{\Omega}$, $\bar{\Upsilon}$, $\bar{\eta}_0$ and $\bar{v}$ are known bounds. Finally the equations of motion (4.72) and (4.73) can be rewritten into the following form:

$$\left\{ \begin{array}{rcl} \dot{\mathbf{x}} & = & \mathbf{A_c}\mathbf{x} + \mathbf{B}\mathbf{u} + \mathbf{g}(\mathbf{x}, \mathbf{y}, t), \\ \dot{\mathbf{y}} & = & \mathbf{A_r}\mathbf{y} + \mathbf{f}(\mathbf{x}, \mathbf{y}, t) \end{array} \right. \tag{4.75}$$

where the parameters of the matrices $\mathbf{A_c}$, $\mathbf{B}$ and $\mathbf{A_r}$ are known. The functions $\mathbf{g}$ and $\mathbf{f}$ include the uncertain coupling effects.

$$\mathbf{A_c} = \begin{pmatrix} 0 & 0 & 1 & 0 \\ 0 & 0 & 0 & 1 \\ -\dfrac{k_1 + k_2}{M} & \dfrac{ak_1 - bk_2}{M} & -\dfrac{c_1 + c_2}{M} & \dfrac{ac_1 - bc_2}{M} \\ \dfrac{ak_1 - bk_2}{J} & -\dfrac{a^2k_1 + b^2k_2}{J} & \dfrac{ac_1 - bc_2}{J} & -\dfrac{a^2c_1 + b^2c_2}{J} \end{pmatrix} \tag{4.76}$$

$$\mathbf{B} = \begin{pmatrix} 0 & 0 \\ 0 & 0 \\ -1 & -1 \\ \dfrac{aM}{J} & -\dfrac{bM}{J} \end{pmatrix}, \quad \text{and} \quad \mathbf{g} = \begin{pmatrix} 0 \\ 0 \\ g_3 \\ g_4 \end{pmatrix} \tag{4.77}$$

Here for $t \in [0, t_f]$:

$$\begin{array}{rcl} g_3(\mathbf{x}, \mathbf{y}, t) & := & -\dfrac{k}{M}z - \dfrac{1}{M}[k(\xi(t) - a) + cv]\Theta - \dfrac{c}{M}\dot{z} - \dfrac{c}{M}(\xi(t) - a)\dot{\Theta} - \dfrac{k}{M}\eta - \dfrac{c}{M}\dot{\eta} + \dfrac{k}{M}\eta_0 \\ & & + \dfrac{k_1}{M}z_{1,0} + \dfrac{k_2}{M}z_{2,0} + g \end{array} \tag{4.78}$$

$$\begin{array}{rcl} g_4(\mathbf{x}, \mathbf{y}, t) & := & -\dfrac{k}{J}(\xi(t) - a)z - \dfrac{1}{J}[k(\xi(t) - a)^2 + cv(\xi(t) - a)]\Theta - \dfrac{c}{J}(\xi(t) - a)\dot{z} - \dfrac{c}{J}(\xi(t) - a)^2\dot{\Theta} \\ & & - \dfrac{k}{J}(\xi(t) - a)\eta - \dfrac{c}{J}(\xi(t) - a)\dot{\eta} + \dfrac{k}{J}(\xi(t) - a)\eta_0 - \dfrac{ak_1}{J}z_{1,0} + \dfrac{bk_2}{J}z_{2,0} \end{array} \tag{4.79}$$

while, for $t > t_f$,

$$g_3 := \frac{k_1}{M}z_{1,0} + \frac{k_2}{M}z_{2,0} + g \quad g_4 := -\frac{ak_1}{J}z_{1,0} + \frac{bk_2}{J}z_{2,0} \tag{4.80}$$

$$\mathbf{A_r} := \begin{pmatrix} 0 & 1 \\ -\omega_0 & -\sigma_0 \end{pmatrix} \quad \mathbf{f}(\mathbf{x},\mathbf{y},t) := \begin{pmatrix} 0 \\ \mathbf{f}_2 \end{pmatrix} \tag{4.81}$$

For $t \in [0, t_f]$,

$$\mathbf{f}_2 = -\frac{k}{m}z - \frac{1}{m}[k(\xi(t)-a)+cv]\Theta - \frac{c}{m}\dot{z} - \frac{c}{m}(\xi(t)-a)\dot{\Theta} - \Delta\omega\eta - \Delta\sigma\dot{\eta} + \frac{k}{m}\eta_0 - g \tag{4.82}$$

and for $t > t_f$,

$$\mathbf{f}_2 = -\Delta\omega\eta - \Delta\sigma\dot{\eta} + \frac{k}{m}\eta_0 - g \tag{4.83}$$

Denote $\mathbf{e} = (e_1, e_2)^T$

$$e_i(\mathbf{x},\mathbf{y},t) = e_{i,1}(t)z + e_{i,2}(t)\Theta + e_{i,3}(t)\dot{z} + e_{i,4}(t)\dot{\Theta} + e_{i,5}(t)\eta + e_{i,6}(t)\dot{\eta} + e_{i,7}(t) \tag{4.84}$$

Now, it can be verified that $\mathbf{A_c}$ and $\mathbf{A_r}$ are stable matrices and the function $\mathbf{e}(\mathbf{x},\mathbf{y},\cdot)$ is continuous for all t except a set $\{0, t_f\}$ and there exist known non-negative scalars α_i^c, α_i^r, δ_i, such that, for all $\mathbf{x},\mathbf{y}$ and t, one has

$$\mathbf{g} \;=\; [\,\mathbf{B}_1\,,\,\mathbf{B}_2\,]\,[\,\mathbf{e}_1\,,\,\mathbf{e}_2\,]^T \tag{4.85}$$

where

$$\mathbf{B}_1 = \begin{pmatrix} 0 \\ 0 \\ -1 \\ \dfrac{aM}{J} \end{pmatrix}, \quad \mathbf{B}_2 = \begin{pmatrix} 0 \\ 0 \\ -1 \\ -\dfrac{bM}{J} \end{pmatrix} \tag{4.86}$$

and

$$\|\mathbf{e}_i(\mathbf{x},\mathbf{y},t)\| \;\leq\; \alpha_i^c\|\mathbf{x}\| + \alpha_i^r\|\mathbf{y}\| + \delta_i \tag{4.87}$$

with

$$\alpha_i^c = \sqrt{\alpha_1^2+\alpha_2^2+\alpha_3^2+\alpha_4^2} \qquad \alpha_i^r = \sqrt{\alpha_5^2+\alpha_6^2} \qquad \delta_i = \alpha_7 \tag{4.88}$$

where

$$\alpha_1 = \bar{\Omega} \qquad \alpha_3 = \bar{\Upsilon} \qquad \alpha_5 = \bar{\Omega} \qquad \alpha_6 = \bar{\Upsilon}$$

$$\alpha_2 = \begin{cases} \dfrac{1}{(a+b)}\left(\bar{\Omega}a^2 + (a\bar{\Omega} + \bar{\Upsilon}\bar{v})a + a\bar{\Upsilon}\bar{v}\right), & \text{if } a \geq b \\ \dfrac{1}{(a+b)}\left(\bar{\Omega}b^2 + (b\bar{\Omega} + \bar{\Upsilon}\bar{v})b + b\bar{\Upsilon}\bar{v}\right), & \text{if } a < b \end{cases} \qquad \alpha_4 = \begin{cases} \dfrac{2a^2}{(a+b)}\bar{\Upsilon}, & \text{if } a \geq b \\ \dfrac{2b^2}{(a+b)}\bar{\Upsilon}, & \text{if } a < b \end{cases}$$

$$\alpha_7 = \max\left\{\frac{1}{(a+b)}\left[\bar{\Omega}(a+b)\bar{\eta}_0 + \frac{(a+b)k_1z_{1,0}+g}{M}\right], \frac{1}{(a+b)}\left[\bar{\Omega}(a+b)\bar{\eta}_0 + \frac{(a+b)k_2z_{2,0}+ag}{M}\right]\right\}$$

Indeed, solving the linear system $\mathbf{g} = \mathbf{B}\,\mathbf{e}$, it is easy to get that $\mathbf{e} = (e_1, e_2)^T$, where

$$e_1 = \frac{-bMg_{c,3} + Jg_{c,4}}{(a+b)M} \quad ; \quad e_2 = -\frac{aMg_{c,3} + Jg_{c,4}}{(a+b)M} \tag{4.89}$$

4.2.1 Controller Design

The objective of active control is to attenuate the vibration of the bridge induced by a crossing truck through the uncertain coupling between the dynamics of the bridge and the truck. The controller design should only consider the feedback information of the bridge, while that of the truck is considered unknown. By taking into account this control challenge, two active controllers are designed, the first one is based on the Lyapunov stability theory, while the second on the Sliding Mode Control theory.

Controller 1

Define a candidate Lyapunov function:

$$V(\boldsymbol{x}) \quad = \quad \frac{1}{2}\boldsymbol{x}^T(t)\boldsymbol{P}\boldsymbol{x}(t) \tag{4.90}$$

By using equation (4.75), the derivative of V($\boldsymbol{x}$) is obtained

$$\dot{V}(\boldsymbol{x}) \quad = \quad \boldsymbol{x}^T\boldsymbol{P}\boldsymbol{B}_1u_1 + \boldsymbol{x}^T\boldsymbol{P}\boldsymbol{B}_2u_2 + \boldsymbol{x}^T\boldsymbol{P}\boldsymbol{B}_1e_1 + \boldsymbol{x}^T\boldsymbol{P}\boldsymbol{B}_2e_2 - \frac{1}{2}\boldsymbol{x}^T\boldsymbol{Q}\boldsymbol{x} \leq H(\boldsymbol{x},\boldsymbol{u}) + H(\boldsymbol{y}) \tag{4.91}$$

where

$$H(\boldsymbol{y}) \quad =: \quad (\alpha_1^r||\boldsymbol{x}^T\boldsymbol{P}\boldsymbol{B}_1|| + \alpha_2^r||\boldsymbol{x}^T\boldsymbol{P}\boldsymbol{B}_2||)\cdot||\boldsymbol{y}|| \tag{4.92}$$

and

$$H(\boldsymbol{x},\boldsymbol{u}) \quad =: \quad H_1(\boldsymbol{x},\boldsymbol{u}_1) + H_2(\boldsymbol{x},\boldsymbol{u}_2) - \frac{1}{2}\boldsymbol{x}^T\boldsymbol{Q}\boldsymbol{x} \tag{4.93}$$

where

$$H_i(\boldsymbol{x},\boldsymbol{u}_i) \quad = \quad \delta_i||\boldsymbol{x}^T\boldsymbol{P}\boldsymbol{B}_i|| + \alpha_i^c||\boldsymbol{x}^T\boldsymbol{P}\boldsymbol{B}_i||\cdot||\boldsymbol{x}|| + \boldsymbol{x}^T\boldsymbol{P}\boldsymbol{B}_iu_i \tag{4.94}$$

Since the state variable $\boldsymbol{y}(t)$ of the coupled uncertain subsystem (the truck) is usually not measurable, the objective of control is to minimize the $\dot{V}(\boldsymbol{x})$ by making the $H(\boldsymbol{x},\boldsymbol{u}) < 0$. Denote $\boldsymbol{u}_i^d(t)$ as the "desired" control signal (without taking into account the actuator dynamics). Then the following "desired " control law will be used to minimize the equation (4.94):

$$\boldsymbol{u}_i^d = -\boldsymbol{k}_i^c\boldsymbol{x} - (\delta_i + \alpha_i^c||\boldsymbol{x}||)sgn(\boldsymbol{x}^T\boldsymbol{P}\boldsymbol{B}_i) \quad ; \quad \boldsymbol{k}_i^c \quad = \quad \frac{1}{4}\boldsymbol{B}_i^T\boldsymbol{P} \tag{4.95}$$

It is easy to verify that $H(\boldsymbol{x},\boldsymbol{u}) < 0$ is accomplished. In practice, the continuous approximation is used for the control law (4.115) to attenuate the high-frequency chattering

$$sgn(\cdot) \Longrightarrow \frac{(\cdot)}{|(\cdot)| + \gamma} \tag{4.96}$$

where $0 < \gamma < 1$. Thus, the corresponding continuous "desired" control law is

$$\boldsymbol{u}_i^d \quad = \quad -\boldsymbol{k}_i^c\boldsymbol{x} - (\delta_i + \alpha_i^c||\boldsymbol{x}||)\frac{\boldsymbol{x}^T\boldsymbol{P}\boldsymbol{B}_i}{|\boldsymbol{x}^T\boldsymbol{P}\boldsymbol{B}_i| + \gamma_i} \tag{4.97}$$

Now, assume that a hydraulic actuator is used for the implementation of the control action generated by the "desired" controllers (4.115) or (4.117). The dynamic behavior of the hydraulic actuator is described by the following equation ([33]):

$$v_i(t) \quad = \quad P_{v_i}\dot{u}_i(t) + P_{l_i}u_i(t) + P_{a_i}\dot{z}(t), \quad i = 1,2 \tag{4.98}$$

where

$$P_{v_i} = \frac{C_{v_i}}{4\beta_i P_{a_i}}, \qquad P_{l_i} = \frac{C_{l_i}}{P_{a_i}}, \qquad P_{a_i} > 0 \tag{4.99}$$

The equation (4.98) represents the internal dynamics of a hydraulic actuator's chamber, with $u_i(t)$ being the average output actuator force, $v_i(t)$ the total fluid flow rate of the actuator's chamber, P_{a_i} the actuator effective piston's area, C_{v_i} the chamber's volume, β_i the bulk modulus of the hydraulic fluid, C_{l_i} the coefficient of leakage and $\dot{z}_i(t)$ the velocity of the piston.

Denote $\tilde{\boldsymbol{u}}(t)$ as the tracking error between the "real" control action $\boldsymbol{u}(t)$ and the "desired" control action $\boldsymbol{u}_d(t)$; i.e.,

$$\tilde{\boldsymbol{u}}(t) = \boldsymbol{u}(t) - \boldsymbol{u}_d(t) \tag{4.100}$$

By taking into account the actuator dynamics, the control force to be applied to the bridge platform take the form

$$v_i(t) = P_{v_i}\dot{u}_i^d(t) + P_{l_i}u_i^d(t) + P_{a_i}\dot{z}(t), \qquad i = 1, 2 \tag{4.101}$$

Define a new Lyapunov function candidate $V(\boldsymbol{x}, \tilde{\boldsymbol{u}})$

$$V(\boldsymbol{x}, \tilde{\boldsymbol{u}}) = V_1(\boldsymbol{x}) + V_2(\tilde{\boldsymbol{u}}) \tag{4.102}$$

with

$$V_1(\boldsymbol{x}) = \frac{1}{2}\boldsymbol{x}^T\boldsymbol{P}\boldsymbol{x} \qquad V_2(\tilde{\boldsymbol{u}}) = \frac{1}{2}\tilde{\boldsymbol{u}}^T\boldsymbol{P}_l^{-1}\boldsymbol{P}_v\tilde{\boldsymbol{u}} \tag{4.103}$$

where

$$\boldsymbol{P}_l = \text{diag}(P_{l_1}, P_{l_2}) \qquad \text{and} \qquad \boldsymbol{P}_v = \text{diag}(P_{v_1}, P_{v_2})$$

The controller design is made through the minimization of the derivative of a Lyapunov function candidate. From the eqn.(4.100)

$$\boldsymbol{u}(t) = \boldsymbol{u}_d(t) + \tilde{\boldsymbol{u}}(t) \tag{4.104}$$

Then, the derivative of $V(\boldsymbol{x}, \tilde{\boldsymbol{u}})$ is obtained as follows by using eqns. (4.115), (4.98) and (4.100):

$$\dot{V}(\boldsymbol{x}, \tilde{\boldsymbol{u}}) \leq H(\boldsymbol{x}, \boldsymbol{u}, \tilde{\boldsymbol{u}}) + H(\boldsymbol{y}) \tag{4.105}$$

where

$$\begin{aligned} H(\boldsymbol{x}, \boldsymbol{u}, \tilde{\boldsymbol{u}}) &=: H(\boldsymbol{x}, \boldsymbol{u}) - \tilde{\boldsymbol{u}}^T\tilde{\boldsymbol{u}} - \frac{1}{4}\boldsymbol{x}^T\boldsymbol{P}\boldsymbol{B}\boldsymbol{B}^T\boldsymbol{P}\boldsymbol{x} + \boldsymbol{x}^T\boldsymbol{P}\boldsymbol{B}\tilde{\boldsymbol{u}} \\ &= H(\boldsymbol{x}, \boldsymbol{u}) - (\tilde{\boldsymbol{u}} - \frac{1}{2}\boldsymbol{x}^T\boldsymbol{P}\boldsymbol{B})^T(\tilde{\boldsymbol{u}} - \frac{1}{2}\boldsymbol{x}^T\boldsymbol{P}\boldsymbol{B}) \leq H(\boldsymbol{x}, \boldsymbol{u}) < 0 \end{aligned} \tag{4.106}$$

Therefore, the "real" control action $\boldsymbol{u}(t)$ (taking into account the actuator dynamics) can minimize the derivative of Lyapunov function $\dot{V}(\boldsymbol{x}, \tilde{\boldsymbol{u}})$ by making $H(\boldsymbol{x}, \boldsymbol{u}, \tilde{\boldsymbol{u}}) < 0$, which is similar to the case when a "desired" control action $\boldsymbol{u}_d(t)$ (without taking into account the actuator dynamics) is applied to the bridge platform.

Controller 2

Define a sliding function as follows

$$\boldsymbol{\sigma}(t) = \boldsymbol{D}\boldsymbol{x}(t) \qquad \text{with} \qquad \sigma_i(t) = \boldsymbol{d}_i^T \boldsymbol{x}(t) \qquad (i = 1, 2) \tag{4.107}$$

where $\boldsymbol{D} = [\boldsymbol{d}_1, \boldsymbol{d}_2]^T \in I\!R^{2\times 4}$ is a matrix to be chosen by the designer in order to guarantee the asymptotic stability of the closed-loop system in sliding mode

$$\dot{\boldsymbol{x}}(t) = \left[\boldsymbol{I}_4 - \boldsymbol{B}_c(\boldsymbol{D}\boldsymbol{B}_c)^{-1}\boldsymbol{D}\right]\boldsymbol{A}_c\boldsymbol{x}(t) \tag{4.108}$$

For the system (4.75), a simple choice for $\boldsymbol{D}$ is

$$\boldsymbol{D} = \begin{pmatrix} 1 & 0 & 1 & 0 \\ 0 & 1 & 0 & 1 \end{pmatrix} \tag{4.109}$$

Consequently, the following two sliding functions are defined

$$\sigma_1(t) = \dot{z}(t) + z(t); \qquad \sigma_2(t) = \dot{\Theta}(t) + \Theta(t) \tag{4.110}$$

In order to design the sliding mode controller, define a Lyapunov function candidate:

$$V(\boldsymbol{\sigma}) = \frac{1}{2}\boldsymbol{\sigma}^T(t)\boldsymbol{\sigma}(t) \tag{4.111}$$

The derivative of the Lyapunov function is obtained as follows:

$$\dot{V}(\boldsymbol{\sigma}) \;=\; \boldsymbol{\sigma}^T\dot{\boldsymbol{\sigma}} = \boldsymbol{\sigma}^T\left[\boldsymbol{D}\boldsymbol{A}_c\boldsymbol{x} + \boldsymbol{D}\boldsymbol{B}_c\boldsymbol{u} + \boldsymbol{D}\boldsymbol{B}_c\boldsymbol{e}(\boldsymbol{x}, \boldsymbol{y}, t)\right] \le H(\boldsymbol{x}, \boldsymbol{u}) + H(\boldsymbol{y}) \tag{4.112}$$

where

$$H(\boldsymbol{x}, \boldsymbol{u}) \;=:\; \boldsymbol{\sigma}^T\{\boldsymbol{D}\boldsymbol{A}_c\boldsymbol{x} + \boldsymbol{D}\boldsymbol{B}_c\boldsymbol{u}\} + ||\boldsymbol{\sigma}^T|| \cdot ||\boldsymbol{D}\boldsymbol{B}_c|| \cdot \{\delta_c + \alpha_c^c||\boldsymbol{x}||\} \tag{4.113}$$

$$H(\boldsymbol{y}) \;=:\; \alpha_c^r||\boldsymbol{\sigma}^T|| \cdot ||\boldsymbol{D}\boldsymbol{B}_c|| \cdot ||\boldsymbol{y}|| \tag{4.114}$$

Since $\boldsymbol{y}(t)$ is usually not measurable, the objective of the sliding mode control is to minimize σ by making negative $\dot{V}(\boldsymbol{\sigma})$ and explicitly $H(\boldsymbol{x}, \boldsymbol{u}) < 0$. If we denote $\boldsymbol{u}_d(t)$ as the "desired" control signal (without taking into account the actuator dynamics), then the following "desired " sliding mode control law will be used for the generation of sliding motion:

$$\boldsymbol{u}_d \;=\; -\boldsymbol{k}_c\boldsymbol{x} - (\boldsymbol{D}\boldsymbol{B}_c)^{-1}\{\psi_0 + \psi_1|z| + \psi_2|\Theta| + \psi_3|\dot{z}| + \psi_4|\dot{\Theta}|\}\left[sgn\left(\sigma_1\right), sgn\left(\sigma_2\right)\right]^T \tag{4.115}$$

where

$$\boldsymbol{k}_c = \frac{1}{4}\boldsymbol{D}\boldsymbol{B}_c\boldsymbol{D} + (\boldsymbol{D}\boldsymbol{B}_c)^{-1}\boldsymbol{D}\boldsymbol{A}_c; \qquad \text{and} \qquad \psi_i > \sqrt{2}\alpha_i||\boldsymbol{D}\boldsymbol{B}_c||; \qquad i = 1, 2, 3, 4 \tag{4.116}$$

It is easy to verify that if the controller gains are chosen to accomplish the relationships eqns.(4.116)) then $H(\boldsymbol{x}, \boldsymbol{u}) < 0$. Approximating the control law (4.115) to attenuate the high-frequency chattering, the corresponding continuous "desired" sliding mode control law is

$$\boldsymbol{u}_d \;=\; -\boldsymbol{k}_c\boldsymbol{x} - (\boldsymbol{D}\boldsymbol{B}_c)^{-1}\{\psi_0 + \psi_1|z| + \psi_2|\Theta| + \psi_3|\dot{z}| + \psi_4|\dot{\Theta}|\}\left[\frac{\sigma_1}{|\sigma_1| + \gamma_1}\;,\; \frac{\sigma_2}{|\sigma_2| + \gamma_2}\right]^T \tag{4.117}$$

By including the actuator dynamics of the hydraulic device and applying the control force $\boldsymbol{v}(t) = [v_1(t), v_2(t)]^T$ (4.98) to the bridge platform a new Lyapunov function candidate $V(\boldsymbol{\sigma}, \tilde{\boldsymbol{u}})$ is defined as

$$V(\boldsymbol{\sigma}, \tilde{\boldsymbol{u}}) = V_1(\boldsymbol{\sigma}) + V_2(\tilde{\boldsymbol{u}}); \quad V_1 = \frac{1}{2}\boldsymbol{\sigma}^T\boldsymbol{\sigma}; \quad V_2(\tilde{\boldsymbol{u}}) = \frac{1}{2}P_l^{-1}P_v\tilde{\boldsymbol{u}}^T\tilde{\boldsymbol{u}} \tag{4.118}$$

Then a derivative of $V(\boldsymbol{\sigma}, \tilde{\boldsymbol{u}})$ is obtained as:

$$\dot{V}(\boldsymbol{\sigma}, \tilde{\boldsymbol{u}}) \leq H(\boldsymbol{x}, \boldsymbol{u}, \tilde{\boldsymbol{u}}) + H(\boldsymbol{y}) \tag{4.119}$$

where

$$\begin{aligned} H(\boldsymbol{x}, \boldsymbol{u}, \tilde{\boldsymbol{u}}) &=: H(\boldsymbol{x}, \boldsymbol{u}) - \frac{1}{4}\boldsymbol{\sigma}^T \boldsymbol{B}_c^T \boldsymbol{D}^T \boldsymbol{D}\boldsymbol{B}_c\boldsymbol{\sigma} + \boldsymbol{\sigma}^T \boldsymbol{D}\boldsymbol{B}_c\tilde{\boldsymbol{u}} - \tilde{\boldsymbol{u}}^T\tilde{\boldsymbol{u}} \\ &= H(\boldsymbol{x}, \boldsymbol{u}) - (\tilde{\boldsymbol{u}} - \frac{1}{2}\boldsymbol{D}\boldsymbol{B}_c\boldsymbol{\sigma})^T(\tilde{\boldsymbol{u}} - \frac{1}{2}\boldsymbol{D}\boldsymbol{B}_c\boldsymbol{\sigma}) \leq H(\boldsymbol{x}, \boldsymbol{u}) < 0 \end{aligned} \tag{4.120}$$

Therefore, the "real" control action $\boldsymbol{u}(t)$ (taking into account the actuator dynamics) can minimize the derivative of Lyapunov function $\dot{V}(\boldsymbol{\sigma}, \tilde{\boldsymbol{u}})$ by making $H(\boldsymbol{x}, \boldsymbol{u}, \tilde{\boldsymbol{u}}) < 0$, which is similar to the case when a "desired" control action $\boldsymbol{u}_d(t)$ (without taking into account the actuator dynamics) is applied to the bridge platform.

4.2.2 Numerical Results

An actively suspended bridge platform is considered as the main system and the excitation is induced by a truck when it crosses the bridge. The platform is excited by the crossing of the truck for time $t \in [0, 6]$ seconds, and after $t = 6$ seconds no excitation is evolved between the platform and the truck.

The following parameters are used for the numerical simulation:
Nominal parameters and bounds for uncertainties: $\bar{\eta}_0 = 1$ [m], $\omega_0 = 40$ [N/(m kg)], $\bar{\omega} = 20$ [N/(m kg)], $\sigma_0 = 1$ [Ns/(m Kg)], $\bar{\sigma} = 5$ [Ns/(m Kg)], $\bar{\Omega} = 5$ [N/(m kg)], $\bar{\Upsilon} = 0.5$ [Ns/(m Kg)], $\bar{v} = 8.33$ [m/s] ($\bar{v} = 30$ [km/h]), $k_0 = 4 \cdot 10^5$ [N/m], $c_0 = 10^4$ [Ns/m].
Bridge: $M = 10^5$ Kg, $J = 2 \cdot 10^7$ Kg m^2, $a = b = 25$ m, $k_i = 4 \cdot 10^6$ N/m and $c_i = 4 \cdot 10^4$ N s/m for each $i = 1, 2$. $z_{1,0} = z_{2,0} = -0.125$ m, which correspond to the equilibrium position for the platform without truck and no control.
Truck: The parameters of the truck, which are unknown for the controller design, are the following: $m = 10^4$ Kg, $v = 8.33$ m/s (= 30 Km/h), $k = 4 \cdot 10^5$ N/m, $c = 10^4$ N s/m, $\eta_0 = 0.75$ m.
Hydraulic Actuator: The parameters of the hydraulic actuator are the following: $P_a = 2.4 \times 10^{-2}$, $P_v = 3.57 \times 10^3$ and $P_l = 1.99 \times 10^{-5}$.
With the above parameters, we obtain: $\boldsymbol{\alpha} = [\,5\,,\,129.165\,,\,0.5\,,\,12.5\,,\,5\,,\,0.5\,,\,500.0025\,]^T$

The Lyapunov control law obtained in equations (4.101) and (4.117) has been numerically implemented. The time history of structural vibration of the bridge platform for the uncontrolled case (dash line) and the controlled case (solid line) are shown in figures 4.12 to 4.19. Concretely, figures 4.12 and 4.13 show the main effect of the control, which is to add damping to the bridge platform. Without control, the platform has very low damping, thus exhibiting a highly oscillatory response. The damping coefficients of the two end supports are $c_1 = c_2 = 4 \times 10^4$ N s/m, which corresponds to a damping factor of 4.5% approximately. The control modifies this behavior, forcing a practically overdamped response. It is seen how the vertical deflection z of the center of mass of the platform evolves slowly but smoothly towards its equilibrium position with the truck. After $t = 6$ seconds the excitation disappears and the platform deflection evolves to recover the initial equilibrium position. Figures 4.14 and 4.15 show that the inclination Θ of the bridge has not been significantly improved because the linear control. Figures 4.16 and 4.17 show the dynamic of the truck. Finally, in figures 4.18 and 4.19 the control signals u_1 and u_2 are displayed, which are feasible for practical actuators.

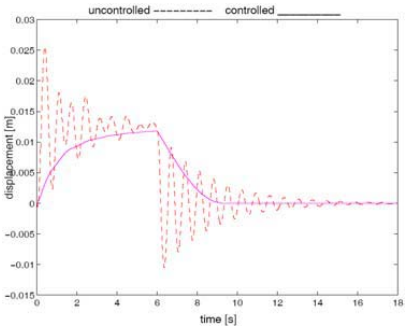

Figure 4.12: Vertical displacement of the bridge

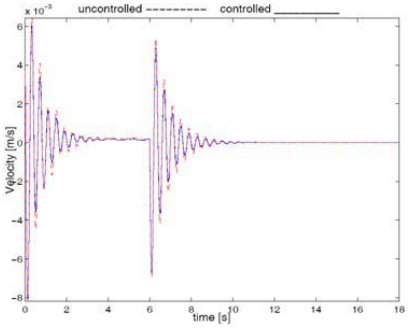

Figure 4.15: Inclination velocity of the bridge

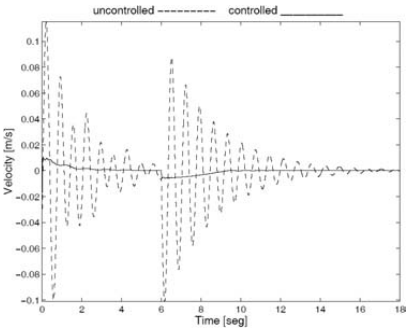

Figure 4.13: Vertical velocity of the bridge

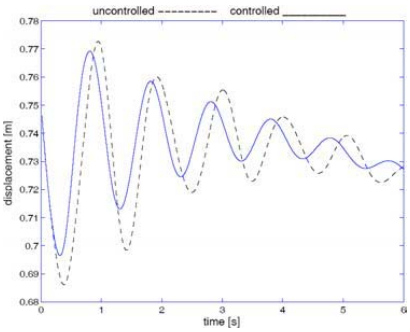

Figure 4.16: Vertical vibration of the truck

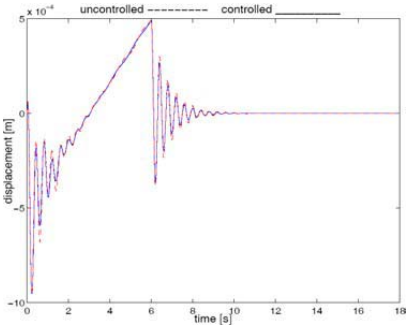

Figure 4.14: Inclination of the bridge

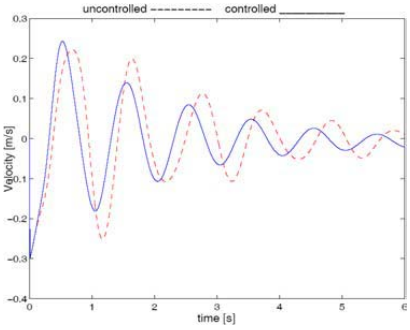

Figure 4.17: Vertical velocity of the truck

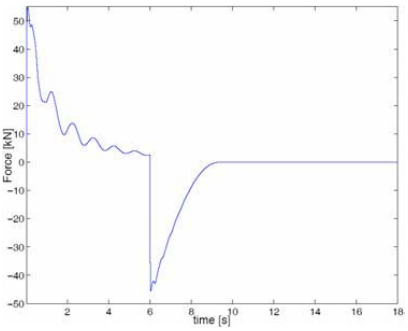

Figure 4.18: Control force of the 1st actuator

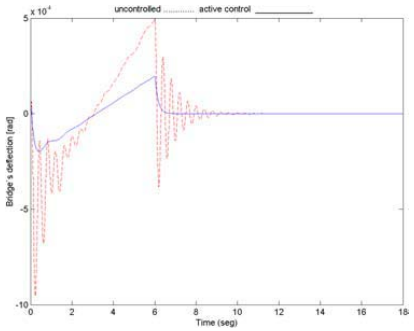

Figure 4.21: Inclination of the bridge

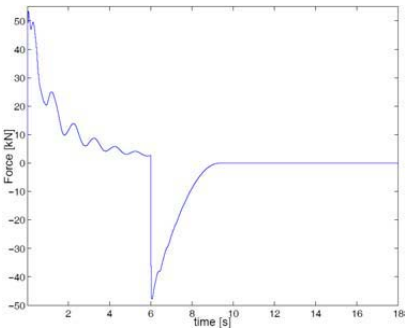

Figure 4.19: Control force of the 2nd actuator

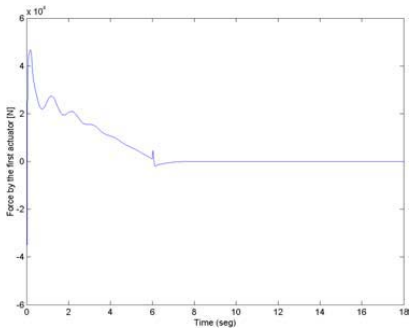

Figure 4.22: Control force of the 1st actuator

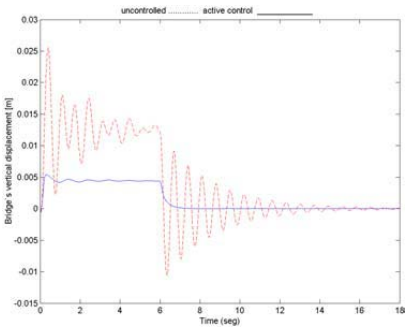

Figure 4.20: Vertical vibration of the bridge

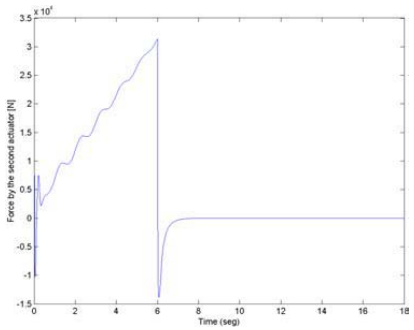

Figure 4.23: Control force of the 2nd actuator

In the sliding mode controller design The matrix $\boldsymbol{D}$ is chosen as

$$\boldsymbol{D} = \begin{pmatrix} 1 & 0 & 1 & 0 \\ 0 & 1 & 0 & 1 \end{pmatrix},$$

in order to have a reasonable trade-off between performance and control effort and the controller gains are chosen as follows : $\boldsymbol{\Psi} = (\psi_0, \psi_1, \psi_2, \psi_3, \psi_4)^T = (1 \times 10^{-3}, 10, 258.33, 1, 25)^T$

Figures 4.20 to 4.23 show the dynamic behaviour of the controlled and uncontrolled structure. It is seen how the vertical deflection z of the center of mass of the platform evolves slowly but smoothly towards its equilibrium position with the truck ($z = 0.125m$). After $t = 6$ seconds the excitation disappears and the platform deflection evolves to recover the initial equilibrium position. Figure 4.21 shows that the inclination Θ of the bridge has been significantly improved. Figures 4.22 and 4.23 display the control signals u_1 and u_2, which are feasible for practical actuators too.

Two active control schemes, Lyapunov based controller and sliding mode controller, have been numerically verified. It has been shown that vibration attenuation of a main system excited by an temporarily coupled uncertain subsystem has been achieved, while actuator dynamics (time delay and friction force) have been adequately taken into account in order to have a control design closer to the real operation conditions of the hydraulic actuator.

4.3 Structural System C: Full Scale Two-Span Bridge

Consider a two-span bridge supported by three columns. At each of the three joints between the columns and the superstructure, can exist active or semiactive control systems as illustrated in Figure 4.24.

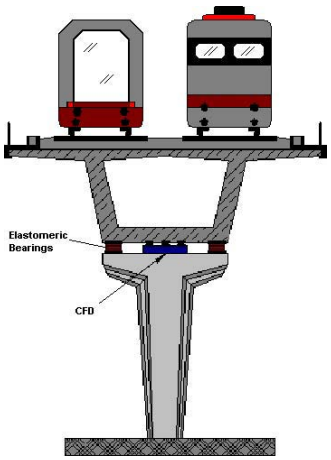

Figure 4.24: Example of a bridge prototype section with controllable friction devices (CFD) and elastomeric bearings.

A finite element model is available to describe the dynamic behavior of the bridge [14]. Initially, the model has 3 degrees of freedom (DOF) in the directions (x, y, z) at each node. Figure 4.25 shows the model configuration for half of the bridge. In this case, we study the dynamic

behavior of the beam structure in the transversal direction x only, where the seismic excitation and the control forces are applied. After a model reduction by using static condensation, the dynamic behavior of the beam structure and the supports is reasonably represented by the displacements of the 10 nodes that are highlighted in figure 4.25. Their equation of motion is the following:

$$\boldsymbol{M}\ddot{\boldsymbol{x}} + \boldsymbol{C}\dot{\boldsymbol{x}} + \boldsymbol{K}\boldsymbol{x} = \boldsymbol{F}\,, \tag{4.121}$$

where $\boldsymbol{x} = [\,x_1\,,\,x_2\,,\,\cdots\,,\,x_{10}\,]^T \in I\!R^{\,n}$ represents the transversal displacements of each node. The vector $\boldsymbol{F} \in I\!R^{\,n}$ describes the external excitation force, such as a seismic action. $\boldsymbol{M}$, $\boldsymbol{C}$ and $\boldsymbol{K} \in I\!R^{\,10\times 10}$ are the positive definite mass, damping and stiffness matrices, respectively, with

$$\boldsymbol{M} = \mathrm{diag}(\,[\,m_1\,m_2\,\ldots\,m_{10}]\,)$$

The damping matrix has been obtained with the Rayleigh-damping relation $\boldsymbol{C} = \alpha\boldsymbol{M} + \beta\boldsymbol{K}$, α and β being positive constants. The following are the numerical values for $\boldsymbol{M}$, and $\boldsymbol{K}$

$\boldsymbol{M} = \mathrm{diag}([0.6677,\ 1.7238,\ 0.2369,\ 0.6940,\ 0.4658,\ 1.3524,\ 0.4809,\ 1.7238,\ 0.2329,\ 0.3470]\times 10^4\,Kg,$

$$\boldsymbol{K}= \begin{bmatrix} 0.676 & -0.028 & -0.470 & -0.581 & 0.135 & 0.056 & 0.224 & -0.058 & -0.001 & -0.037 \\ -0.028 & 0.815 & 0.012 & -0.158 & 0.172 & -0.056 & 0.055 & -0.020 & 0.002 & -0.006 \\ -0.470 & 0.012 & 0.531 & 0.178 & -0.279 & 0.178 & -0.139 & 0.056 & -0.008 & 0.016 \\ -0.581 & -0.158 & 0.178 & 1.741 & -0.688 & -1.023 & 0.085 & -0.095 & 0.094 & 0.194 \\ 0.135 & 0.172 & -0.279 & -0.688 & 1.091 & 0.093 & -0.484 & 0.108 & 0.038 & 0.095 \\ 0.056 & -0.056 & 0.178 & -1.023 & 0.093 & 2.460 & -0.831 & -0.310 & 0.082 & -1.015 \\ 0.224 & 0.055 & -0.139 & 0.085 & -0.484 & -0.831 & 1.550 & 0.282 & -0.473 & 0.074 \\ -0.058 & -0.020 & 0.056 & -0.095 & 0.108 & -0.310 & 0.282 & 1.052 & 0.104 & -0.091 \\ -0.001 & 0.002 & -0.008 & 0.094 & 0.038 & 0.082 & -0.473 & 0.104 & 0.583 & -0.314 \\ -0.037 & -0.006 & 0.016 & 0.194 & 0.095 & -1.015 & 0.074 & -0.091 & -0.314 & 0.986 \end{bmatrix} \times 10^9 N/m.$$

The damping matrix $\boldsymbol{C}$ is obtained with the Rayleigh-damping relation with α=0.52075 and β=0.00325.

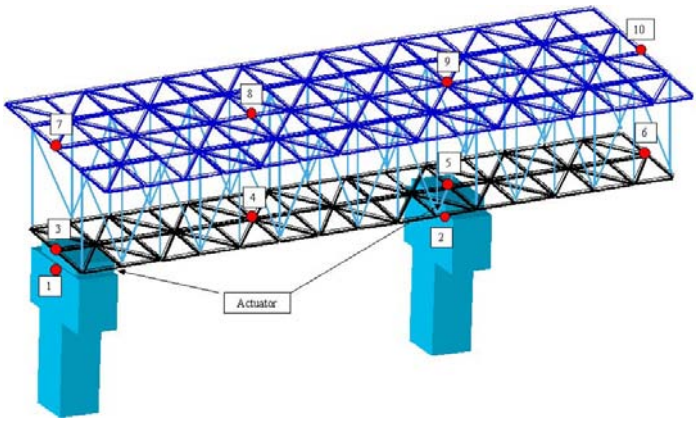

Figure 4.25: Finite element scheme of half of the bridge.

The nodes where the control devices are placed, will be referred as the controlled nodes, since they are the only nodes directly influenced by the friction devices. The following equations

are used to describe the dynamics of the controlled nodes:

$$\ddot{x}_1 = -\frac{1}{m_1}\left[c_{1,3}(\dot{x}_1+\dot{x}_3)+f_{1,3}+k_{1,3}(x_1-x_3)+m_1\ddot{x}_g\right] \tag{4.122}$$

$$\ddot{x}_2 = -\frac{1}{m_2}\left[c_{2,5}(\dot{x}_2-\dot{x}_5)+f_{2,5}+k_{2,5}(x_2-x_5)+m_2\ddot{x}_g\right] \tag{4.123}$$

$$\begin{aligned}\ddot{x}_3 = -\frac{1}{m_3}\big[&c_{1,3}(\dot{x}_3-\dot{x}_1)-f_{1,3}+k_{3,1}(x_3-x_1)+c_{3,4}(\dot{x}_3-\dot{x}_4)+k_{3,4}(x_3-x_4)+c_{3,7}(\dot{x}_3-\dot{x}_7)\\ &+k_{3,7}(x_3-x_7)+c_{3,8}(\dot{x}_3-\dot{x}_8)+k_{3,8}(x_3-x_8)+m_3\ddot{x}_g\big]\end{aligned} \tag{4.124}$$

$$\begin{aligned}\ddot{x}_5 = -\frac{1}{m_5}\big[&c_{2,5}(\dot{x}_2-\dot{x}_2)-f_{2,5}+k_{5,2}(x_5-x_2)+c_{5,4}(\dot{x}_5-\dot{x}_4)+k_{5,4}(x_5-x_4)+c_{5,6}(\dot{x}_5-\dot{x}_6)\\ &+k_{5,6}(x_5-x_6)+c_{5,8}(\dot{x}_5-\dot{x}_8)+k_{5,8}(x_5-x_8)+c_{5,9}(\dot{x}_5-\dot{x}_9)+k_{5,9}(x_5-x_9)\\ &+c_{5,10}(\dot{x}_5-\dot{x}_{10})+k_{5,10}(x_5-x_{10})-m_5\ddot{x}_g\big]\end{aligned} \tag{4.125}$$

where $\ddot{x}_g(t)$ is the ground acceleration. The above equations are extracted from the model (4.121) and augmented with the functions $f_{1,3}$ and $f_{2,5}$, which represent the friction forces between the corresponding nodes due to the controllable friction devices.

4.3.1 Control Configuration 1

The first control configuration uses Controllable Friction Devices (CFD) put in parallel to elastomeric bearings at each controlled nodes. Such control devices are semiactive because friction force can be controlled by means of a small energy source, and additional energy is not delivered to the structure. It is assumed that the friction forces supplied by the CFD devices have the following form:

$$f_{i,j}(\dot{x}_i,\dot{x}_j,t)=\gamma_{i,j}(t)\,(\dot{x}_i-\dot{x}_j);\quad i=1,3;\quad j=2,5\,, \tag{4.126}$$

where $\gamma_{i,j}(t)$ are time functions which describe on-line controlled modifications of the damping characteristics of the devices. It is assumed that these functions can take any value within prescribed bounds such that

$$c^*_{i,j}+\gamma_{i,j}=c^*_{i,j}+[0,\ \delta_{i,j}]\in\left[c^-_{i,j},\ c^+_{i,j}\right];\quad \{i,j\}=\{(1,3),(2,5)\}) \tag{4.127}$$

where ${c_{i,j}}^{\pm}$ are known constants (prescribed bounds). They define extreme allowable values for the total effective damping between nodes, where

$$c^*_{i,j}=\frac{c^+_{i,j}+c^-_{ij}}{2}\quad\text{and}\quad \delta_{i,j}=\frac{c^+_{i,j}-c^-_{ij}}{2}\,. \tag{4.128}$$

Now consider that each friction device has a control actuator driven by a control signal $u_{i,j}$ and assume that there is a first order time lag, such that the following model is adopted to relate the control signal $u_{i,j}$ and the damping signal $\gamma_{i,j}$:

$$u_{i,j}(t)=\frac{1}{\delta_{i,j}}\left\{\tau_{i,j}\dot{\gamma}_{i,j}(t)+\gamma_{i,j}(t)\right\}, \tag{4.129}$$

where $\tau_{i,j}$ is a time constant. Then, the effective control forces (4.126) supplied by the friction devices can be written in the form

$$\phi_{i,j}(\dot{x}_i,\dot{x}_j,t)=\delta_{i,j}u_{i,j}\,(\dot{x}_i-\dot{x}_j)-\tau_{i,j}\dot{\gamma}_{i,j}(\dot{x}_i-\dot{x}_j) \tag{4.130}$$

By substituting the expression (4.130) for the pairs of nodes $(1,3)$ and $(2,5)$ into their equations of motion (4.125), the following equations are obtained:

$$\begin{aligned}
\ddot{x}_1 &= -\frac{1}{m_1}\left[(c_{1,3}+\delta_{1,3}u_{1,3}-\tau_{1,3}\dot{\gamma}_{1,3})\,(\dot{x}_1-\dot{x}_3)+k_{1,3}(x_1-x_3)+m_1\ddot{x}_g\right]\\
\ddot{x}_2 &= -\frac{1}{m_2}\left[(c_{2,5}+\delta_{2,5}u_{2,5}-\tau_{2,5}\dot{\gamma}_{2,5})\,(\dot{x}_2-\dot{x}_5)+k_{2,5}(x_2-x_5)-m_2\ddot{x}_g\right]\\
\ddot{x}_3 &= -\frac{1}{m_3}\left[(c_{1,3}+\delta_{1,3}u_{1,3}-\tau_{1,3}\dot{\gamma}_{1,3})\,(\dot{x}_3-\dot{x}_1)+k_{3,1}(x_3-x_1)+c_{3,4}(\dot{x}_3-\dot{x}_4)+k_{3,4}(x_3-x_4)\right.\\
&\quad \left.+c_{3,7}(\dot{x}_3-\dot{x}_7)+k_{3,7}(x_3-x_7)+c_{3,8}(\dot{x}_3-\dot{x}_8)+k_{3,8}(x_3-x_8)+m_3\ddot{x}_g\right]\\
\ddot{x}_5 &= -\frac{1}{m_5}\left[(c_{2,5}+\delta_{2,5}u_{2,5}-\tau_{2,5}\dot{\gamma}_{2,5})\,(\dot{x}_5-\dot{x}_2)+k_{5,2}(x_5-x_2)+c_{5,4}(\dot{x}_5-\dot{x}_4)+k_{5,4}(x_5-x_4)\right.\\
&\quad +c_{5,6}(\dot{x}_5-\dot{x}_6)+k_{5,6}(x_5-x_6)+c_{5,8}(\dot{x}_5-\dot{x}_8)+k_{5,8}(x_5-x_8)+c_{5,9}(\dot{x}_5-\dot{x}_9)\\
&\quad \left.+k_{5,9}(x_5-x_9)+c_{5,10}(\dot{x}_5-\dot{x}_{10})+k_{5,10}(x_5-x_{10})+m_5\ddot{x}_g\right]
\end{aligned}$$

Controller Design

The control objective is now to generate the signals $u_{i,j}$ through a feedback control law which use information from the couples of nodes $(1-3),(2-5)$. Two controllers have been designed for this problem. The first controller is based on based on the Lyapunov stability theory and the second one is based on the QFT approach.

Controller 1

Write the state space equation for the controlled nodes as follows:

$$\dot{\boldsymbol{z}}(t)=\boldsymbol{A}\boldsymbol{z}(t)+\boldsymbol{B}(\boldsymbol{z},t)\boldsymbol{u}(t)+\boldsymbol{C}(\boldsymbol{z},t)\boldsymbol{\Upsilon}(t)+\boldsymbol{E}(\boldsymbol{z},t)\boldsymbol{z}_A(t)+\boldsymbol{F}(t), \tag{4.131}$$

where $\boldsymbol{z}(t)=[x_1,x_2,x_3,x_5,\dot{x}_1,\dot{x}_2,\dot{x}_3,\dot{x}_5]^T$, $\boldsymbol{u}(t)=[u_{1,3},u_{2,5}]^T$, $\boldsymbol{\Upsilon}(t)=[\dot{\gamma}_{1,3},\dot{\gamma}_{2,5}]^T$
$\boldsymbol{z}_A(t)=[x_4,x_6,x_7,x_8,x_9,x_{10},\dot{x}_4,\dot{x}_6,\dot{x}_7,\dot{x}_8,\dot{x}_9,\dot{x}_{10}]^T$
and

$$\boldsymbol{B}(\boldsymbol{z},t)=\begin{pmatrix} c0_(4,1) & c0_(4,1)\\ \dfrac{\delta_{1,3}(\dot{x}_3-\dot{x}_1)}{m_1} & 0\\ 0 & \dfrac{\delta_{2,5}(\dot{x}_5-\dot{x}_2)}{m_2}\\ -\dfrac{\delta_{1,3}(\dot{x}_3-\dot{x}_1)}{m_3} & 0\\ 0 & -\dfrac{\delta_{2,5}(\dot{x}_5-\dot{x}_2)}{m_5}\end{pmatrix} \qquad \boldsymbol{A}=\begin{pmatrix} 0_(4,4) & 1_(4,4)\\ M_1^{-1}K_1 & M_1^{-1}C_1\end{pmatrix}$$

$$\boldsymbol{C}(\boldsymbol{z},t)=\begin{pmatrix} 0_{(4,1)} & 0_{(4,1)}\\ -\dfrac{\tau_{1,3}(\dot{x}_3-\dot{x}_1)}{m_1} & 0\\ 0 & -\dfrac{\tau_{2,5}(\dot{x}_5-\dot{x}_2)}{m_2}\\ \dfrac{\tau_{1,3}(\dot{x}_3-\dot{x}_1)}{m_3} & 0\\ 0 & \dfrac{\tau_{2,5}(\dot{x}_5-\dot{x}_2)}{m_5}\end{pmatrix} \qquad \boldsymbol{F}(\boldsymbol{z},t)=\begin{bmatrix} 0_(4,1)\\ 1/m_1\\ 1/m_2\\ 1/m_3\\ 1/m_5\end{bmatrix}\ddot{x}_g(t)$$

The matrix $\boldsymbol{E}(\boldsymbol{z},t)\in I\!R^{8\times 12}$ is not explicitly written for the sake of brevity.
Define the Lyapunov function candidate

$$V(\boldsymbol{z},t)=\frac{1}{2}\boldsymbol{z}^T(t)\boldsymbol{P}\boldsymbol{z}(t)\,, \tag{4.132}$$

By using equation (4.131), the derivative of $V(\boldsymbol{z},t)$ is obtained:

$$\dot{V}(\boldsymbol{z},t) = -\frac{1}{2}\boldsymbol{z}^T\boldsymbol{Q}\boldsymbol{z} + \boldsymbol{z}^T\boldsymbol{P}\boldsymbol{F} + \boldsymbol{z}^T\boldsymbol{P}\boldsymbol{b}_{1,3}(\boldsymbol{z})u_{1,3} + \boldsymbol{z}^T\boldsymbol{P}\boldsymbol{b}_{2,5}(\boldsymbol{z})u_{2,5} + \boldsymbol{z}^T\boldsymbol{P}\boldsymbol{c}_{1,3}(\boldsymbol{z})\dot{\gamma}_{1,3} + \boldsymbol{z}^T\boldsymbol{P}\boldsymbol{c}_{2,5}(\boldsymbol{z})\dot{\gamma}_{2,5} + \boldsymbol{z}^T\boldsymbol{P}\boldsymbol{E}\boldsymbol{z}_A \tag{4.133}$$

where $b_{1,3}$ and $b_{2,5}$ correspond to the first an second column of $\boldsymbol{B}$, respectively. Similarly, $c_{1,3}$ and $c_{2,5}$ correspond to the first an second column of $\boldsymbol{C}$. By comparing terms between $b_{i,j}$ and $c_{i,j}$ it is found that:

$$\boldsymbol{c}_{i,j} = -\frac{\tau_{i,j}}{\delta_{i,j}}\boldsymbol{b}_{i,j} = -T_{i,j}\boldsymbol{b}_{i,j}, \qquad \text{for} \quad \{i,j\} = \{(1,3),(2,5)\} \tag{4.134}$$

with $T_{i,j} = \dfrac{\tau_{i,j}}{\delta_{i,j}}$

The control objective is to minimize $\dot{V}(\boldsymbol{z},t)$ for every $(\boldsymbol{z},t)$. The intuition underlying this objective is to reduce the system response $\boldsymbol{z}$ by forcing the associated energy $\boldsymbol{z}^T\boldsymbol{P}\boldsymbol{z}$ to be as negative as possible. Then, the semiactive control signals that result in the minimum of $\dot{V}(\boldsymbol{z},t)$ for $u_{i,j}(t)$ are

$$u_{i,j} = -\text{sgn}(\boldsymbol{z}^T\boldsymbol{P}\boldsymbol{b}_{i,j}), \quad \text{for} \quad \{i,j\} = \{(1,3),(2,5)\}. \tag{4.135}$$

Stability Analysis

The analysis related to the negativeness of the time derivative of the Lyapunov function (4.132) is as follows.
By substituting (4.134) and (4.135) into (4.133), we write

$$\dot{V}(\boldsymbol{z},t) = -\frac{1}{2}\boldsymbol{z}^T\boldsymbol{Q}\boldsymbol{z} - \theta_{1,3}(\boldsymbol{z},\dot{\gamma}_{1,3}) - \theta_{2,5}(\boldsymbol{z},\dot{\gamma}_{2,5}) + \boldsymbol{z}^T\boldsymbol{P}\boldsymbol{E}\boldsymbol{z}_A + \boldsymbol{z}^T\boldsymbol{P}\boldsymbol{F}\,. \tag{4.136}$$

where

$$\theta_{1,3}(\boldsymbol{z},\dot{\gamma}_{1,3}) = \boldsymbol{z}^T\boldsymbol{P}\boldsymbol{b}_{1,3}[\text{sgn}(\boldsymbol{z}^T\boldsymbol{P}\boldsymbol{b}_{1,3}) + T_{1,3}\dot{\gamma}_{1,3}] \quad \theta_{2,5}(\boldsymbol{z},\dot{\gamma}_{2,5}) = \boldsymbol{z}^T\boldsymbol{P}\boldsymbol{b}_{2,5}[\text{sgn}(\boldsymbol{z}^T\boldsymbol{P}\boldsymbol{b}_{2,5}) + T_{2,5}\dot{\Delta}_{2,5}]$$

Let us analyze the sign of $\theta_{1,3}$ and $\theta_{2,5}$. Consider a time interval $[t_1,t_2]$ where $\boldsymbol{z}^T\boldsymbol{P}\boldsymbol{b}_{1,3} > 0$. Then, $u_{1,3}(t) = 1$ for all $t \in [t_1,t_2]$. By solving the differential equation (4.129), we obtain

$$\gamma_{1,3}(t) = -\delta_{1,3}[1 - e^{-(t-t_1)/\tau_{1,3}}], \quad \dot{\gamma}_{1,3}(t) = -\frac{1}{T_{1,3}}e^{-(t-t_1)/\tau_{1,3}} \geq -\frac{1}{T_{1,3}}, \quad \forall t \in [t_1,t_2], \tag{4.137}$$

Then, we have that $\theta_{1,3}(\boldsymbol{z},\dot{\gamma}_{1,3}) \geq 0$ for all $t \in [t_1,t_2]$. Consequently, it is proved that $\theta_{1,3}(\boldsymbol{z},\dot{\gamma}_{1,3}) \geq 0$ for all $t \geq 0$. Following a similar reasoning, it can be proved that $\theta_{2,5}(\boldsymbol{z},\dot{\gamma}_{2,5}) \geq 0$ for all $t \geq 0$.

From the above analysis, it is concluded that the terms $\theta_{1,3}$ and $\theta_{2,5}$ reduce the time derivative of the Lyapunov function in (4.133) except at particular time instants where $\theta_{1,3} = \theta_{2,5} = 0$.

Numerical Results

The seismic excitation has been that of the *El Centro* (1940) earthquake. The semiactive control laws (4.135) have been used with the following matrix obtained by solving the Lyapunov equation

(4.132), with $\boldsymbol{Q}$ being the identity matrix:

$$\boldsymbol{P} = \begin{bmatrix} 258.4290 & 0.0000 & -29.4716 & -0.0000 & 0.3411 & 0.0000 & 0.1210 & -0.0000 \\ -0.0000 & 179.5009 & -0.0000 & 32.3173 & -0.0000 & 0.0842 & -0.0000 & 0.0227 \\ -29.4716 & 0.0000 & 116.4699 & -0.0000 & -0.3128 & 0.0000 & -0.1209 & -0.0000 \\ 0.0000 & 32.3173 & 0.0000 & 146.6417 & -0.0000 & 0.1876 & -0.0000 & -0.0227 \\ 0.3411 & -0.0000 & -0.3128 & -0.0000 & 0.0369 & 0.0000 & 0.0144 & -0.0000 \\ -0.0000 & 0.0842 & -0.0000 & 0.1876 & -0.0000 & 0.0117 & -0.0000 & -0.0017 \\ 0.1210 & -0.0000 & -0.1209 & 0.0000 & 0.0144 & 0.0000 & 0.0049 & -0.0000 \\ 0.0000 & 0.0227 & -0.0000 & -0.0227 & 0.0000 & -0.0017 & 0.0000 & -0.0016 \end{bmatrix}.$$

The semiactive device is characterized by time constants $\tau_{1,3} = \tau_{2,5} = 0.01\,s$, and $\delta_{1,3} = 7.6613 \times 10^5\,Ns/m$, $\delta_{2,5} = 2.8079 \times 10^5\,Ns/m$.

Figures 4.26(a) to 4.27(b) show the time histories of the transversal displacements and velocities of the nodes 3 and 5 respectively, both for the uncontrolled case and for the case with the semiactive control. We may observe a significant reduction in the response when the semiactive controlled devices are in operation. Notice that these nodes are included in the state vector $\boldsymbol{z}$, whose reduction is the objective of the control design. The effective forces supplied by the controllable friction devices at the nodes 3 and 5 ($\phi_{1,3}$ and $\phi_{2,5}$) are shown in Figures 4.29(a) and 4.29(b). Although this study has not gone into the physical design of the devices, the level of forces required to control the system seems to be feasible. It is also interesting to look at the response of the nodes that are not in the control objective. Figures 4.28(a) and 4.28(b) show the displacement and velocity of node 8, which is located in the middle between the two semiactive controllers (see Figure 4.24). The displacement response obtained when the controllers are in operation exhibits a significant reduction with respect to the uncontrolled one.

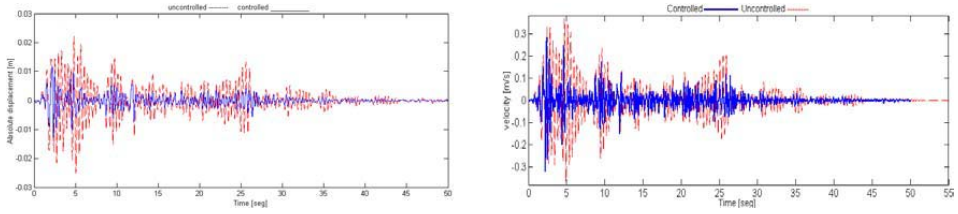

(a) displacement (b) Velocity

Figure 4.26: dynamics of node 3

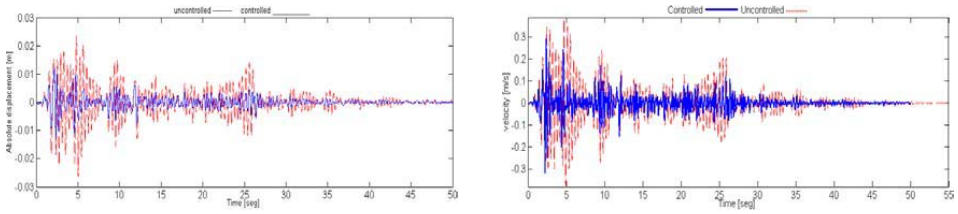

(a) displacement (b) Velocity

Figure 4.27: dynamics of node 5

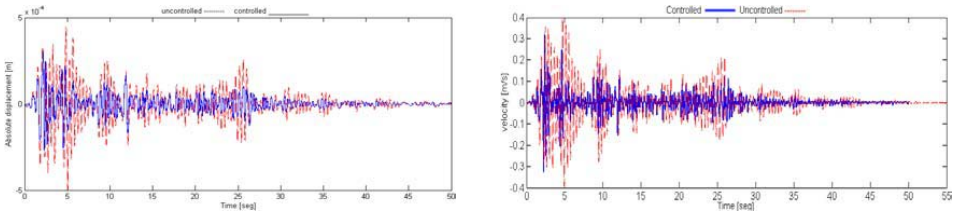

(a) displacement (b) Velocity

Figure 4.28: dynamics of node 8

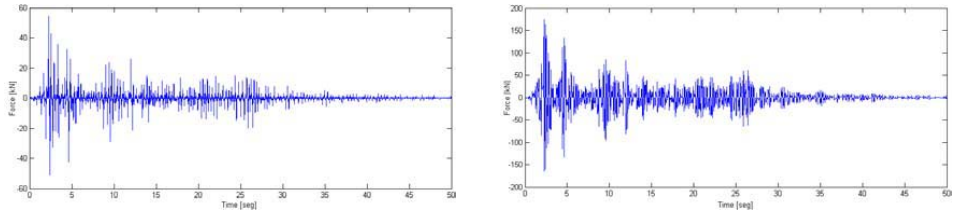

(a) $\phi_{1,3}$ (b) $\phi_{2,5}$

Figure 4.29: Control forces

Controller 2

The second controller is based on the QFT control theory. The control objective is to attenuate structural vibrations when an uncertain but bounded seismic force F_g acts on the transversal direction of the structure and stiffness and damping parameters are considered uncertain, varying about 5% of their nominal value. A bounded noise signal is considered to be present in the measurement of displacement.

Natural frequencies in the transversal direction presented in the structure are: [2.55 11.24 27.05 35.62 51.72 58.19 70.50 82.76 94.08 159.44] [Hz]. For simplicity of design, it is considered that the nodes 1 and 2 behave as rigid bodies. Then, the nodes to be directly controlled corresponds to those of the immediately upper side where the control devices are installed (nodes 3 and 5). The dynamic behavior of the structure at the controlled nodes $i = 3, 5$, is rewritten as follows:

$$m_i\ddot{x}_i + c_i\dot{x}_i + k_i x_i = m_i\ddot{x}_g - f_{i,j} + f_{pd_i}; \qquad i = 3, 5 \tag{4.138}$$

with m_i, c_i, k_i the mass, damping and stiffness of the node i respectively, x_i the transversal displacement at the node i, $\phi_{i,j}$ the control force applied at the node i and

$$f^i_{pd} = c_{i2}(\dot{x}_i - \dot{x}_2) + c_{i3}(\dot{x}_i - \dot{x}_3) + \ldots + c_{i8}(\dot{x}_i - \dot{x}_8) + k_{i2}(x_i - x_2) + k_{i3}(x_i - x_3) + \ldots + k_{i8}(x_i - x_8)$$

the force applied by the others nodes on the node i. c_{ij} and k_{ij} are respectively the damping and stiffness between the node i and node j. For this case, we are going to consider that the control device can develop a continuous friction force controlled by a continuous command voltage $u_{i,j}$, such that $f_{i,j} = u_{i,j}\delta_{i,j}(\dot{x}_i - \dot{x}_j)$. Thus the control force is limited to $|f^{max}_{i,j}| = u^{max}_{i,j}\delta_{i,j}max(|\dot{x}_i - \dot{x}_j|)$.

From equation (4.138) the transfer function of the plants to be controlled are obtained as:

$$P_{i,j}(s) = \frac{X_i(s)}{f_{pd_i}(s) - f_{i,j}(s)} = \frac{1}{m_i s^2 + c_i s + k_i} \tag{4.139}$$

Local QFT controllers are designed for each plant. In the controller design, the uncertain but bounded term f_{pd_i} is not measurable and not directly controllable. Thus it is considered with the unknown seismic force F_0 as disturbance to the input of the plant. By using the QFT MATLAB toolbox, the final nominal loops found are those shown in figures 4.30(a) and 4.30(b). The controller functions $G_i(s)$ derived for each control device (i=3,5) are respectively:

$$G_{1,3}(s) = \frac{161.1s^2 + 162.1s + 1}{0.0044s^2 + 1.004s + 1} \qquad G_{2,5}(s) = 0.99\frac{151.6s^2 + 152.6s + 1}{0.01s^2 + 1.01s + 1} \tag{4.140}$$

Then the control commands are computed as: $u_{i,j} = G_{i,j}x_i/(\delta_{i,j}(\dot{x}_i - \dot{x}_j))$ if $(\dot{x}_i - \dot{x}_j) \neq 0$, sgn($G_{i,j}x_i$)=sgn($\dot{x}_i - \dot{x}_j$) and $0 \leq |G_{i,j}x_i| < u_{i,j}^{max}\delta_{i,j}|(\dot{x}_i - \dot{x}_j)|$, else $u_{i,j} = 0$.

Numerical Results

El Centro earthquake acceleration was applied as disturbance signal. The control force developed by the actuator at the node 3 is presented in figure 4.32, while figures 4.31(a) and 4.31(b) show that the displacement and velocity at both controlled and uncontrolled nodes have been attenuated.

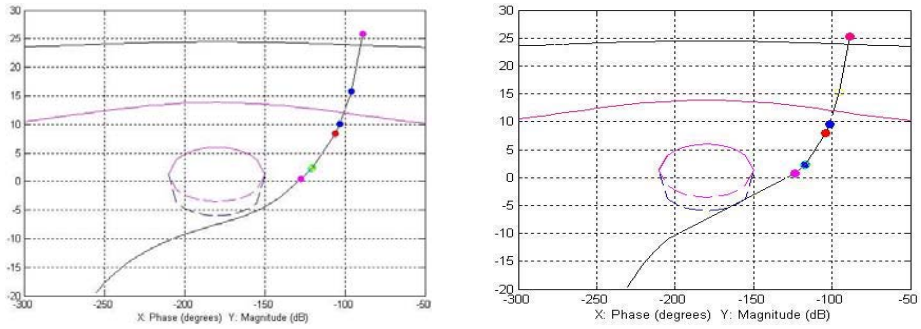

(a) Controller 3 (b) Controller 5

Figure 4.30: Final loop shaping L_N

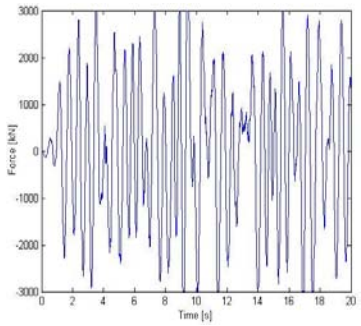

Figure 4.32: Control force at the node 3.

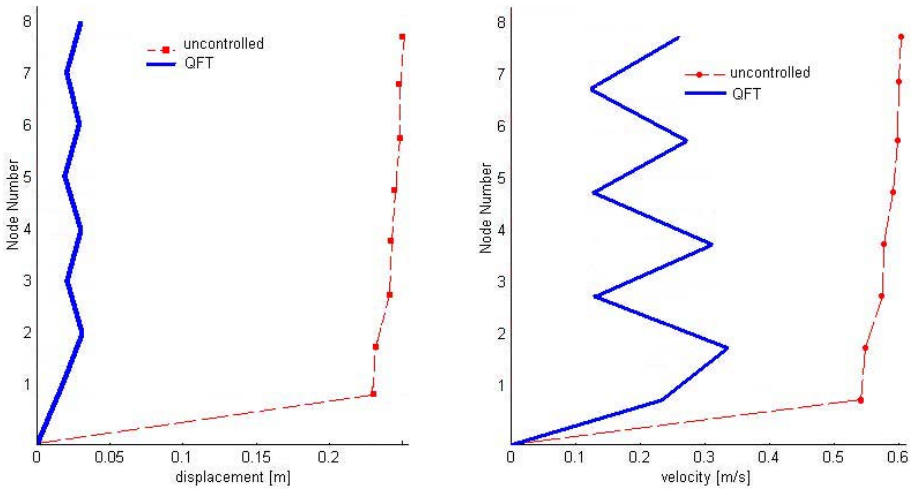

(a) Displacement (b) Velocities

Figure 4.31: Peak absolute vibration profiles

4.3.2 Control Configuration 2

The second control configuration consists of a hybrid control system. It is composed of a hysteretic passive isolator plus a MR damper installed at each joint between the column and the superstructure, such as shown in figure 4.33. Identical control systems are installed at both nodes. Here, the piers of the structure where the control system is supported, are considered rigid bodies.

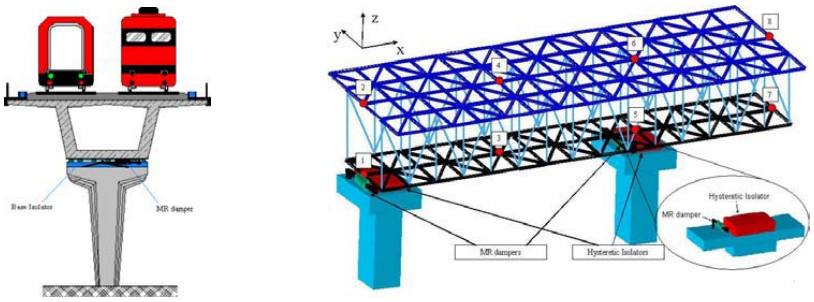

(a) Frontal View (b) DOF model

Figure 4.33: Full Scale Two-Span Bridge

By including the forces added by the new control configuration, we can rewrite the motion equation for each controlled node (3 and 5), as follows:

$$\ddot{x}_i = -\frac{1}{m_i}\left[c_i\dot{x}_i + f_{pd_i} + \Phi_i(\dot{x}_i, t) + m_i\ddot{x}_g + f_{c_i}\right] \tag{4.141}$$

with

$$\begin{array}{ll} \Phi_i = \Lambda_i k_i x_i + (1-\Lambda_i) D_i k_i z_1 & \dot{z}_1 = D_i^{-1}[-\gamma_1 |\dot{x}_i| z_1 |z_1|^{n_1-1} - \beta_1 \dot{x}_i |z_1|^{n_1} + A_1 \dot{x}_i] \\ f_{ci}(\dot{x}_i, t) = -\delta_i \dot{x}_i - \alpha_i z_2 & \dot{z}_2 = -\gamma_2 |\dot{x}_i| z_2 |z_2|^{n_2-1} - \beta_2 \dot{x}_i |z_2|^{n_2} + A_2 \dot{x}_i] \\ f_{pd_i} = \boldsymbol{c}_{di} \boldsymbol{\Delta \dot{x}}_{di} + \boldsymbol{k}_{di} \boldsymbol{\Delta x}_{di} & \end{array} \tag{4.142}$$

The isolation scheme is modelled as a single degree of freedom system with m_i, c_i and k_i being the mass, damping and stiffness parameters of the controlled nodes, respectively. x_i represents the absolute transversal displacement at the ith node controlled. The restoring force Φ_i characterizes the hysteretic behavior of the isolator, which usually consists of inelastic rubber bearings. The dynamics of both isolator and MR damper is described by means of the so-called Bouc-Wen model in the form of the equations (4.142). The restoring force is represented by the superposition of an elastic component $k_i x_i$ and a hysteretic component $(1-\Lambda_i) D_i k_i z_1$, where $D_i > 0$ is the yield constant displacement and $\Lambda_i \in [0\ 1]$ is the post to pre-yielding stiffness ratio. The MR damper force is represented by a linear part related to the transversal velocity plus a nonlinear part related to the nonlinear variable z_1. $\boldsymbol{c}_{di} = [c_{i_1}\ c_{i_2}\ \ldots\ \boldsymbol{c_{i_j}}]$ and $\boldsymbol{k}_{di} = [k_{i_1}\ k_{i_2}\ \ldots\ k_{i_j}]$. $\boldsymbol{\Delta y}_d = [y - y_1\ y - y_2\ \ldots\ y - y_j]$ is the relative displacement vector between the controlled node and the other ones. For control purposes, the equation predicting the behavior of the MR damper for a time-varying command voltage input u_i is as follows:

$$\alpha_i = \alpha_i(u_i) = \alpha_{a_i} + \alpha_{bi} u_i \qquad \text{and} \qquad \delta_i = \delta_i(u_i) = \delta_{ai} + \delta_{bi} u_i \tag{4.143}$$

Assumption 1. Displacements and velocities at the controlled nodes are measurable.
Assumption 2. The unknown seismic excitation $\ddot{x}_g(t)$ is bounded by $|\ddot{x}_g(t)| \leq X_0$ for all $t \geq 0$, where X_0 is a known positive constant.
Under the assumption 2, it is easy to verify that the unknown disturbance force $f_{gi}(t) = m_i \ddot{x}_g(t)$ is bounded by $|f_{gi}(t)| \leq F_{gi}$ for all $t \geq 0$, with F_{gi} being some known positive constant.

Controller Design

The control objective is to design a backstepping controller such that the closed-loop system is globally stable and consequently the structural vibration is attenuated. Since nonlinear MR dampers and hysteretic isolators are used in this problem, the backstepping technique is adequate to design the controller.
First, rewrite the dynamic equation (4.141) into the following state equation:

$$\begin{array}{ll} \dot{y}_1 = y_2 & \dot{y}_2 = \dfrac{1}{m_3}\left[c_i y_2 + f_{pd_3} + \Phi_3 + f_{c3} - f_{g3}\right] \\ \dot{y}_3 = y_4 & \dot{y}_4 = \dfrac{1}{m_5}\left[c_5 y_4 + f_{pd_5} + \Phi_5 + f_{c5} - f_{g5}\right] \end{array} \tag{4.144}$$

where $y_1 = x_3$, $y_2 = \dot{x}_3$, $y_3 = x_5$ and $y_4 = \dot{x}_5$.
Then the following standard variables are used for controller backstepping design:

$$\begin{array}{llll} e_1 = y_1; & \dot{e}_1 = y_2; & e_1\dot{e}_1 = e_1 y_2; & \eta_1 = -h_1 e_1; \quad \dot{\eta}_1 = -h_1 y_2; \\ e_2 = y_2 - \eta_1; & \dot{e}_2 = \dot{y}_2 + h_1 y_2; & e_2\dot{e}_2 = e_2(\dot{y}_2 + h_1 y_2); & \\ e_3 = y_3; & \dot{e}_3 = y_4; & e_3\dot{e}_3 = e_3 y_4; & \eta_2 = -h_3 e_3; \quad \dot{\eta}_2 = -h_3 y_4; \\ e_4 = y_4 - \eta_2; & \dot{e}_2 = \dot{y}_4 + h_3 y_4; & e_4\dot{e}_4 = e_4(\dot{y}_4 + h_3 y_4); & \end{array} \tag{4.145}$$

By using equations (4.144) and (4.145), we obtain:

$$\begin{array}{l} e_2\dot{e}_2 = -\dfrac{e_2}{m_3}\left[c_3 y_2 + f_{pd3} - f_{g3} + \Lambda k_3 y_1 + (1-\Lambda_3) D_3 k_3 z_{1_3} + \delta_{a3} y_2 + \alpha_{a3} z_{2_3} + (\delta_{b3} y_2 + \alpha_{b3} z_{2_3}) u_3\right] \\ e_4\dot{e}_4 = -\dfrac{e_4}{m_5}\left[c_5 y_4 + f_{pd5} - f_{g5} + \Lambda_5 k_5 y_3 + (1-\Lambda_5) D_5 k_5 z_{1_5} + \delta_{a3} y_4 + \alpha_{a3} z_{2_5} + (\delta_{b5} y_4 + \alpha_{b5} z_{2_5}) u_5\right] \end{array} \tag{4.146}$$

In order to achieve the asymptotic error suppression, the following control law is derived for giving the commanding voltage signal to the MR damper:

$$u_3 = -\frac{-(c_3+\delta_{a3}-m_3h_1)y_2-\Lambda_3k_3y_1-f_{pd3}+f_{g3}-(1-\Lambda_3)D_3k_3z_{1_3}-\alpha_{a3}z_{2_3}+m_3e_1+h_2e_2}{\delta_{b3}y_2+\alpha_{b3}z_{2_3}}$$
$$u_5 = -\frac{-(c_5+\delta_{a5}-m_5h_3)y_4-\Lambda_5k_5y_3-f_{pd5}+f_{g5}-(1-\Lambda_5)D_5k_5z_{1_3}-\alpha_{a5}z_{2_5}+m_5e_3+h_4e_4}{\delta_{b5}y_4+\alpha_{b5}z_{2_5}} \quad (4.147)$$

However, since f_{pdi}, f_{gi}, z_{1_i} and z_{2_i} contain unmeasurable variables, the control law 4.147 is not implementable in practice. In order to overcome the measurement limitation problem, some considerations and estimations are made.

Estimation of the evolutionary variables z_{1_i} and z_{2_i}: Since the variables z_{1_i} and z_{2_i} (i=3,5) cannot be directly measured and its right computation depends on the initial value $z_{1_i}(0)$ and $z_{2_i}(0)$, estimated values $\hat{z}_{1_i}$ and $\hat{z}_{2_i}$ are obtained, by means of the next equations:

$$\begin{aligned}
\dot{\hat{z}}_{1_3} &= D_3^{-1}[-\gamma_1|y_2||\hat{z}_{1_3}|^{n_1-1}-\beta_1y_2|\hat{z}_{1_3}|^{n_1}+A_1y_2]-\frac{(1-\Lambda)D_3k_3}{m_3}e_2\\
\dot{\hat{z}}_{2_3} &= -\gamma_2|y_2||\hat{z}_{2_3}|^{n_2-1}-\beta_2y_2|\hat{z}_{2_3}|^{n_2}+A_2y_2\\
\dot{\hat{z}}_{1_5} &= D_5^{-1}[-\gamma_1|y_4||\hat{z}_{1_5}|^{n_1-1}-\beta_1y_4|\hat{z}_{1_5}|^{n_1}+A_1y_5]-\frac{(1-\Lambda)D_5k_5}{m_5}e_4\\
\dot{\hat{z}}_{2_5} &= -\gamma_2|y_4||\hat{z}_{2_5}|^{n_2-1}-\beta_2y_2|\hat{z}_{2_5}|^{n_2}+A_2y_4
\end{aligned} \quad (4.148)$$

Define $\tilde{z}=z-\hat{z}$ as the estimation error between the real value z and the estimated value $\hat{z}$, then

$$z_{1_i}=\hat{z}_{1_i}+\tilde{z}_{1_i}; \qquad \dot{z}_{1_i}=\dot{\hat{z}}_{1_i}+\dot{\tilde{z}}_{1_i}; \quad \text{and} \quad z_{2_i}=\hat{z}_{2_i}+\tilde{z}_{2_i}; \qquad \dot{z}_{2_i}=\dot{\hat{z}}_{2_i}+\dot{\tilde{z}}_{2_i} \quad (4.149)$$

By taking $\tilde{z}_{2_3}=e_2$ and $\tilde{z}_{2_5}=e_4$, the denominators of the commanding voltage signals u_i can be replaced by

$$\delta_{b3}y_2+\alpha_{b3}z_{2_3}=\alpha_{b3}(\dot{\hat{z}}_{2_3}+\dot{\tilde{z}}_{2_3})+\delta_{b3}y_2=\alpha_{b3}(\dot{\hat{z}}_{2_3}+e_2)+\delta_{b3}y_2$$
$$\delta_{b5}y_4+\alpha_{b5}z_{2_5}=\delta_{b5}y_4+\alpha_{b5}(\dot{\hat{z}}_{2_5}+\dot{\tilde{z}}_{2_5})=\alpha_{b5}(\dot{\hat{z}}_{2_5}+e_4)+\delta_{b5}y_4$$

Now, based upon the bounded values of f_{gi} the estimated values of z_{1_i} and z_{2_i}, and considering that f_{pd_i} is not controllable, an implementable law is adopted for the backstepping control:

$$u_3 = -\frac{-(c_3+\delta_{a3}-m_3h_1)y_2-\Lambda k_3y_1+F_3sgn(e_2)-(1-\Lambda_3)D_3k_3\hat{z}_{1_3}-\alpha_{a3}\hat{z}_{2_3}+m_3e_1}{\delta_{b3}y_2+\alpha_{b3}(\hat{z}_{2_3}+e_2)} \quad (4.150)$$

$$u_5 = -\frac{-(c_5+\delta_{a5}-m_5h_3)y_4-\Lambda k_5y_3+F_5sgn(e_4)-(1-\Lambda_5)D_5k_5\hat{z}_{1_5}-\alpha_{a5}\hat{z}_{2_5}+m_5e_3}{\delta_{b5}y_4+\alpha_{b5}(\hat{z}_{2_5}+e_4)} \quad (4.151)$$

for all $\delta_{b3}y_2+\alpha_{b3}(\hat{z}_{2_3}+e_2)\neq 0$ and $\delta_{b5}y_4+\alpha_{b5}(\hat{z}_{2_5}+e_4)\neq 0$, otherwise u_3=0 and u_5=0.

Stability Analysis

In order to verify the closed-loop stability, the following Lyapunov function candidate is defined:

$$V = \frac{1}{2}e_1^2+\frac{1}{2}e_2^2+\frac{1}{2}e_3^2+\frac{1}{2}e_4^2+\frac{1}{2}\tilde{z}_{1_3}^2+\frac{1}{2}\tilde{z}_{2_3}^2+\frac{1}{2}\tilde{z}_{1_5}^2+\frac{1}{2}\tilde{z}_{2_5}^2 \quad (4.152)$$
$$\dot{V} = e_1\dot{e}_1+e_2\dot{e}_2+e_3\dot{e}_3+e_4\dot{e}_4+\tilde{z}_{1_3}\dot{\tilde{z}}_{1_3}+\tilde{z}_{2_3}\dot{\tilde{z}}_{2_3}+\tilde{z}_{1_5}\dot{\tilde{z}}_{1_5}+\tilde{z}_{2_5}\dot{\tilde{z}}_{2_5} \quad (4.153)$$

By using the equations (4.146), (4.148) and (4.151) and replacing them in (4.153), negativity of $\dot{V}$ can be demonstrated:

$$\begin{aligned}\dot{V} &= \frac{1}{m_3}\left[F_3|e_2| - f_{g3}e_2\right] - h_1 e_1^2 - h_2 e_2^2 - (\gamma_1 - \beta_1)D_3^{-1}|y_2|\tilde{z}_{1_3}^2 - (\gamma_2 - \beta_2)|y_2|\tilde{z}_{2_3}^2 + \\ &\quad \frac{1}{m_5}\left[F_5|e_4| - f_{g5}e_4\right] - h_3 e_3^2 - h_4 e_4^2 - (\gamma_1 - \beta_1)D_5^{-1}|y_4|\tilde{z}_{1_5}^2 - (\gamma_2 - \beta_2)|y_4|\tilde{z}_{2_5}^2 \leq 0\end{aligned}$$

Therefore, stability of the closed-loop system is ensured.

Numerical Results

The couple of base isolator plus MR damper installed at each one of the two joints of the structure (nodes 3 and 5), contain identical hysteretic dynamics. For the nodes 3 and 5:

$$\boldsymbol{k}_{d_3} = [0.5317,\ -0.4708,\ -0.2799,\ 0.1781,\ -0.1394,\ 0.1786,\ -0.0089,\ 0.0165] \times 10^6\ (kN/m)$$

$$\boldsymbol{k}_{d_5} = [-0.1394,\ 0.2243,\ -0.4844,\ 0.0856,\ 1.5509,\ -0.8317,\ -0.4735,\ 0.0741] \times 10^6\ (kN/m)$$

, while the values for vectors $\boldsymbol{c}_{d_3}$ and $\boldsymbol{c}_{d_5}$ are computed according with the Rayleigh-damping relation. γ_1=β_1 =1.8×10^2 m^{-1}, A_1=72, α=0.6, k=5.9×10^3 kN/m, D=0.6, γ_2=β_2=3×10^2 m^{-1}, A_2=120, δ_a=1.25×10^2 kN·s/m, δ_b=75 kN·s/mV, λ_a=6.25×10^4, λ_b=3.75×10^4, F_g=4.28×10^2 kN, h_1=1.5 and h_2=0.2918.
El Centro earthquake has been studied as the external seismic excitation. Passive (pure base isolation) and hybrid (base isolation + semiactive control) were studied. The time histories of absolute displacements and velocities at the controlled node 1 and 5 are shown in figures 4.34(a)-4.36.

Additionally, figures 4.37 and 4.38 present the absolute displacement and velocity of the beam at the uncontrolled node 4 . It is seen that the absolute displacement of both the controlled and uncontrolled nodes has been significant reduced by using the semiactive controllers such that the isolator can work safely within its elastic region and the structural acceleration has been kept small so that the human comfort is guaranteed. Figure 4.34 presents the hysteretic behaviour of the MR dampers during the seismic excitation.

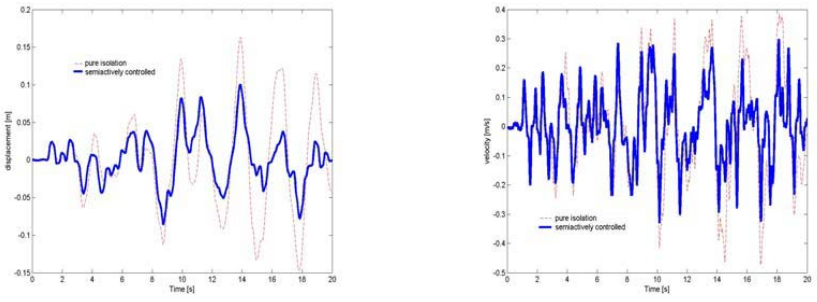

(a) Node 1 (b) Node 5

Figure 4.34: Dynamics of the node 1

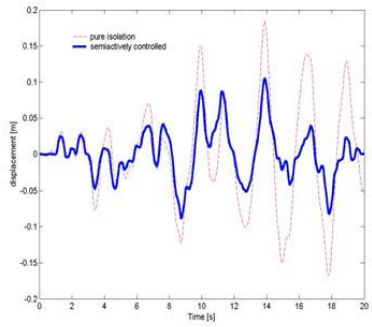

Figure 4.35: Displacement of node 5

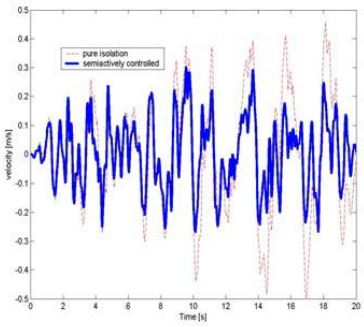

Figure 4.38: Velocity of node 4

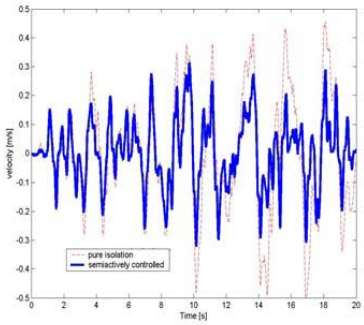

Figure 4.36: Velocity of node 5

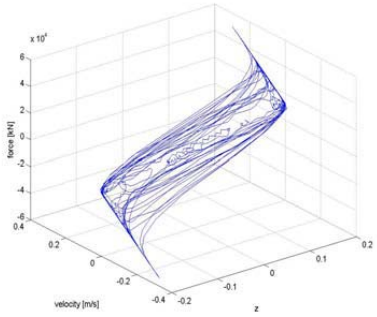

Figure 4.39: Hysteretic behaviour of the MR damper at the node 2

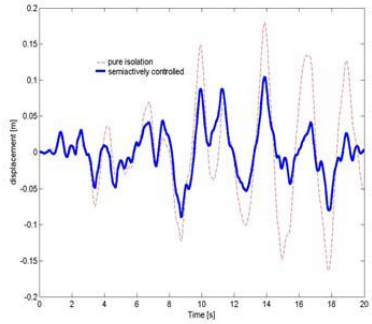

Figure 4.37: Displacement of node 4

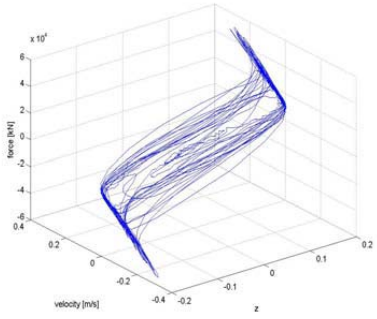

Figure 4.40: Hysteretic behaviour of the MR damper at the node 5

Chapter 5

Experimental Verification

This chapter presents the most important experimental results obtained on three experimental prototypes. The control configuration of the experimental prototypes contains one o more control problems presented in chapter 3 and studied in chapter 4. Different control control approaches studied in chapter 4 are implemented.

5.1 Experimental Prototype A. 6-story test building semiactively controlled

Consider a linear building structure controlled by means of nonlinear semiactive MR dampers installed at the lower floors, as shown in the figure 5.3. It is assumed that the control forces provided by the control devices are adequate to keep the response of the primary structure from exciting the linear region. The motion equation of the structure can be written as:

$$\boldsymbol{M}_s\ddot{\boldsymbol{x}} + \boldsymbol{C}_s\dot{\boldsymbol{x}} + \boldsymbol{K}_s\boldsymbol{x} = \boldsymbol{\Lambda}\boldsymbol{f} - \boldsymbol{M}_s\boldsymbol{\Gamma}\ddot{x}_g \tag{5.1}$$

where $\boldsymbol{x}$ =vector of the relative displacements of the floors of the structure, $\ddot{x}_g$ ground acceleration, $\boldsymbol{f} = [f_1, f_2, \ldots, f_m]^T$: vector of measured control forces, defined by (5.7)-(5.10) and generated by the n MR dampers, Γ = column vector of ones, and Λ = vector determined by the placement of the MR dampers in the structure. The $\boldsymbol{M}_s$, $\boldsymbol{C}_s$, $\boldsymbol{K}_s$ matrices take the form:

$$\boldsymbol{M}_s = \text{diag}([m_1, m_2, \ldots, m_n]) \tag{5.2}$$

$$\boldsymbol{K}_s = \begin{bmatrix} k_1+k_2 & -k_2 & 0 & \ldots & 0 \\ -k_2 & k_2+k_3 & -k_3 & \ldots & 0 \\ 0 & -k_3 & k_3+k_4 & \ldots & 0 \\ \vdots & \vdots & \vdots & \vdots & \vdots \\ 0 & 0 & 0 & \ldots & k_n \end{bmatrix} \tag{5.3}$$

$$\boldsymbol{C}_s = \begin{bmatrix} c_1+c_2 & -c_2 & 0 & \ldots & 0 \\ -c_2 & c_2+c_3 & -c_3 & \ldots & 0 \\ 0 & -c_3 & c_3+c_4 & \ldots & 0 \\ \vdots & \vdots & \vdots & \vdots & \vdots \\ 0 & 0 & 0 & \ldots & c_n \end{bmatrix} \tag{5.4}$$

where m_i, k_i, c_i are respectively, the mass, stiffness and damping parameters in the floor i. Equation (5.1) in state space form is as follows:

$$\dot{\boldsymbol{z}} = \boldsymbol{A}\boldsymbol{z} + \boldsymbol{B}\boldsymbol{f} + \boldsymbol{E}\ddot{x}_g \tag{5.5}$$

$$\boldsymbol{y} = \boldsymbol{C}\boldsymbol{z} + \boldsymbol{D}\boldsymbol{f} \tag{5.6}$$

where $\boldsymbol{z}$ = state vector and $\boldsymbol{y}$ = vector of measured outputs. Measurements available in this system to determine the control action are the absolute accelerations of all floors of the structure and the MR damper control forces. The ith MR damper can not be directly commanded to generate a specified force f_i, because its response is dependent on the local motion at the nodes of the structure where the MR damper is attached. By commanding the voltage v_i applied on the MR dampers through the current driver, forces can be increased or decreased. The next considerations should be taken into account in the design of control laws: (1). The control voltage to the ith device is bounded within the range $u_i = [0, u_{max}]$, (2). For a fixed set of states, the magnitude of the applied force $|f_i|$ increases when u_i increases and viceversa. (3). The unknown seismic excitation $\ddot{x}_g(t)$ is bounded by $|\ddot{x}_g(t)| \leq X_0$ for all $t \geq 0$ where X_0 is a known positive constant.

5.1.1 Semiactive Control Devices

The semiactive control device used here is the MR damper. A simple mechanical model for the MR damper such is shown in figure 5.1 has been previously developed and experimental results [109, 108] have demonstrated that it accurately predicts the behavior of a MR damper. The MR damper force is represented by means of the following equation:

$$f = \delta\Delta\dot{q} + \alpha z \tag{5.7}$$
$$\dot{z} = -\gamma|\Delta\dot{q}|z|z|^{n-1} - \beta\Delta\dot{q}|z|^n + A_a\Delta\dot{q} \tag{5.8}$$

with $\Delta q = q_i - q_j$ the difference of displacement at the ends of the device and z a evolutionary variable that accounts for the history dependence of the response. The parameters γ, β, n and A_a can be adjusted to control the linearity in the unloading and the smoothness of the transition from the pre-yield to the post-yield region.[21, 97]. The parameters of the MR damper generally depend on the commanding voltage signal u. Thus, for control purposes this dependence is formulated as

$$\alpha = \alpha(u) = \alpha_a + \alpha_b u \qquad \delta = \delta(u) = \delta_a + \delta_b u \tag{5.9}$$

The dynamics introduced by the current driver circuit are considered to be a first-order time lag in the response of the device to changes in the command input. It it is expressed as:

$$\dot{u} = -\eta(u - v) \tag{5.10}$$

where v is the command voltage applied to the control circuit.

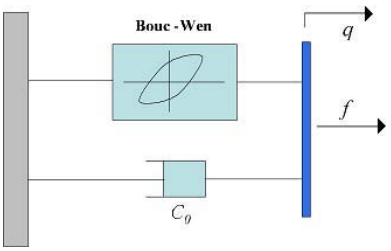

Figure 5.1: Mechanical model of the MR damper

5.1.2 Experimental Setup

An experimental model has been designed and constructed at the WUSCEEL research group. This test structure is a 6-story, single bay, steel frame, shown in the figure 5.2. The structure is 188 cm tall and has a mass of 147 kg, distributed uniformly among the floors. A couple of MR dampers is installed between the ground and first floor, and other couple between the first and second floors of the structure. The control force of the devices being applied to the structure is sensed by means of force transducers (PCB Piezotronics) placed in series with the MR damper. Absolute accelerations are measured at each floor of the structure by means of capacitive accelerometers (PCB Piezotronics, Depew, New York). The eight measurements obtained from these devices are those used by the controller. Data acquisition, control actions and system evaluation are implemented using a DSP-based real time control system by dSpace, Inc., Paderbon, Germany. This system includes a 16-bit 16-analog input PC board (DSP2003) and a 16-bit 8-analog output PC board (DSP2101).

Figure 5.2: Photograph of the test structure

The MR dampers used in the experiment are prototype devices, obtained from Lord Corp. for testing and evaluation. It consists of two steel parallel plates (see figure 5.4) whose dimensions are 4.45×1.9×2.5 cm. Forces are generated in the device when the moving plate, coated with a thin foam saturated with MR fluid, slides between the two parallel plates. An electromagnet consisting of a coil installed at one end of the devices, produces the magnetic field applied on the MR fluid of the saturated foam. The center plate of the device is 0.495 cm thick, resulting in a gap of 0.071 cm, thus a maximum force of 29 N can be generated by each device. Such force is approximately 1.6% the weight of the structure. Power is supplied to the device by means of a current amplifier where an output DC current between 0-1.2 Amp is present when an input voltage between 0-4 volts is applied.

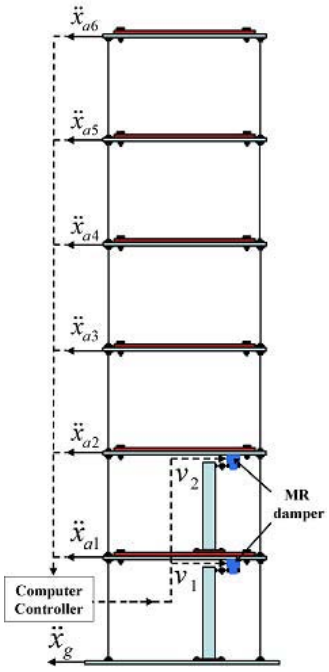

Figure 5.3: Schematic diagram of the test structure

Ground excitations are obtained by means of a uniaxial seismic simulator, which consists of a 1.5×1.5 m^2 aluminium sliding table (PEGASUS) mounted on high-precision, low friction, linear bearings. A schematic diagram of the experiment is presented in the figure 5.3.

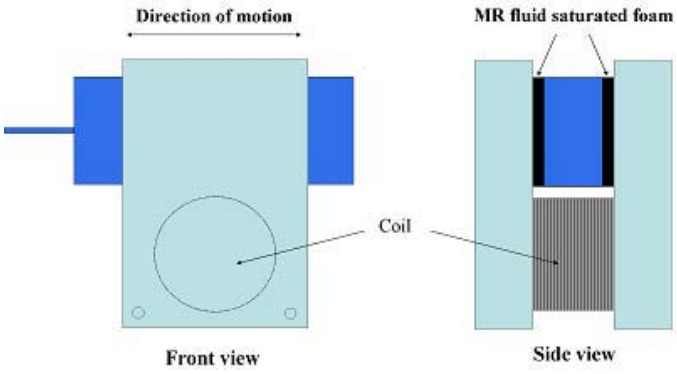

Figure 5.4: Schematic diagram of shear mode MR damper

5.1.3 Identification of the System

Identification of Test Structure

In order to identify the present MIMO system a hybrid identification technique is used. The reason to use a hybrid technique is due to that all the experimental input/output relationships

are not available in this kind of systems. An ideal situation for identification would be that all the input/output relationships (ground/ith floor acceleration and forces/ith floor acceleration) be available, however for this problem only ground/ith floor acceleration relationships are available. An analytical model is updated by using identified modal parameters and optimization algorithms in order to obtain closer real dynamics of the structure.

The methodology followed is: i). A white noise acceleration is used to excite the structure at the ground level. ii). Then, experimental transfer functions from the ground to the ith floor are obtained. iii). The Eigensystem Realization Algorithm (ERA) is applied to estimate the dynamic properties of the experimental structure (i.e. damping factors and natural frequencies). The finite impulse responses for each floor are required as inputs for the algorithm. Such responses are computed by applying the Inverse Fast Fourier Transform IFFT on each transfer function. iv). Based on the identified damping factors and natural frequencies, the mass and stiffness parameters of the analytical model are optimized by using the FMINCON function implemented in MATLAB and using as objective function the sum of the square error between the experimental and computed magnitude data at each frequency of the transfer functions. vi). Then damping matrix is optimized by using the same optimization function and defining as objective function the sum of the square errors between the experimental and computed acceleration values for each time sample, when a white noise excitation is applied at the ground during n seconds. The damping matrix is computed based on the method proposed in [34] whose equation is as follows:

$$\boldsymbol{C}_s = \boldsymbol{M}_s \boldsymbol{\Phi} \text{diag}(2\boldsymbol{h}_e[2\pi \boldsymbol{f}_e]) \boldsymbol{\Phi}^T \tag{5.11}$$

with $\boldsymbol{\Phi} = [\phi_1\ \phi_2\ \ldots\ \phi_n]$ the modal matrix, where ϕ_i are the eigenvectors of $\boldsymbol{M}_s^{-1}\boldsymbol{K}_s$, $\boldsymbol{f}_e$ are the frequencies and $\boldsymbol{h}_e$ the damping factors estimated by using the ERA. The initial parameters used to optimize the damping matrix correspond to the damping factors, while natural frequencies are maintained constant during the optimization. The identification process is graphically represented in the figure 5.5.

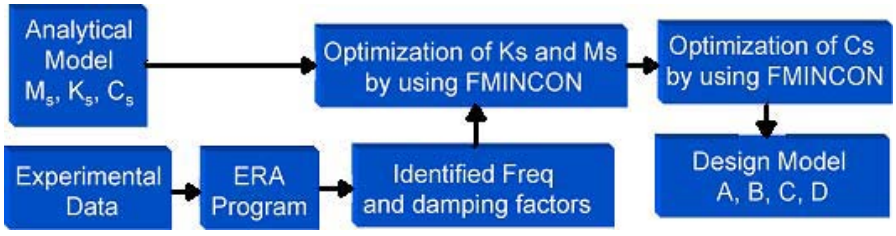

Figure 5.5: Schematic diagram of the procedure used to identify the structure

Obtention of the Analytical Model

In order to obtain an adequate model of the structure that can be used to control design purposes, the lumped-mass approach is considered. Thus, the linear equation (5.1) is used with stiffness of each floor k_i=273 (N/cm) and mass m_i=0.227 (N·s^2/cm). The natural damping factor was assumed 1% for each floor and the natural frequencies obtained are: [1.39 4.08 6.54 8.62 10.19 11.18] (Hz).

Obtention of experimental transfer functions

A white noise signal is used to excite the structure at the ground during 300 seconds. Accelerations of each floor and the ground are recorded and transfer functions from de ground acceleration to each floor acceleration are obtained directly from the data acquisition system.

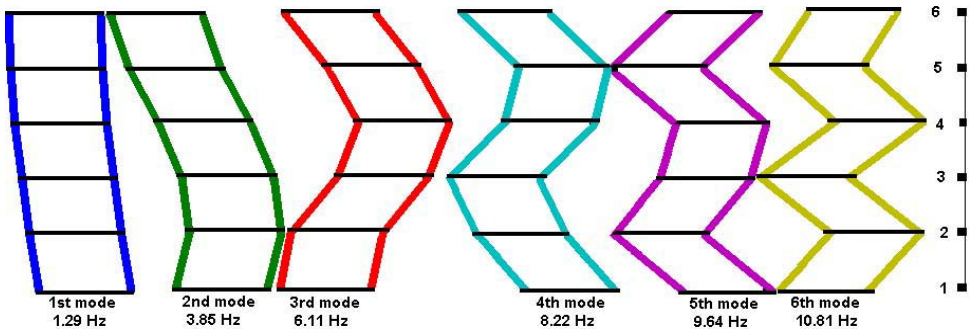

Figure 5.6: Mode shapes of the experimental structure

Estimation of modal parameters

The damping factors and natural frequencies of the experimental structure are estimated by using ERA. This algorithm consists in building a Hankel matrix by using the finite impulse responses of each floor and according to the number of poles used to represent the transfer functions [34]. In this case since the structure is 6-DOF, 12 poles are used. The natural frequencies and damping factors estimated are: [1.29 3.85 6.11 8.22 9.64 10.81] (Hz) and [1.38 0.71 0.64 0.56 0.48 0.91] (%). The identified mode shapes of the structure are shown in figure 5.6.

Optimization of M_s and K_s

Based on the mass and stiffness matrices obtained in the analytical model and the damping matrix obtained by using the equation (5.11), with the experimental damping factors and the analytical eigenvectors of $M_s^{-1}K_s$, the stiffness and mass parameters are optimized in order to obtain an analytical transfer function close to the experimental one. The FMINCON function implemented in MATLAB is used, with the analytical stiffness and mass parameters used as initial values and a objective function defined as the sum of the square errors between the the experimental and analytical transfer function magnitude at each analysis frequency. Because the last mode of the structure is close to 12 Hz, the transfer functions are analyzed up to 15 Hz. Figure 5.7 presents the plot of a transfer function (from ground acceleration to the fourth floor) obtained by using the experimental data, the analytical model, and the model with the optimized damping and mass parameters .

Optimization of C_s

After obtaining the optimal values for M_s and K_s, the damping factors are optimized by using the FMINCON function. The damping factors estimated with ERA are used as initial values and the objective function corresponds to the sum of the square errors resulting between the experimental and computed accelerations at each floor when a with white noise of length 30 seconds is used as ground acceleration. The resulting optimal damping factors are : [4.95 1.16 0.76 0.41 0.20 0.24]

%. Experimental natural frequencies are maintained constant and damping matrix is computed by using the equation (5.11). Figure 5.8 presents the experimental and computed, by using the optimized parameters of M_s, K_s and C_s, acceleration at the fourth floor for a withe noise ground acceleration.

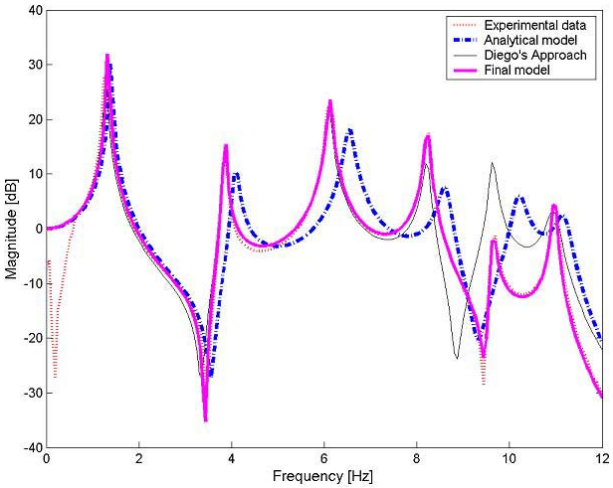

Figure 5.7: Analytical and experimental transfer functions from ground to fourth floor acceleration

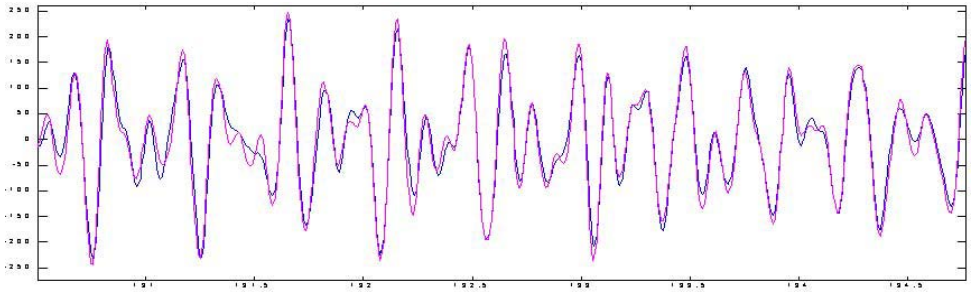

Figure 5.8: Analytical and experimental fourth floor acceleration minimizing Cs

5.1.4 Identification of MR dampers

The identification of the MR dampers consists of two stages. The first stage consists of identifying the MR dampers separately. It means to use an experimental configuration such that different kind of displacements can be applied to each device and experimental displacement, velocity and force measurements of the device are used to identify the parameters, based on the MR damper dynamics equations (5.7)-(5.10). The second stage consists in updating the MR damper parameters after being installed in the structure. In order to update such values, a variety of representative tests, including sinusoidal excitations at different frequencies and amplitudes being applied at the ground of the structure, are performed. Three configurations are studied: (1) Two MR dampers installed between the base and the first floor (2) Two MR dampers

installed between the first and second floor and (3) two MR dampers on each of the fist two floors of the structure. Forces generated in each MR damper and accelerations of each floor are recorded to identify and optimize the MR damper parameters. The FMINCON optimization function is used to determine the optimal values. The values obtained in stage 1 are used as initial values and the objective function is defined as the error between the experimental and predicted accelerations of all floors. Predicted responses are obtained using the optimal M_s, C_s and K_s matrices and updating the MR damper parameters of equations (5.7)-(5.10). The optimal parameters obtained are: δ_a=0.0454; δ_b=0.0195; A_a=12; γ=300; β=300; η=80;. While the parameters α_a and α_b varied between the four MR dampers in ranges of $\in [45, 60]$ and $\in [45, 90]$, respectively.

An integrated system model is obtained by using the optimal parameters of both structure and MR damper after being installed in the structure. Some graphic results are shown in the figures 5.9 and 5.10.

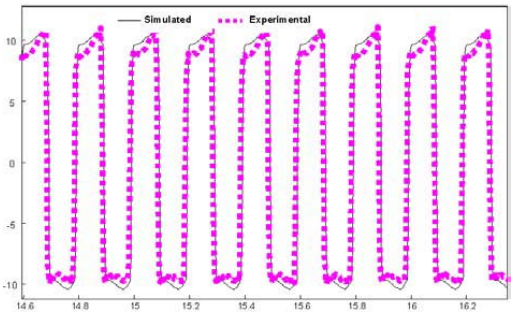

Figure 5.9: Experimental and simulated MR damper forces

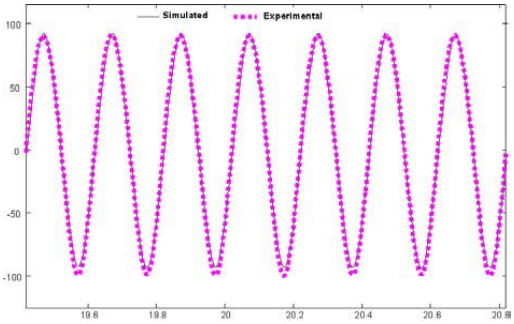

Figure 5.10: Experimental and simulated third floor acceleration with the optimized MR damper parameters

5.1.5 Semiactive Control Algorithms

Different semiactive control algorithms for this kind of control systems have been already studied [46, 47]. However, this study includes new control approaches based on Backstepping and QFT control techniques studied in chapter 4.

Backstepping Controller

Reordering equation (5.1), the motion equations for nodes 1 and 2, where the MR dampers are installed, are expressed as

$$\begin{aligned}\ddot{x}_1 &= -\frac{1}{m_1}\left[\sum_{i=2}^{n} m_i\ddot{x}_i + \sum_{i=1}^{n} m_i\ddot{x}_g + k_1x_1 + c_1\dot{x}_1 + f_1\right]\\ \ddot{x}_2 &= -\frac{1}{m_2}\left[\sum_{i=3}^{n} m_i\ddot{x}_i - k_1x_1 - c_1\dot{x}_1 + (k_1+k_2)x_2 + (c_1+c_2)\dot{x}_2 + f_2 + \sum_{i=2}^{n} m_i\ddot{x}_g\right]\end{aligned} \tag{5.12}$$

Rewrite the above dynamic equations into the following state equation:

$$\begin{aligned}\dot{y}_1 &= y_2 \qquad\qquad \dot{y}_3 = y_4\\ \dot{y}_2 &= -\frac{1}{m_1}\left[\sum_{i=2}^{n} m_i\ddot{x}_i + \sum_{i=1}^{n} m_i\ddot{x}_g + k_1y_1 + c_1y_2 + f_1\right]\\ \dot{y}_4 &= -\frac{1}{m_2}\left[\sum_{i=3}^{n} m_i\ddot{x}_i - k_1y_1 - c_1y_2 + (k_1+k_2)y_3 + (c_1+c_2)y_4 + f_2 + \sum_{i=2}^{n} m_i\ddot{x}_g\right]\end{aligned} \tag{5.13}$$

where $y_1 =: x_1$, $y_2 =: \dot{x_1}$, $y_3 =: x_2$ and $y_4 =: \dot{x_2}$.
The control objective is to design a backstepping controller such that the closed-loop system is globally stable and consequently the structural vibration is attenuated. Thus, the following standard variables, typically adopted in the literatures of backstepping control, are used for controller design:

$$\begin{array}{llll} e_1 = y_1; & \dot{e}_1 = y_2; & e_1\dot{e}_1 = e_1y_2; & \alpha_1 = -h_1e_1;\\ e_2 = y_2 - \alpha_1; & \dot{e}_2 = \dot{y}_2 + h_1y_2; & e_2\dot{e}_2 = e_2(\dot{y}_2 + h_1y_2) & \\ e_3 = y_3; & \dot{e}_3 = y_4; & e_3\dot{e}_3 = e_3y_4; & \alpha_2 = -h_3e_3;\\ e_4 = y_4 - \alpha_2; & \dot{e}_4 = \dot{y}_4 + h_3y_4; & e_4\dot{e}_4 = e_4(\dot{y}_4 + h_3y_4) & \end{array} \tag{5.14}$$

By replacing (5.13) into (5.14) and (5.14) it is obtained:

$$\begin{aligned} e_2\dot{e}_2 &= -\frac{e_2}{m_1}\left[\sum_{i=2}^{n} m_i\ddot{x}_i + \sum_{i=1}^{n} m_i\ddot{x}_g + k_1y_1 + (c_1 - m_1h_1)y_2 + f_1\right]\\ e_4\dot{e}_4 &= -\frac{e_4}{m_2}\left[\sum_{i=3}^{n} m_i\ddot{x}_i + \sum_{i=2}^{n} m_i\ddot{x}_g - k_1y_1 - c_1y_2 + (k_1+k_2)y_3 + (c_1+c_2-m_2h_3)y_4 + f_2\right]\end{aligned} \tag{5.15}$$

In order to achieve the asymptotic error suppression, the following control law is derived

$$f_1 = -\sum_{i=2}^{n} m_i\ddot{x}_i - \sum_{i=1}^{n} m_i\ddot{x}_g - k_1y_1 - (c_1 - m_1h_1)y_2 + m_1e_1 \tag{5.16}$$

$$f_2 = -\sum_{i=3}^{n} m_i\ddot{x}_i - \sum_{i=2}^{n} m_i\ddot{x}_g + k_1y_1 + c_1y_2 - (k_1+k_2)y_3 - (c_1+c_2)y_4 + m_2e_3 \tag{5.17}$$

However, the control laws 5.16 and 5.17 are not implementable in practice since they contain unmeasurable variables, such as z, $\ddot{x}_g$ and states. Ground acceleration is considered uncertain but bounded, while states are estimated using a Kalman state estimator. On other hand, a voltage command in place of a force command is required for the MR dampers. In order to overcome this problem, two control law approaches are used. The first controller computes the equivalent command voltage based on the equation (5.7), the force value obtained from (5.16 and 5.17) and

a estimated value of the evolutionary z. The controller 2 uses the modified Clipped-Optimal control algorithm used in [109] to compute the equivalent command voltage.

Backstepping Controller 1 (BE_1)

By using (5.7) and (5.9), and the desired force values f_1 and f_2 obtained in (5.16) and (5.17) the following control law is obtained:

$$u_i = \frac{f_i - \alpha_{a_i} z_i + \delta_{a_i} \Delta y_i}{\alpha_{b_i} z_i + \delta_{b_i} \Delta y_i}; \quad i = 1, 2 \tag{5.18}$$

with $\Delta y_1 = y_2$ and $\Delta y_2 = y_4 - y_2$. Since the variable z_i cannot be directly measured, an estimated value $\hat{z}_i$ is obtained:

$$\dot{\hat{z}}_i = -\gamma_i |\Delta y_i| \hat{z}_i |\hat{z}_i|^{n-1} - \beta_i \Delta y_i |\hat{z}_i|^n + A_i \Delta y_i \tag{5.19}$$

Define $\tilde{z}_i = z_i - \hat{z}_i$ as the estimation error between the real value z_i and the estimated value $\hat{z}_i$, then

$$z_i = \tilde{z}_i + \hat{z}_i; \qquad \dot{\tilde{z}}_i = \dot{z}_i - \dot{\hat{z}}_i \tag{5.20}$$

By taking $\tilde{z}_1 = e_2$, $\tilde{z}_2 = e_4$, the denominator of the commanding voltage signals u_1 and u_2 can be replaced by $\delta_{b_1} y_2 + \alpha_{b_1} \hat{z}_1 + \alpha_{b_1} \tilde{z}_1 = \delta_{b_1} y_2 + \alpha_{b_1} \hat{z}_1 + \alpha_{b_1} e_2$ and $\delta_{b_2}(y_4 - y_2) + \alpha_{b_2} \hat{z}_2 + \alpha_{b_2} \tilde{z}_2 = \delta_{b_2}(y_4 - y_2) + \alpha_{b_2} \hat{z}_2 + \alpha_{b_2} e_4$.
Now, an implementable law, based upon the bounded values of X_0 and the estimated values of z_i, is adopted for the backstepping control:

$$u_1 = \frac{1}{\alpha_{b_1}(\hat{z}_1 + e_2) + \delta_{b_1} y_2} \left[-\sum_{i=2}^{n} m_i \ddot{x}_i - k_1 y_1 - (-m_1 h_1 c_1 + \delta_{a_1}) y_2 + m_1 e_1 - \alpha_{a_1} z_1 - \sum_{i=1}^{n} m_i X_0 sgn(e_2) \right] \tag{5.21}$$

$$u_2 = \frac{1}{\alpha_{b_2}(\hat{z}_2 + e_4) + \delta_{b_2}(y_4 - y_2)} \left[-\sum_{i=3}^{n} m_i \ddot{x}_i + k_1 y_1 + (c_1 + \delta_{a_2}) y_2 - (k_1 + k_2) y_3 - (c_1 + c_2 + \delta_{a_2}) y_4 - \alpha_{a_2} z_2 + m_2 e_3 - \sum_{i=2}^{n} m_i X_0 sgn(e_4) \right] \tag{5.22}$$

for all $\alpha_{b_1}(\hat{z}_1 + e_2) + \delta_{b_1} y_2 \neq 0$ and $\alpha_{b_2}(\hat{z}_2 + e_4) + \delta_{b_2}(y_4 - y_2) \neq 0$, otherwise $u_i = 0$. Moreover, for some types of MR dampers [21]-[97], the constraints $\gamma \geq \beta \geq 0$ and $n = 1$ must be satisfied by the control law.

Stability Analysis
In order to verify the closed-loop stability, the following Lyapunov function candidate is defined:

$$V = \frac{1}{2} e_1^2 + \frac{1}{2} e_2^2 + \frac{1}{2} e_3^2 + \frac{1}{2} e_4^2 + \frac{1}{2} \tilde{z}_1^2 + \frac{1}{2} \tilde{z}_2^2 \tag{5.23}$$

$$\dot{V} = e_1 \dot{e}_1 + e_2 \dot{e}_2 + e_3 \dot{e}_3 + e_4 \dot{e}_4 + \tilde{z}_1 \dot{\tilde{z}}_1 + \tilde{z}_2 \dot{\tilde{z}}_2 \tag{5.24}$$

From equations (5.15)-(5.17), (5.21)-(5.22), one obtains:

$$e_1 \dot{e}_1 = e_1 y_2 \qquad e_3 \dot{e}_3 = e_3 y_4$$

$$e_2\dot{e}_2 = -\frac{e_2}{m_1}\left[-\sum_{i=1}^{n} m_i[\ddot{x}_g - X_0 sgn(e_2)] + \alpha_{a_1}\tilde{z}_1 + m_1 e_1\right] \quad (5.25)$$

$$= -\frac{1}{m_1}\sum_{i=1}^{n} m_i[X_0|e_2| - \ddot{x}_g e_2] - e_1 e_2 - h_2 e_2^2$$

$$e_4\dot{e}_4 = -\frac{e_4}{m_2}\left[\sum_{i=2}^{n}[\ddot{x}_g - X_0 sgn(e_4)] + \alpha_{a_2}\tilde{z}_2 + m_2 e_3\right] \quad (5.26)$$

$$= -\frac{1}{m_2}\sum_{i=2}^{n} m_i[X_0|e_4| - \ddot{x}_g e_4] - e_3 e_4 - h_4 e_4^2$$

with $h_2 = \dfrac{\alpha_{a_1}}{m_1}$ and $h_4 = \dfrac{\alpha_{a_2}}{m_2}$.
From equations (5.8), (5.19)-(5.20), one gets:

$$\tilde{z}_i\dot{\tilde{z}}_i = \tilde{z}_i\left(\dot{z}_i - \dot{\hat{z}}_i\right) = -\tilde{z}_i\left[\gamma_i|\Delta y_i|\left(z_i|z_i|^{n-1} - \hat{z}_i|\hat{z}_i|^{n-1}\right) - \beta_i\Delta y_i\left(|z|^n - |\hat{z}_i|^n\right)\right] \quad (5.27)$$

For $n = 1$,

$$\tilde{z}_i\dot{\tilde{z}}_i = -\gamma_i|\Delta y_i|\tilde{z}_i^2 - \beta_i\Delta y_i\tilde{z}_i\left(|z_i| - |\hat{z}_i|\right) \leq -\left(\gamma_i - \beta_i\right)|\Delta y_i|\tilde{z}_i^2 \leq 0 \quad (5.28)$$

Finally, the derivative Lyapunov function becomes:

$$\dot{V} = -\frac{1}{m_1}\sum_{i=1}^{n} m_i\left[X_0|e_2| - \ddot{x}_g e_2\right] - \frac{1}{m_2}\sum_{i=2}^{n} m_i\left[X_0|e_4| - \ddot{x}_g e_4\right] - h_2 e_2^2 - h_4 e_4^2 - \left(\gamma_1 - \beta_1\right)|y_2|\tilde{z}_1^2 -$$
$$\left(\gamma_2 - \beta_2\right)|y_4 - y_2|\tilde{z}_2^2 \leq 0 \quad (5.29)$$

Therefore, stability of the closed-loop system is ensured.

Backstepping Controller 2 (BE_2)
The controller consists in to use the desired forces f_1 and f_2 obtained in 5.16 and 5.17, respectively, and to obtain an equivalent command voltage by using the modified clipped-optimal technique. This technique was proposed in [18] for controlling a single MR damper and in [19] for multiple MR devices, and experimentally verified in [107]. This algorithm consists in appending m force feedback loops to induce each MR damper to produce approximately a desired control force. Then, a command voltage signal is obtained as follows: When the i-th MR damper is providing the desired optimal force (i.e. $f_i = f_{c_i}$) the voltage applied to the MR damper should remain at the present value. If the magnitude of the desired optimal force is between the minimal force f_{0_i} and the maximum force f_{max_i}, and the two forces have the same sign, the voltage applied to the current driver is derived from a linear relation, experimentally obtained, between the output force and the input voltage which takes the form: $f_i = f_{0_i} + m(u_i - u_{0_i})$. Otherwise, the commanded voltage is set to zero. Thus, the control law for the i-th MR damper, using the modified clipped-optimal is stated as:

$$\begin{cases} u_i = u_{0_i} + m^{-1}(f_i - f_{0_i}) & \text{if } \begin{cases} \text{sgn}(f_i) = \text{sgn}(f_{c_i}) \\ |f_{0_i}| \leq |f_{c_i}| \leq |f_{i_{max}}| \end{cases} \\ u_i = u_{max} & \text{if } \begin{cases} \text{sgn}(f_i) = \text{sgn}(f_{c_i}) \\ |f_{c_i}| > |f_{i_{max}}| \end{cases} \\ u_i = 0 & \text{otherwise} \end{cases}$$

This control approach is graphically represented in figure 5.11

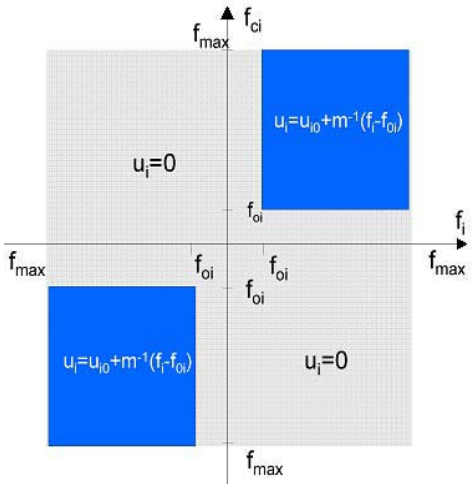

Figure 5.11: Graphical representation of the Clipped-Optimal control technique

QFT Controller

a QFT controller is implemented in order to avoid destructive structural vibration modes. The objective is to reduce vibrations produced by an uncertain disturbance acting at the base of the structure and that could excite the structure at the natural frequencies. Because MR damper contains nonlinearities, a hybrid approach is used. It consists in finding a desired command force based on QFT design and computing the equivalent command voltage based on the modified clipped-optimal control technique. Two controllers are implemented in order to exploit some of the advantages offered by QFT. The design of the first controller based on the analytical model, while the design of second controller is based on experimental transfer functions from the ground to the first floor and from the ground to second floor.
The next considerations are taken into account for control design purposes:
i) The mass, damping and stiffness parameters for the first and second floor are considered unknown values varying between [0.97 1.03] times their nominal value (i.e. $m_i = [0.971.03]{*}m_{i_N}$, $c_i = [0.971.03] * c_{i_N}$ and $k_i = [0.971.03] * k_{i_N}$, for i=1,2).
ii). The earthquake acceleration is considered as uncertain but bounded; i.e. $|\ddot{x}_g(t)| \leq X - 0$ for all $t \geq 0$.
iii). Only acceleration measurements in each floor are available. A noise percentage of 5% is considered in this measurements.
The design specifications for the QFT controller are:
i) The magnitude of the transfer functions from the ground to the first and second floor for the controlled structure must be less than 60% of the uncontrolled structure.
ii) The acceleration for floors 1 and 2 must be less than 0.01g when noise is present in the feedback signal measurement.

QFT Controller 1 (QFT_1)
By rewriting the motion equations of the structure for the first and second floor we have:

$$m_1\ddot{x}_1 + c_1\dot{x}_1 + k_1x_1 = \sum_{i=2}^{6} m_i\ddot{x}_i + \sum_{i=1}^{6} m_i\ddot{x}_g - f_1 \tag{5.30}$$

$$m_2\ddot{x}_2 + c_2(\dot{x}_2 - \dot{x}_1) + k_2(x_2 - x_1) = \sum_{i=3}^{6} m_i\ddot{x}_i + \sum_{i=2}^{6} m_i\ddot{x}_g - f_2 \tag{5.31}$$

Transforming the above equations to the laplace domain:

$$\ddot{x}_1(s) = \frac{s^2}{m_1s^2 + c_1s + k_1}\left[\sum_{i=1}^{6} m_i\ddot{x}_g - \left(\sum_{i=2}^{6} m_i\ddot{x}_i + f_1\right)\right] \tag{5.32}$$

$$\ddot{x}_2(s) = \frac{s^2}{m_2s^2 + c_2s + k_2}\left[\sum_{i=2}^{6} m_i\ddot{x}_g - \left(\sum_{i=3}^{6} m_i\ddot{x}_i + f_2 - (c_2s + k_2)\ddot{x}_1(s)\right)\right] \tag{5.33}$$

By following the structure of the LTI system presented in figure 5.12 two controllers G_1 and G_2, for controlling plants P_1 and P_2,respectively, are designed.

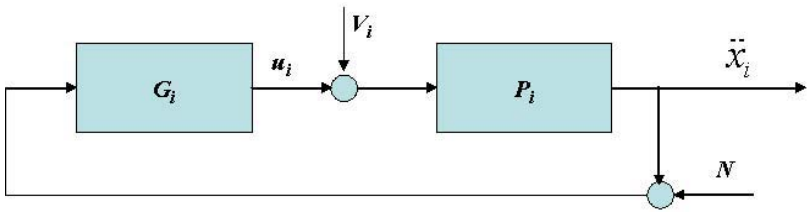

Figure 5.12: LTI system for floors 1 and 2 and using the analytical model

The transfer functions for such plants are derived from equations (5.32) and (5.33) as:

$$P_1(s) = \frac{s^2}{m_1s^2 + c_1s + k_1} \qquad P_2(s) = \frac{s^2}{m_2s^2 + c_2s + k_2} \tag{5.34}$$

The control inputs $u_1 = G_1\ddot{x}_1$ and $u_2 = G_2\ddot{x}_2$ are related with the desired forces for the floors 1 and 2 by means of the following equations:

$$u_1 = \sum_{i=1}^{6} m_i\ddot{x}_g + f_1 \tag{5.35}$$

$$u_2 = \sum_{i=3}^{6} m_i\ddot{x}_i + f_2 - (c_2s + k_2)\ddot{x}_1 \tag{5.36}$$

Thus the desired forces f_1 and f_2 can be found by manipulating the above equations. The terms of the right hand of equations (5.35)-(5.36), related with the ground acceleration ($\sum_{i=j}^{6} m_i\ddot{x}_g$, j=1,2), are considered as a unknown disturbances at input of the plant with maximum values of ($D_1 = \sum_{i=1}^{6} \max(m_i)X_0$, $D_2 = \sum_{i=2}^{6} \max(m_i)X_0$).
By using the QFT MATLAB Toolbox the final loops $L_1 = G_1P_1$ and $L_2 = G_2P_2$ are obtained. They are shown in figures 5.13 and 5.14.

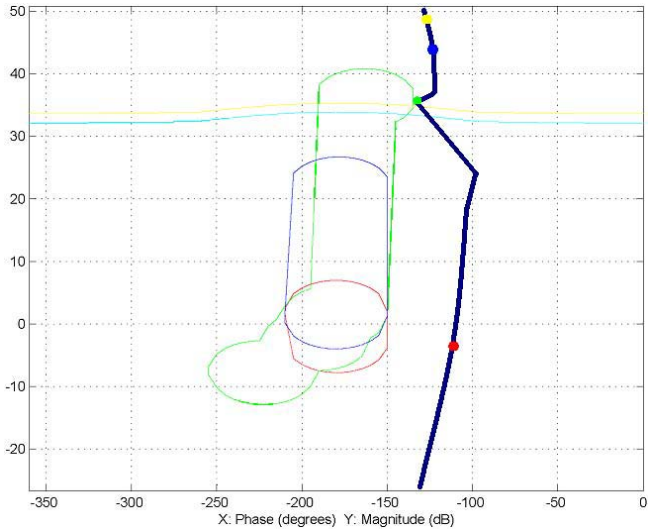

Figure 5.13: Final loop L_N for G_1

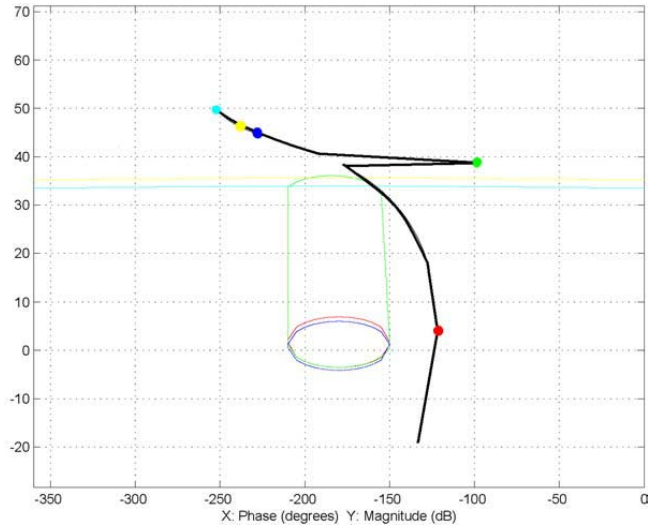

Figure 5.14: Final loop L_N for G_2

The controllers G_1 and G_2 derived from the final loops L_1 and L_2 are respectively:

$$G_1 = 0.674\frac{0.1225s^2 + 1.122s + 1}{0.01118s^3 + 0.0186s^2 + 1.007s + 1} \qquad G_2 = 0.8\frac{0.4127s^2 + 1.413^s + 1}{0.0009s^3 + 0.0321s^2 + 1.031s + 1}$$

Finally, the command voltage is found by using the modified clipped-optimal technique and based on the desired command forces computed from the equations (5.35) and (5.36).

QFT Controller 2 (QFT_2)

The design of the second QFT controller is based on the experimental transfer functions from the ground acceleration to the each floor where the MR dampers are installed (floors 1 and 2). As shown in figure 5.15, a disturbance V related with the ground acceleration is presented at the input of each plant, while the control signal U for each plant is related with the desired control forces by means of the following equations:

$$u_1(s) = G_1(s)\ddot{x}_1(s) = f_1 - f_2 \tag{5.37}$$

$$u_2(s) = G_2(s)\ddot{x}_2(s) = f_2 \tag{5.38}$$

By using equations (5.37) and (5.38), the desired command forces f_1 and f_2 are obtained.

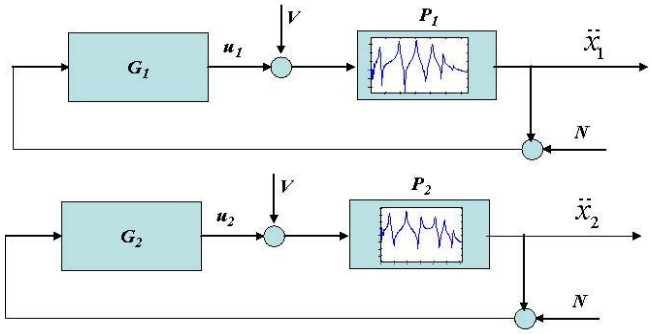

Figure 5.15: LTI system for floors 1 and 2 and using the experimental transfer functions

The final loops obtained for G_1 and G_2 are shown in figures 5.16 and 5.17, repesctively.

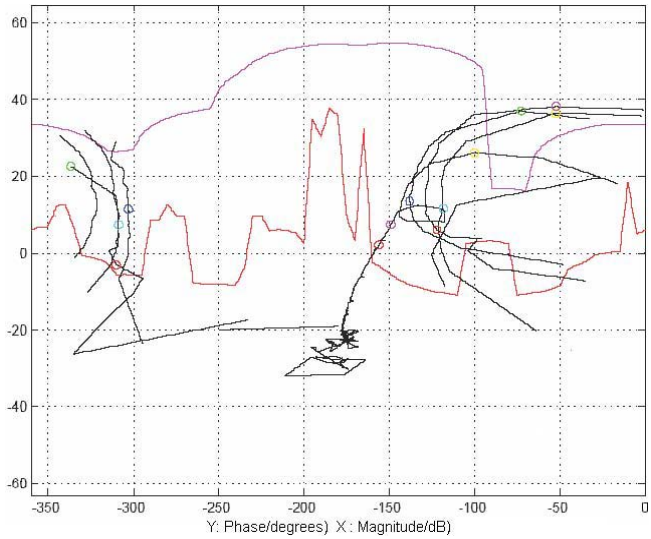

Figure 5.16: Final Loop L_N for the controller G_1

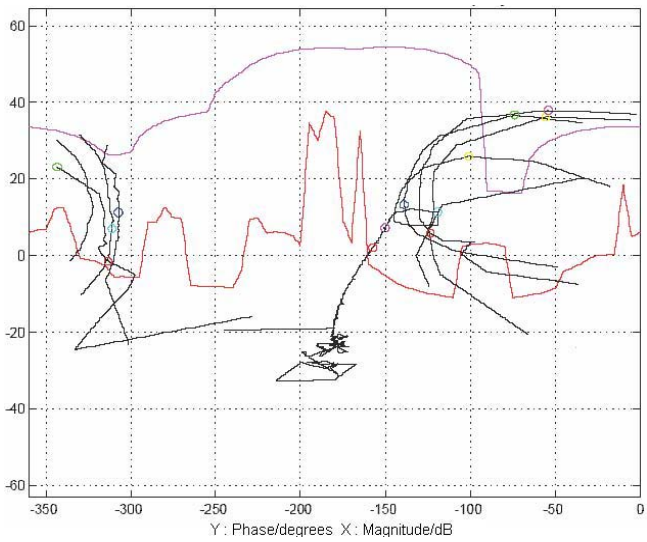

Figure 5.17: Final Loop L_N for the controller G_2

The transfer functions G_1 and G_2 derived from the final loops L_1 and L_2, respectively, are the following:

$$G_1 = 0.4\frac{0.2532s^3 + 1.453s^2 + 2.2s + 1}{0.07983s^3 + 0.6449s^2 + 1.565s + 1} \qquad G_2 = 0.4\frac{0.3689s^3 + 1.935s^2 + 2.566s + 1}{0.101s^3 + 0.7366s^2 + 1.636s + 1} \tag{5.39}$$

5.1.6 Experimental Results

The semiactive backstepping and QFT controllers are implemented on the 6-story test building. Four kind of excitations are applied on the structure, three earthquakes (*El Centro*, Gebze and Mexico) and a random white noise acceleration, in order to demonstrate the effectiveness and robustness of the controllers. For *El Centro* earthquake acceleration three excitation amplitudes (50, 100 and 125 % of its nominal value, referred as low, medium and high), are applied in order to analyze the performance of the control system for different amplitude levels. Additionally, two additional controllers (Lyapunov stability theory controller and Sliding Mode Controller) and passive *on* state MR damper configuration are implemented in order to compare the performance of the proposed controllers. Quantitative evaluation of the controllers is made by using five evaluation criteria [93]. The first evaluation criterion considers the normalized peak floor accelerations

$$J_1 = \max_{i,t}\left(\frac{|\ddot{x}_{ai}(t)|}{\ddot{x}_a^{max}}\right) \tag{5.40}$$

where the absolute acceleration of the ith floor of the structure $\ddot{x}_{ai}(t)$ is normalized by the maximum peak acceleration presented in the structure in the uncontrolled configuration and denote as $\ddot{x}_a^{max}$.
The second evaluation criterion considers the normed peak floor acceleration response

$$J_2 = \max_{i,t}\left(\frac{\|\ddot{x}_{ai}(t)\|}{\|\ddot{x}_a^{max}\|}\right) \tag{5.41}$$

Table 5.1: Uncontrolled Structural Responses

Amplitude	$\lvert\ddot{x}_a^{max}\rvert$	$\lVert\ddot{x}_a^{max}\rVert$	$\lvert F_b^{max}\rvert$	$\lVert F_b^{max}\rVert$
El Centro Earthquake				
Low	113,86	2396	34,6	781
Medium	229,14	4254	66,8	1495
High	351,12	6564	96,9	2244
Gebze Earthquake				
Low	89,7	1572	29,6	2866
Medium	111,27	1872	55,3	4603
High	237,6	3470	49,3	5318
Mexico Earthquake				
Low	397,9	995	107,9	1313
Medium	864,7	2085	188,2	2190

where $\|\ddot{x}_{ai}(t)\| = \sqrt{\int_0^{tf} \ddot{x}_{ai}^2(t)dt}$; and the absolute accelerations of the ith floor $\ddot{x}_{ai}(t)$, are normalized by $\|\ddot{x}_a^{max}\|$.
The third evaluation criterion considers the maximum base shear generated in the controlled configuration

$$J_3 = \max_t \left| \sum_{i=1}^{6} \frac{m_i \ddot{x}_{ai}(t)}{F_b^{max}} \right| \tag{5.42}$$

where F_b^{max} is the maximum base shear in the uncontrolled configuration.
The fourth evaluation criterion corresponds to the normed/nondimensionalized base shear.

$$J_4 = \frac{\left\| \left| \sum_{i=1}^{6} m_i \ddot{x}_{ai}(t) \right| \right\|}{\|F_b^{max}\|} \tag{5.43}$$

where $\|F_b^{max}\| = \left\| \left| \sum_{i=1}^{6} m_i \ddot{x}_{ai}(t) \right| \right\|$ is the maximum normed uncontrolled base shear.
And the fifth evaluation criterion used here is a measure of the maximum control force per device, given by

$$J_5 = \max_{t,i} \left(\frac{|f_i(t)|}{W} \right) \tag{5.44}$$

where $f_i(t)$ is the force generated by the ith control device over the time story of each earthquake and W = 1,446 N = weight of the structure.

Figures 5.20 and 5.21 show the response profiles of the peak acceleration measurements for low and medium levels of *El Centro* earthquake, while figure 5.22 and 5.23 show those of high levels of Mexico and Gebze earthquake, respectively. The above figures show clearly the effectiveness of the controllers proposed for different kind of earthquakes. Additionally it is seen that peak responses are reduced for all the floors of the structure. The passive-on configuration results in general improves the structural responses with respect to the uncontrolled case, however in the particular case for *El Centro* low amplitude, the third criterion is worst. This means that structural responses are not ever improved by maintaining the MR dampers in a constant voltage. For different types and levels of excitation, the proposed controllers perform

better than the passive-on case and significant vibration reduction is obtained. The backstepping controllers improve the structural response in a similar way than the Sliding Mode Controller or Lyapunov controller, while the QFT controllers improve the structural responses better than the others controllers implemented. For *El Centro* and Low amplitude Gebze earthquakes the controller QFT_1 reduction of the normed peak acceleration (evaluation criterion J_1) is under 50%, while for Medium and high amplitude Gebze and Mexico earthquakes the reduction is under 63%. The QFT_2 controller is the second best for the evaluation criterion J_1. In general, the same behaviour is observed for the evaluation criteria J_2 to J_4. According to evaluation criteria J_5, small control forces are required for all the semiactive control configurations implemented and they result to be in general smaller than the passive-on case. Figures 5.18-5.19 show the time history of the third and sixth floor acceleration, respectively, for a small excitation of El Centro earthquake. It is seen that no only the peak responses are reduced, but also the response throughout the earthquake. In general, the same behaviour is observed for all the controllers implemented.

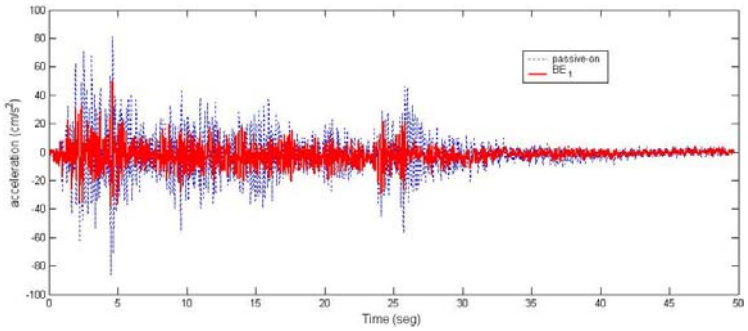

Figure 5.18: Third floor acceleration for small amplitude El Centro earthquake

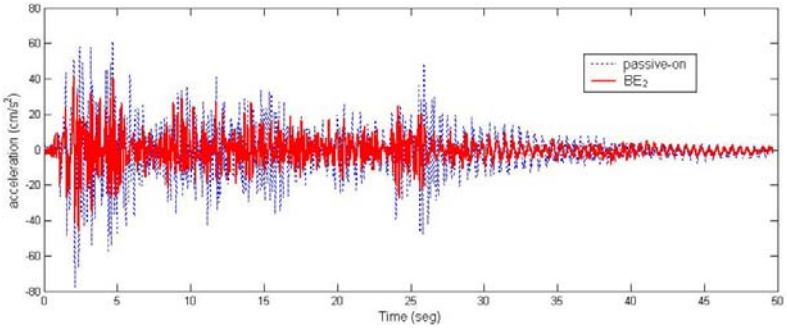

Figure 5.19: Sixth floor acceleration for small amplitude El Centro earthquake

Table 5.2: Normalized Experimental Responses

Control strategy	J_1	J_2	J_3	J_4	J_5
Low amplitude El Centro earthquake					
Passive on	0,8159	0,4256	1,1107	0,5711	0,0499
BE+Clipped	0,6252	0,4080	0,8519	0,7654	0,0432
BE+$\hat{z}$	0,6554	0,3432	0,8063	0,4298	0,0078
QFT_1	0,4179	0,2525	0,4296	0,3158	0,0241
QFT_2	0,4748	0,2430	0,5472	0,3318	0,0155
Lyapunov	0,7965	0,3997	0,8462	0,5341	0,0507
SMC	0,6149	0,3557	0,8447	0,5342	0,0380
Medium Amplitude El Centro earthquake					
Passive on	0,6350	0,2804	0,6077	0,3244	0,0159
BE+Clipped	0,5178	0,3533	0,6649	0,6090	0,0440
BE+$\hat{z}$	0,5802	0,3637	0,6993	0,4507	0,0516
QFT_1	0,4633	0,2428	0,5574	0,3120	0,0451
QFT_2	0,5262	0,2691	0,5938	0,3197	0,0269
Lyapunov	0,6182	0,4009	0,8462	0,4960	0,0566
SMC	0,5639	0,3282	0,5999	0,4262	0,0457
High amplitude El Centro earthquake					
Passive on	0,6965	0,2996	0,7183	0,3369	0,0146
BE+Clipped	0,5119	0,3050	0,6229	0,5264	0,0428
BE+$\hat{z}$	0,5705	0,3046	0,6105	0,3727	0,0554
QFT_1	0,4720	0,2283	0,5889	0,3003	0,0491
QFT_2	0,5747	0,2581	0,6692	0,3116	0,0389
Lyapunov	0,5259	0,3382	0,6898	0,4221	0,0570
SMC	0,4846	0,2917	0,5617	0,3673	0,0423
Low amplitude Gebze earthquake					
Passive on	0,8250	0,4530	0,8423	0,5252	0,0407
BE+Clipped	0.6123	0.3021	0.4122	0.3342	0.0128
BE+$\hat{z}$	0,6054	0,3126	0,4052	0,3521	0,0227
QFT_1	0,4105	0,2394	0,3974	0,2521	0,0149
QFT_2	0,4051	0,2470	0,3855	0,2700	0,0144
Lyapunov	0,7902	0,3793	0,6567	0,4053	0,0348
SMC	0,5897	0,3087	0,3973	0,3234	0,0512

Table 5.3: Normalized Experimental Responses Part 2

Control strategy	J_1	J_2	J_3	J_4	J_5
Medium amplitude Gebze earthquake					
Passive-on	0,8236	0,4985	0,7654	0,4567	0,0360
BE+Clipped	0,6296	0,3399	0,4065	0,2055	0,0143
BE+$\hat{z}$	0,6026	0,3432	0,4158	0,1998	0,0192
QFT_1	0,6258	0,3418	0,4197	0,2236	0,0101
QFT_2	0,6165	0,3365	0,4203	0,2173	0,0103
Lyapunov	0,8721	0,5091	0,7089	0,3844	0,0407
SMC	0,6070	0,3296	0,3951	0,2085	0,0360
High amplitude Gebze earthquake					
Passive-on	0,6250	0,4250	0,7856	0,5254	0,0472
BE+Clipped	0,4766	0,3451	0,7658	0,5433	0,0378
BE+$\hat{z}$	0,4666	0,3513	0,7342	0,5332	0,042
QFT_1	0,3661	0,2469	0,4971	0,3434	0,0383
QFT_2	0,4020	0,2647	0,5018	0,3282	0,0192
Lyapunov	0,5689	0,3642	0,6465	0,4434	0,0432
SMC	0,4793	0,3520	0,7471	0,5810	0,0415
Low amplitude Mexico earthquake					
Passive-on	0,6892	0,4527	0,6987	0,4876	0,0551
BE+Clipped	0,6148	0,3871	0,5839	0,4168	0,0496
BE+$\hat{z}$	0,6027	0,3928	0,5921	0,4063	0,0462
QFT_1	0,5256	0,3044	0,5880	0,3617	0,0532
QFT_2	0,5273	0,3005	0,5838	0,3578	0,0489
Lyapunov	0,6720	0,4042	0,6250	0,4523	0,0312
SMC	0,6232	0,3526	0,5382	0,0.4025	0,0501
High amplitude Mexico earthquake					
Passive-on	0,5983	0,3675	0,6910	0,4859	0,0652
BE+Clipped	0,5954	0,3601	0,6812	0,4771	0,0668
BE+$\hat{z}$	0,6126	0,3734	0,6621	0,4523	0,0557
QFT_1	0,5630	0,3208	0,6641	0,4507	0,0596
QFT_2	0,6382	0,3536	0,6757	0,4485	0,0536
Lyapunov	0.5921	0.3521	0.6823	0.4725	0.0572
SMC	0,6042	0,3642	0,6817	0,4806	0,0585

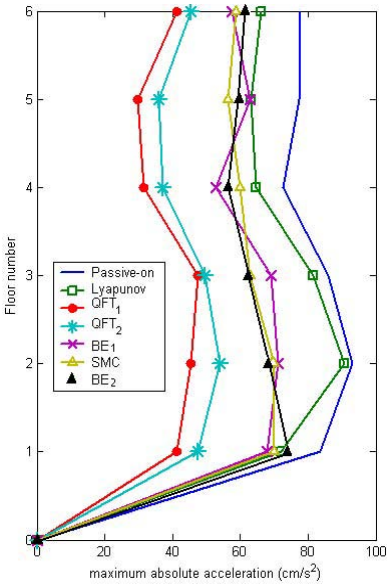

Figure 5.20: Peak absolute acceleration profiles for Low Amplitude El Centro

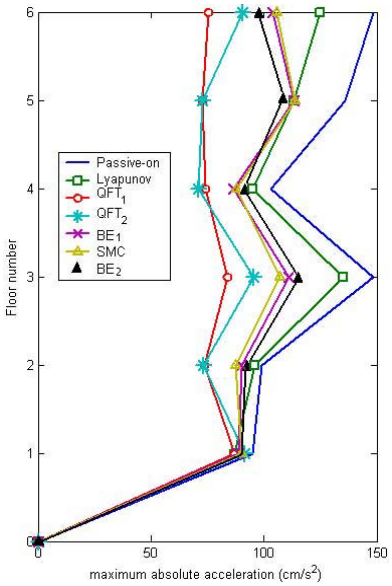

Figure 5.22: Peak absolute acceleration profiles for high Gebze earthquake

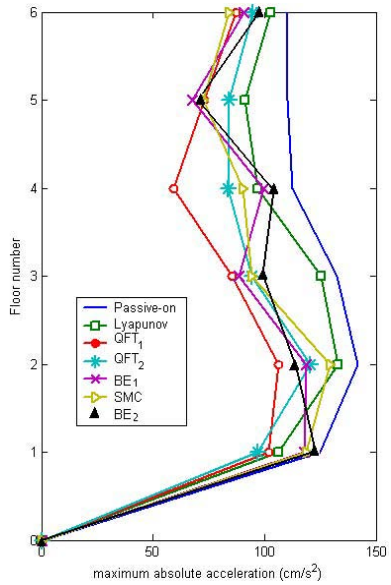

Figure 5.21: Peak absolute acceleration profiles for Medium Amplitude El Centro

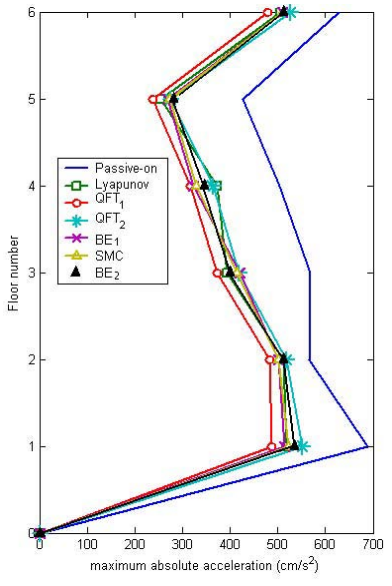

Figure 5.23: Peak absolute acceleration profiles for High Mexico earthquake

5.2 Experiment Prototype 2 : Pseudo-dynamic test sub-structure

Consider a semi-actively controlled two-span bridge with two columns and two joints. The total length of the bridge is 150m. At each joint between the column and the super-structure, there is a Controllable Friction Device (CFD) put in parallel to the elastomeric bearings as illustrated in Figure 4.24.

The model of the bridge has 3 degree of freedom (DOF) in the directions (x,y,z) at each node. However, for experimental tests, only the dynamic behavior of the beam structure in the transversal direction y, where the seismic excitation and control forces are applied, will be studied. A finite element model is obtained and its graphical representation is shown in figure 4.25. The CFDs are located between the nodes 1 and 3 and the nodes 2 and 5, respectively, which are referred to as controlled nodes since they are the only nodes directly influenced by CFDs. After the model reduction by using static condensation, the dynamic behavior of the beam structure is described by the following equation:

$$\boldsymbol{M}\ddot{\boldsymbol{x}} + \boldsymbol{C}\dot{\boldsymbol{x}} + \boldsymbol{K}\boldsymbol{x} = \boldsymbol{F}(t) \tag{5.45}$$

where $\boldsymbol{M}$, $\boldsymbol{C}$ and $\boldsymbol{K}$ are the (10x10) positive definite mass, damping and stiffness matrices, respectively. $\boldsymbol{M}$=diag(m_i) and $\boldsymbol{C} = \alpha\boldsymbol{M} + \beta K$, according to the Rayleigh-damping relation and with α and β being some positive constants. The vector $\boldsymbol{x}$=[x$_1$, x$_2$,. . .,x$_{10}$]^T represents the displacements of each node at the bridge with respect to an inertial frame. $\boldsymbol{F}(t) = \boldsymbol{M}\ddot{x}_g(t)+\Phi(t)$ are external forces induced by the seismic acceleration $\ddot{x}_g(t)$ and supplied by the CFDs with $\Phi(t)$=[-$\phi_{1,3}(t)$, -$\phi_{2,5}(t)$, $\phi_{1,3}(t)$, 0, $\phi_{2,5}(t)$, 0, 0, 0, 0, 0]^T

The CFD is the friction device UHYDE-fbr, which dissipates energy due to solid sliding friction. The name is an abbreviation for **U**we's **HY**steretic **DE**vice, **f** for friction and **br** for bridges. The patented sliding mechanism consists of two-steel plates and a set of bronze inserts. One of the steel plates serves as guidance for the bronze inserts. The other plate has a specially prepared surface, which is in contact with the inserts, forming the sliding surface, as displayed in Figure 5.24.

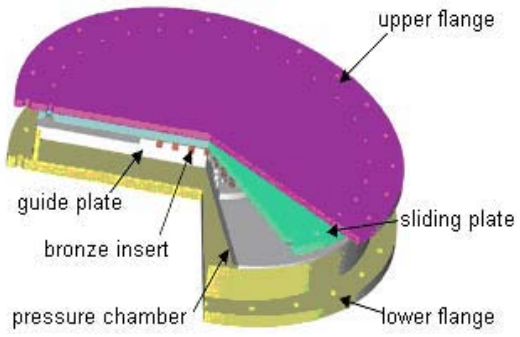

Figure 5.24: Controllable Friction Device (UHYDE-f-br)

While the device itself has an ideal elastic-plastic characteristics, elastic joint stiffness after sliding will remain due to parallel elastomeric bearings. An easy adjustment of the friction force is accomplished by gas pressure. There is an air-tight chamber behind one of the steel plates. A gas tank with electronic control unit varies the pressure, thus changes the normal force at the

sliding surface and the friction force. Quite different force-displacement characteristics, including viscous damping, can be achieved. The gas pressure can also be governed by a control command. Since no external energy is needed for controlling the dynamic behavior of the structure, but only for adjustment of the gas pressure, this concept belongs to the family of semiactive control.

The aim of implementing this experimental prototype is to evaluate experimentally semi-active control strategies applied to a realistic bridge structure subjected to severe earthquake ground motion. For this purpose, the sub-structure pseudo-dynamic test method is used. It allows a realistic full-scale test without having to build a real bridge. There is no other facility in Europe but ELSA in Joint Research Center-ISPRA that allows these tests by using the reaction wall.

5.2.1 Controller design

The control objective is to attenuate the structural vibration based upon two semiactive control algorithms. The first one is a linear controller based on the Lyapunov stability theory and the second one is a nonlinear controller based on the sliding mode control theory. The next considerations are taken into account:
i). The controllers for each device are designed as local controllers.
ii). The earthquake acceleration is considered unknown but bound, such that $|\ddot{x}_g| \leq X_0$ for all $t \geq 0$ with X_0 a known bound.
iii). Measurements of velocity and displacement are only available at the nodes where the control devices are installed.

Lyapunov Stability Theory based Controller

Define the following candidate Lyapunov function:

$$V(t) = \frac{1}{2}\boldsymbol{z_1}^T \boldsymbol{P}_1 \boldsymbol{z}_1 + \frac{1}{2}\boldsymbol{z_2}^T \boldsymbol{P}_2 \boldsymbol{z}_2 \tag{5.46}$$

where $z_1 = [x_1, x_3, \dot{x}_1, \dot{x}_3]^T$ and $z_2 = [x_2, x_5, \dot{x}_2, \dot{x}_5]^T$ correspond to state vectors at the directly controlled nodes. $\boldsymbol{P}_i$ $(i = 1, 2)$ are the positive definite solution of the Lyapunov function $\boldsymbol{P}_i\boldsymbol{A}_i + \boldsymbol{A}_i^T\boldsymbol{P}_i + \boldsymbol{Q}_i = 0$. The design objective is to achieve the maxim dissipation of the energy $\boldsymbol{z}_i^T(t)\boldsymbol{P}_i\boldsymbol{z}_1(t)$ induced by the system response $\boldsymbol{z}_i$ by making $\dot{V}(t)$ as negative as be possible for every $(\boldsymbol{z}_i, t)$.
By rewriting the state space equation (5.45) for $\boldsymbol{z}_1$ and $\boldsymbol{z}_2$ it is obtained:

$$\dot{\boldsymbol{z}}_1(t) = \boldsymbol{A}_1\boldsymbol{z}_1(t) + \boldsymbol{B}_1(t)\phi_{1,3}(t) + \boldsymbol{\Gamma}_1\ddot{x}_g(t) + \boldsymbol{C}_1\boldsymbol{z}_{A_1}(t) \tag{5.47}$$

$$\dot{\boldsymbol{z}}_2(t) = \boldsymbol{A}_2\boldsymbol{z}_2(t) + \boldsymbol{B}_2(t)\phi_{2,5}(t) + \boldsymbol{\Gamma}_2\ddot{x}_g(t) + \boldsymbol{C}_2\boldsymbol{z}_{A_2}(t) \tag{5.48}$$

where $\boldsymbol{z}_{A_1} = [x_2, x_4, \ldots, x_{10}, \dot{x}_2, \dot{x}_4, \ldots, \dot{x}_{10}]^T$, $\boldsymbol{z}_{A_2} = [x_1, x_3, x_4, x_6 \ldots, x_{10}, \dot{x}_1, \dot{x}_3, \dot{x}_4, \dot{x}_6, \ldots, \dot{x}_{10}]^T$, $\boldsymbol{\Gamma}_1 = [0, \ldots, 0\, m_1, m_3]$, $\boldsymbol{\Gamma}_2 = [0, \ldots, 0\, m_2, m_5]$.
By deriving $V(t)$ and replacing 5.47 and 5.48 into the derivative, it is obtained:

$$\begin{aligned}\dot{V}(t) &= -\frac{1}{2}\boldsymbol{z}_1^T\boldsymbol{Q_1}\boldsymbol{z}_1 - \frac{1}{2}\boldsymbol{z}_2^T\boldsymbol{Q_2}\boldsymbol{z}_2 + \boldsymbol{z}_1^T\boldsymbol{P_1}\boldsymbol{\Gamma}_1\ddot{x}_g + \boldsymbol{z}_2^T\boldsymbol{P_2}\boldsymbol{\Gamma}_2\ddot{x}_g + \boldsymbol{z}_1^T\boldsymbol{P_1}\boldsymbol{B}_1\phi_{1,3} + \boldsymbol{z}_2^T\boldsymbol{P_2}\boldsymbol{B}_2\phi_{2,5} + \\ &\quad \boldsymbol{z}_1^T\boldsymbol{P_1}\boldsymbol{C}_1\boldsymbol{z}_{A_1} + \boldsymbol{z}_2^T\boldsymbol{P_2}\boldsymbol{C}_2\boldsymbol{z}_{A_2} \leq H(z_i, \phi_{i,j}) + H(z_{A_i})\end{aligned} \tag{5.49}$$

where

$$\begin{aligned}H(z_i, \phi_{i,j}) &= -\frac{1}{2}\boldsymbol{z}_1^T\boldsymbol{Q_1}\boldsymbol{z}_1 - \frac{1}{2}\boldsymbol{z}_2^T\boldsymbol{Q_2}\boldsymbol{z}_2 + ||\boldsymbol{z}_1^T\boldsymbol{P_1}\boldsymbol{\Gamma}_1||\cdot||\ddot{x}_g|| + ||\boldsymbol{z}_2^T\boldsymbol{P_2}\boldsymbol{\Gamma}_2||\cdot||\ddot{x}_g|| + \boldsymbol{z}_1^T\boldsymbol{P_1}\boldsymbol{B}_1\phi_{1,3} \\ &\quad + \boldsymbol{z}_2^T\boldsymbol{P_2}\boldsymbol{B}_2\phi_{2,5} \\ H(z_{A_i}) &= ||\boldsymbol{z}_1^T\boldsymbol{P_1}\boldsymbol{C}_1||\cdot||\boldsymbol{z}_{A_1}|| + ||\boldsymbol{z}_2^T\boldsymbol{P_2}\boldsymbol{C}_2||\cdot||\boldsymbol{z}_{A_2}||\end{aligned} \tag{5.50}$$

Since the state vectors $\boldsymbol{z}_{A_1}$ and $\boldsymbol{z}_{A_2}$ are considered not measurable, the objective of control is to minimize V by making $H(z_i, \phi_{i,j})$ negative. If $\phi^d_{i,j}$ is denoted as the "desired" control force (without taking into account the actuator dynamics) the next "desired" control law is derived:

$$\phi^d_{1,3} = -\frac{1}{4}\boldsymbol{B}_1^T\boldsymbol{P_1}\boldsymbol{z}_1 - X_0\frac{||\Gamma_1||}{||\boldsymbol{B_1}||}\text{sgn}(\boldsymbol{z}_1^T\boldsymbol{P_1}\boldsymbol{B}_1) \qquad \phi^d_{2,5} = -\frac{1}{4}\boldsymbol{B}_2^T\boldsymbol{P_2}\boldsymbol{z}_2 - X_0\frac{||\Gamma_2||}{||\boldsymbol{B}_2||}\text{sgn}(\boldsymbol{z}_2^T\boldsymbol{P_2}\boldsymbol{\Gamma}_1) \quad (5.51)$$

The dynamic behavior of the UHYDE-fbr device is described by the following equation:

$$u_{i,j}(t) = \frac{1}{k_{f_{i,j}}}(\phi_{i,j} + \tau_{i,j}\dot{\phi}_{i,j})\text{sgn}\{\dot{x}_i(t) - \dot{x}_j(t)\} \qquad \{(i,j)\} = [(1,3),(2,5)] \quad (5.52)$$

where $\phi_{i,j}(t)$ is the average output actuator force, $u_{i,j}(t)$ the voltage signal applied to the actuator, $\tau_{i,j}$ is the actuator time delay and $k_{f_{i,j}}$ is a constant which relates the friction force produced by the actuator with the voltage applied on the electronic control unit that controls the pressure of the gas tank.
By taking into account the actuator dynamics, a control command law $u_{i,j}(t)$ is designed such that the "real" actuator control force $\phi_{i,j}(t)$ tracks asymptotically the "desired" actuator control force $\phi^d_{i,j}(t)$ before obtained. Such control law is defined as:

$$u_{i,j}(t) = \frac{1}{k_{f_{i,j}}}(\phi^d_{i,j} + \tau_{i,j}\dot{\phi}^d_{i,j})\text{sgn}\{\dot{x}_i(t) - \dot{x}_j(t)\} \qquad \{(i,j)\} = [(1,3),(2,5)] \quad (5.53)$$

Denote $\tilde{\phi}_{i,j}(t)$ as the tracking error between the "real" control action $\phi_{i,j}(t)$ and the "desired" control action $\phi_{i,j}(t)$; i.e.,

$$\tilde{\phi}_{i,j} = \phi_{i,j} - \phi^d_{i,j} \qquad \{(i,j)\} = [(1,3),(2,5)] \quad (5.54)$$

Now, redefine a Lyapunov function as:

$$V(\boldsymbol{z}_i, \tilde{\phi}_{i,j}) = V_1(\boldsymbol{z}_i) + V_2(\tilde{\phi}_{i,j}) \quad (5.55)$$

$$V_1(\boldsymbol{z}_i) = \frac{1}{2}\boldsymbol{z_1}^T\boldsymbol{P}_1\boldsymbol{z}_1 + \frac{1}{2}\boldsymbol{z_2}^T\boldsymbol{P}_2\boldsymbol{z}_2 \qquad V_2(\tilde{\phi}_{i,j}) = \frac{1}{2}\tau_{1,3}\tilde{\phi}^2_{1,3} + \frac{1}{2}\tau_{2,5}\tilde{\phi}^2_{2,5} \quad (5.56)$$

From equation (5.54) it is obtained that $\phi_{i,j} = \phi^d_{i,j} + \tilde{\phi}_{i,j}$. By using such relation and equations (5.51)-(5.53) the derivative of $V(\boldsymbol{z}_i, \tilde{\phi}_{i,j})$ is the following:

$$\dot{V}(\boldsymbol{z}_i, \tilde{\phi}_{i,j}) \leq H(z_i, \phi_{i,j}, \tilde{\phi}_{i,j}) + H(z_{A_i}) \quad (5.57)$$

where

$$\begin{aligned} H(z_i, \phi_{i,j}, \tilde{\phi}_{i,j}) &:= H(z_i, \phi_{i,j}) - \tilde{\phi}^2_{1,3} - \tilde{\phi}^2_{2,5}\boldsymbol{z}_1^T\boldsymbol{P_1}\boldsymbol{B}_1\tilde{\phi}_{1,3} + \boldsymbol{z}_2^T\boldsymbol{P}_2\boldsymbol{B}_2\tilde{\phi}_{2,5} \\ &\leq -\frac{1}{2}\boldsymbol{z}_1^T\boldsymbol{Q_1}\boldsymbol{z}_1 - \frac{1}{2}\boldsymbol{z}_2^T\boldsymbol{Q_2}\boldsymbol{z}_2 + (||\boldsymbol{z}_1^T\boldsymbol{P_1}\boldsymbol{\Gamma}_1|| + ||\boldsymbol{z}_2^T\boldsymbol{P_2}\boldsymbol{\Gamma}_2||)(\ddot{x}_g - X_0) \\ &\quad -(\frac{1}{2}\boldsymbol{z}_1^T\boldsymbol{P_1}\boldsymbol{B}_1 - \tilde{\phi}_{1,3})^2 - (\frac{1}{2}\boldsymbol{z}_2^T\boldsymbol{P_2}\boldsymbol{B}_2 - \tilde{\phi}_{2,5})^2 \leq 0 \end{aligned} \quad (5.58)$$

Therefore, the "real" control action $u_{i,j}(t)$ (taking into account the actuator dynamics) can minimize $\dot{V}(\boldsymbol{z}_i, \tilde{\phi}_{i,j})$ by making $H(z_i, \phi_{i,j}, \tilde{\phi}_{i,j}) \leq 0$. Because semiactive characteristics of the control device only positive voltage values can be applied, thus for negative voltage values derived from the control law, the action is $u_{i,j} = 0$.

Sliding Mode Controller

Define sliding functions as follows:

$$\sigma_A = \boldsymbol{D}_1 \boldsymbol{z}_1 \quad \text{with} \quad \sigma_1 = d_i^T z_1 \quad i = 1,3 \tag{5.59}$$
$$\sigma_B = \boldsymbol{D}_2 \boldsymbol{z}_2 \quad \text{with} \quad \sigma_i = d_i^T z_2 \quad i = 2,5 \tag{5.60}$$
$$\tag{5.61}$$

where $D_1 = [d_1 d_3]^T, D_1 = [d_2 d_5]^T \in \boldsymbol{R}^{2\times 4}$ are matrices to be chosen by the designer in order to guarantee the asymptotic stability of the closed-loop system in sliding mode. For the present design, a simple choice for D_i is

$$D_1 = \begin{pmatrix} \lambda_1 & 0 & 1 & 0 \\ 0 & \lambda_3 & 0 & 1 \end{pmatrix} \qquad D_2 = \begin{pmatrix} \lambda_2 & 0 & 1 & 0 \\ 0 & \lambda_5 & 0 & 1 \end{pmatrix} \tag{5.62}$$

with λ_i is a constant to be selected by the designer. Consequently, the following four sliding functions are defined:

$$\sigma_1 = \lambda_1 x_1 + \dot{x}_1 \qquad \sigma_3 = \lambda_3 x_3 + \dot{x}_3 \tag{5.63}$$
$$\sigma_2 = \lambda_2 x_2 + \dot{x}_2 \qquad \sigma_5 = \lambda_5 x_5 + \dot{x}_5 \tag{5.64}$$

When the system is in sliding mode, $\sigma_i(t) = 0$, (i = 1,2,3,5), one has:

$$x_i(t) = x_i(t_s) e^{-(t-t_s)} \tag{5.65}$$

where t_s is the time instant when sliding motion is generated in the system. Thus, the closed-loop control system in sliding mode is exponentially stable.
In order to design the sliding mode controller, define a Lyapunov function candidate:

$$V(t) = \frac{1}{2}\sigma_A^T \sigma_A + \frac{1}{2}\sigma_B^T \sigma_B \tag{5.66}$$

The derivative of the Lyapunov function is obtained as follows:

$$\begin{aligned} \dot{V} &= \sigma_A^T \dot{\sigma}_A + \sigma_B^T \dot{\sigma}_B \\ &= \sigma_A^T D_1 \left[\boldsymbol{A}_1 \boldsymbol{z}_1 + \boldsymbol{B}_1 \phi_{1,3} + \boldsymbol{\Gamma}_1 \ddot{x}_g + \boldsymbol{C}_1 \boldsymbol{z}_{A_1}\right] + \sigma_B^T D_2 \left[\boldsymbol{A}_2 \boldsymbol{z}_2 + \boldsymbol{B}_2 \phi_{2,5} + \boldsymbol{\Gamma}_2 \ddot{x}_g + \boldsymbol{C}_2 \boldsymbol{z}_{A_2}\right] \\ &\leq H(\boldsymbol{z}_i, \phi_{i,j}) + H(z_{A_i}) \end{aligned} \tag{5.67}$$

where

$$\begin{aligned} H(\boldsymbol{z}_i, \phi_{i,j}) &=: \sigma_A^T D_1 \left[\boldsymbol{A}_1 \boldsymbol{z}_1 + \boldsymbol{B}_1 \phi_{1,3}\right] + ||\sigma_A^T|| \cdot ||D_1 \boldsymbol{\Gamma}_1|| \cdot ||\ddot{x}_g|| + \sigma_B^T D_2 \left[\boldsymbol{A}_2 \boldsymbol{z}_2 + \boldsymbol{B}_2 \phi_{2,5}\right] \\ &\quad + ||\sigma_B^T|| \cdot ||D_2 \boldsymbol{\Gamma}_2|| \cdot ||\ddot{x}_g|| \qquad (5.68) \\ H(z_{A_i}) &=: \sigma_A^T D_1 \boldsymbol{C}_1 \boldsymbol{z}_{A_1} + \sigma_B^T D_2 \boldsymbol{C}_2 \boldsymbol{z}_{A_2} \qquad (5.69) \end{aligned}$$

The term $H(z_{A_i})$ is uncontrollable and V will be minimized by making negative $H(\boldsymbol{z}_i, \phi_{i,j})$. Then, the "desired" control force is as follows:

$$\phi_{i,j}^d = -\left\{ \frac{1}{4}\sigma_A \boldsymbol{D}_i \boldsymbol{B}_i + \boldsymbol{B}_i^{-1} \boldsymbol{A}_i \boldsymbol{z}_i - X_0 \frac{||\Gamma_i||}{||\boldsymbol{B}_i||} \mathrm{sgn}(D_i^T \sigma_A) \right\} \qquad \{i,j\} = \{(1,2),(3,5)\} \tag{5.70}$$

By taking into account the actuator dynamics (eq.) a command voltage is obtained by using 5.53. A new candidate Lyapunov function is defined as:

$$V(\boldsymbol{\sigma}_i, \tilde{\phi}_{i,j}) = V_1(\boldsymbol{\sigma}_i) + V_2(\tilde{\phi}_{i,j}) \tag{5.71}$$
$$V_1(\boldsymbol{\sigma}_i) = \sigma_A^T \dot{\sigma}_A + \sigma_B^T \dot{\sigma}_B \qquad V_2(\tilde{\phi}_{i,j}) = \frac{1}{2}\tau_{1,3}\tilde{\phi}_{1,3}^2 + \frac{1}{2}\tau_{2,5}\tilde{\phi}_{2,5}^2 \tag{5.72}$$

By using 5.54, 5.67 and 5.70 it can be demonstrated that:

$$\dot{V}(\boldsymbol{\sigma}_i, \phi_{i,j}) \leq H(\boldsymbol{z}_i, \phi_{i,j}, \tilde{\phi}_{i,j}) + H(z_{A_i}) \tag{5.73}$$

where

$$\begin{aligned} H(\boldsymbol{z}_i, \phi_{i,j}, \tilde{\phi}_{i,j}) &= -\Big\{(||\sigma_1^T||\cdot||D_1\Gamma_1|| + ||\sigma_2^T||\cdot||D_2\Gamma_2||).(X_0 - ||\ddot{x}_g||) + (\frac{1}{2}\boldsymbol{\sigma}_A\boldsymbol{D}_1\boldsymbol{B}_1 - \tilde{\phi}_{1,3})^2 \\ &\quad +(\frac{1}{2}\boldsymbol{\sigma}_B\boldsymbol{D}_2\boldsymbol{B}_2 - \tilde{\phi}_{2,5})^2\Big\} \leq 0 \end{aligned} \tag{5.74}$$

Therefore $V(\boldsymbol{\sigma}_i, \tilde{\phi}_{i,j})$ is minimized. Newly, the condition of $u_{i,j} \in [0 u_{i,j}^{max}]$ should be accomplished.

5.2.2 Experimental Setup

According to the pseudo-dynamic test concept, three joints of this kind are used as test specimen, while the bridge structure is simulated by a computer model. Three joints acting in a horizontal plane, which are the joints of a two-span bridge model, are tested simultaneously in one experiment. A photography of the experiment is presented in figure 5.25, while a schematic diagram is presented in figure 5.26. Using substructuring algorithms, the bridge dynamics are simulated on a computer, the demand of joint displacements is put out. Measured restoring forces are fed back into the computer. Thus, a realistic response of a full-scale bridge is obtained in the tests.

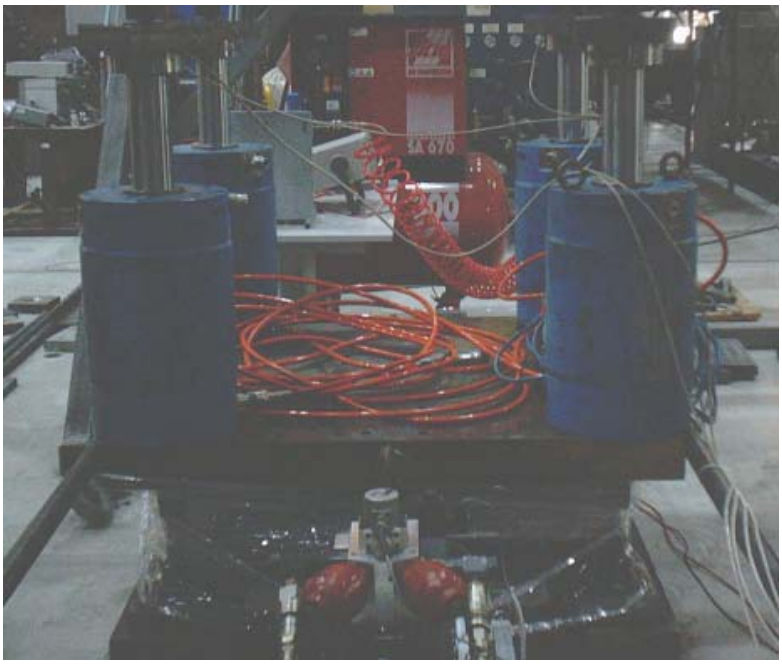

Figure 5.25: Photograph of the pseudo-dynamic test substructure

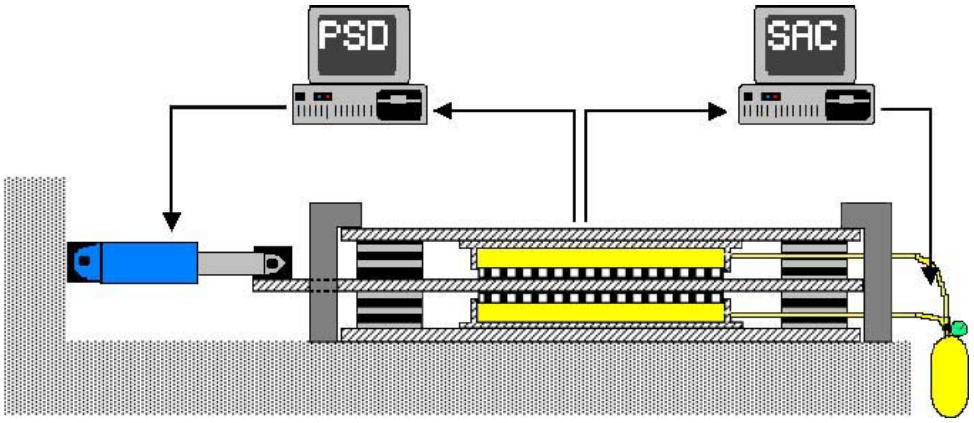

Figure 5.26: Schematic diagram of the test substructure

5.2.3 Experimental results

Experimental tests consistent of controlled displacements and under constant normal force and varying frequency are applied on the CFD device in order to study the influence of the excitation frequency on the the friction coefficient. No significant dependence is established. The average friction coefficient determined is: μ=0.45. A linear relationship is assumed between the normal force (and thus the input voltage), and the friction force (a constant friction coefficient), according to the ranges defined in table 5.4. In laboratory tests, the device deformations are limited to ± 100 mm.

Table 5.4: Magnitudes and range of values for the UHYDE-fbr control device

Value	Normal Force	Friction Force [kN]	Pressure [bar]	Voltage [V]
Minimum	0	0	0	0
Maximum	5000	2250	10	10

Numerical simulations of the optimized passive system under an excitation of a simulated acceleration history according to EC8, soil class B and maximum acceleration of 0.35g indicate a friction force of 2250 kN and maximum device deformation of ± 100 mm. Therefore, the friction force is scaled when feeding back into the pseudodynamic algorithm. The scale factor for the friction force is 1:25. The scale factor for the time in the pseudodynamic test is 1:10.

El Centro scaled acceleration EC8 (see figure 5.27) are applied to the structure by means of the reaction wall, in order to evaluate different control configurations of the device. Three control configurations are defined: uncontrolled, passive-on and semiactive. Experimental results for the first two configurations are available until now, and the semiactive tests will be made in next future. Figure 5.28 presents the experimental displacements at node 3 for the structure with passive-on control, while figures 5.30 and 5.29 the forces delivered ant its dynamic behaviour. Figure 5.31 presents the simulated and experimental displacement at the node 3, for a passive-on ($u_{1,3}$=10v) configuration. It is seen that the simulated response is close to the experimental one, thus the model used both the structure and the actuator are adequate.

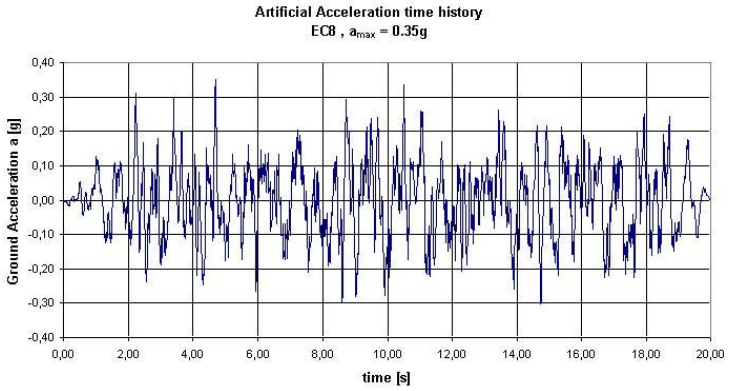

Figure 5.27: El Centro scaled acceleration (EC8)

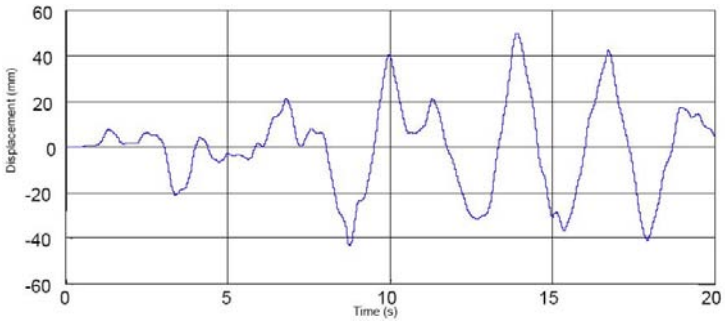

Figure 5.28: Experimental displacement at the node 3

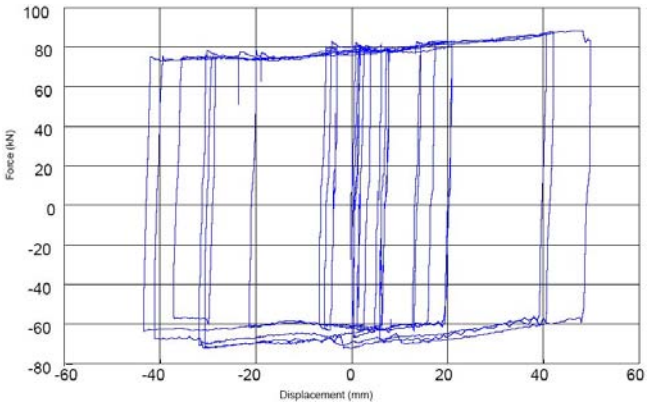

Figure 5.29: Dynamic behaviour of the UHYDE-fbr device in passive-on state

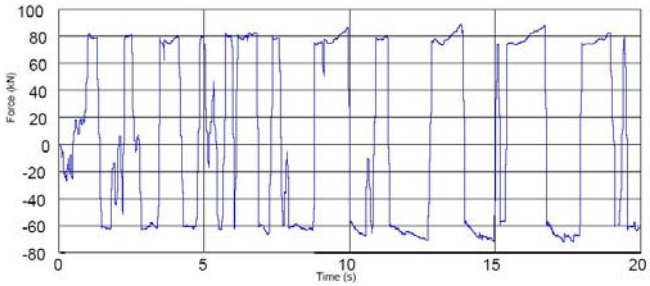

Figure 5.30: Experimental forces delivered by the UHYDE-fbr device in passive-on state

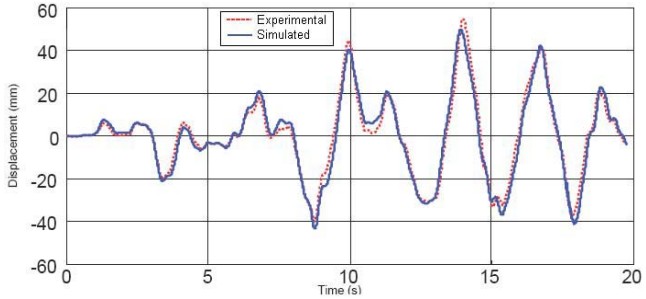

Figure 5.31: Experimental and simulated displacement for the node 3

Numerical simulation were done for the controlled and uncontrolled structure. Figure 5.32 presents the simulated displacement for the node 3. In general, similar responses are obtained for the others nodes. It is seen that structural vibrations are reduced with both SMC controller and Lyapunov stability theory based controller. However the advantage of using the nonlinear controller (SMC) is that parameters of the structure or actuator can be considered uncertain. On the contrary, using directly the Lyapunov controller, the matrix P cannot be solved if some of its elements are uncertain values.

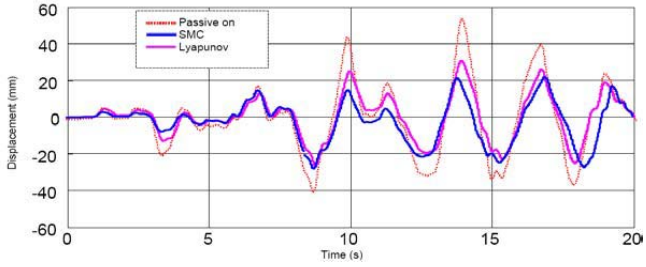

Figure 5.32: Simulated absolute displacement at node 3

5.3 Experimental Prototype 3. 2-story Actively Controlled Test Building

The third experimental prototype corresponds to a 2-story test building fabricated by QUANSER Consulting and available in the MICELab Research Group. A photo of such prototype is shown in figure 5.33. It is actively controlled at the top level by means of an Active Mass Damper (AMD). A voltage of ±5v is applied to the servomotor of the AMD to produce horizontal movement on a carrier medium at the top. Absolute accelerations of both floors can be measured such as the displacement of the AMD. Different kinds of horizontal ground accelerations can be reproduced by means of a shake table whose movement is transmitted by a 1 Hp brushless servomotor. The main specifications of the shake table are: peak acceleration of 2.5g, stroke ±3in and maximum force of 700N. The controllers of both shake table and AMD are implemented on a PC. Signals are recorded from and applied on the structure by using a 16-bit 8-input, 8-output data acquisition card. Controllers are programmed by using Simulink and WinCon software.

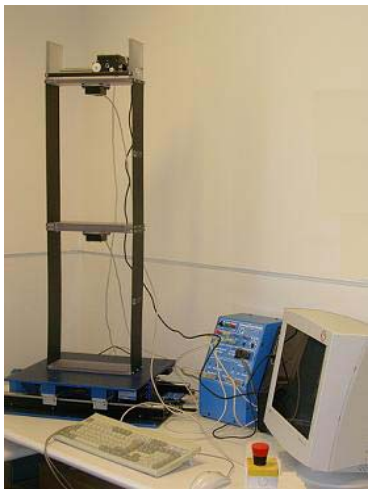

Figure 5.33: Photo of the 2-story test building

An numerical model is provided by Quanser Consulting, which is derived from an equivalent mechanical model (see figure 5.34). The Lagrangian formulation is used to derive the dynamic equations based on the kinetic and potential energies in the system. Finally, the dynamics equations are linearized about the quiescent point and a dynamics equations for the top floor of the structure are obtained. The equations are as follows:

$$m_2\ddot{x}_2 + k_2x_2 + a_1\dot{x}_c = a_2u \tag{5.75}$$

$$m_c\ddot{x}_c + k_2x_2 + a_3\dot{x}_c = a_4u \tag{5.76}$$

where x_2 is the displacement at the second floor, x_c displacement of the cart, u voltage signal applied to the cart motor, m_2 and m_c masses of the second floor and cart, respectively. k_2 corresponds to the equivalent stiffness of the second floor and $a_1 \dots a_4$ are constants values that relate the mechanical and electrical properties of the cart motor.

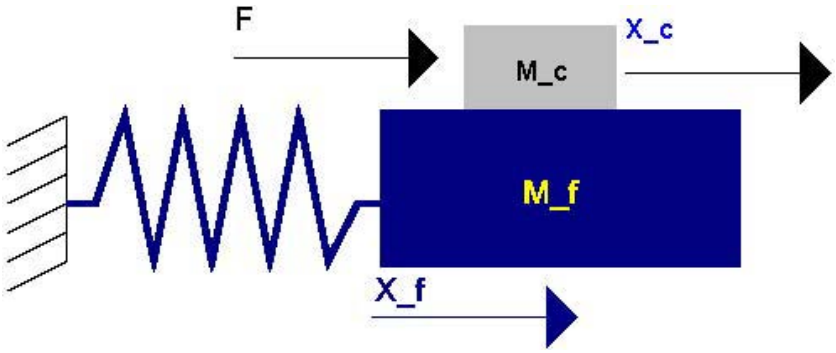

Figure 5.34: Mechanical model for a building with AMD

By substituting system parameters and introducing an integrator for alpha, the following linear model about the quiescent point was obtained.

$$\dot{\boldsymbol{x}} = \boldsymbol{A}\boldsymbol{x} + \boldsymbol{B}u \tag{5.77}$$

(5.78)

with

$$\boldsymbol{A} = \begin{bmatrix} 0 & 0 & 1 & 0 \\ 0 & 0 & 0 & 1 \\ -140.88 & 0 & 0 & 6.68 \\ 140.88 & 0 & 0 & -17.65 \end{bmatrix} \qquad \boldsymbol{B} = \begin{bmatrix} 0 & 0 & -1.49 & 3.95 \end{bmatrix} \tag{5.79}$$

$$\boldsymbol{x} = \begin{bmatrix} x_f & x_c & \dot{x}_f & \dot{x}_c \end{bmatrix} \tag{5.80}$$

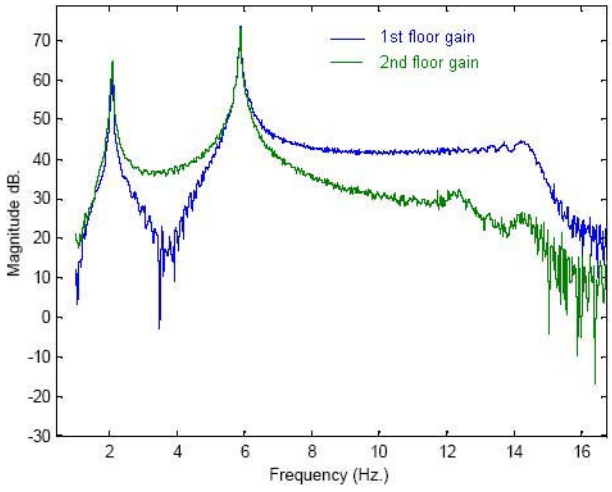

Figure 5.35: Experimental transfer functions from the ground to 1st and 2nd floor

The frequency response for the two floors is obtained by applying a sine sweep signal from 1 Hz to 15 Hz with a 0.2 cm amplitude on the shake table. Figure 5.35 shows the transfer functions from the ground to both floors, where the natural frequencies correspond to [2.08 6.12] [Hz].

The main purpose of using an active controller (AMD) in this experiment is to verify, at laboratory level, the reduction of vibrations of high rise buildings when external forces such as earthquakes act on them. Two goals then should be derived by reducing structural vibrations: To void damages in the structure and maintain human comfort. From the control view point, the objective is to reduce absolute displacement and velocities at the second floor and the cart at the most significant excitation frequencies (included the natural frequencies).

5.3.1 Controller Design

Two controllers are designed. The first is based on the QFT control approach and the second is based on the Lyapunov stability theory.

Controller 1

The QFT controller design is made by making the next considerations. i) The stiffness is an uncertain parameter but bounded around its nominal value [0.97 1.03]*k_{2N}. ii). An uncertain but bounded earthquake acceleration acts as disturbance in the structure and iii). Only measurements of acceleration at the second floor and displacement of the cart are available. Such measurements contain a white noise of around 5% the measured value. The design specifications for the QFT controller are: i) The displacement at the second floor be less than 0.03 m for an uncertain but bounded disturbance and ii) less than 0.005 m when white noise signal is present at the measurement. For design purposes the equations (5.75) and (5.76) are expressed in only one equation. Such equation represents the equivalent plant P of a LTI structure such as that presented in figure 3.2. The system equations represented in Laplace form are:

$$(m_2 s^2 + k_2)x_2(s) + a_1 s x_c(s) = a_2 u(s) \tag{5.81}$$

$$(m_c s^2 + a_3)x_c(s) + k_2 x_2(s) = a_4 u(s) \tag{5.82}$$

By using the above equations, the transfer function of the plant $P(s) = x_2(s)/u(s)$ takes the form:

$$P(s) = \frac{a_2 m_c s + a_2 a_3 - a_1 a4}{m_2 m_c s^3 + m_2 a_3 s^2 + m_c k_c s + k_2 a_3 - k_2 a_1} \tag{5.83}$$

The problem is reduced to design a QFT controller (G) for a SISO LTI system, in the presence of uncertain parameters in the plant, disturbance (V) at the input of the plant and white noise (N) in the measurement. Then, the frequencial specifications are:

$$\left|\frac{PG}{1+PG}\right| = \left|\frac{x_2(j\omega)}{N(j\omega)}\right| \leq W_{s1} \qquad \left|\frac{P}{1+PG}\right| = \left|\frac{x_2(j\omega)}{V(j\omega)}\right| \leq W_{s3} \tag{5.84}$$

Since the displacement cannot be directly measured, a state estimator is used. (See details in the Quanser Innovative Educate Manual). The parametric values are: m_c=0.85 kg, m_2=1.15 kg, k_2=162 N/m, a_1=7.682 N·s/m, a_2=1.7189 N/v, a_3= 20.3024 N·s/m a4= 4.5428 N/v. For the QFT design the bounds are W_{s1}=2 and W_{s3}=5×10^{-4} for all the work frequencies. QFT controller design is done by using the MATLAB QFT toolbox. Figure 5.36 shows the design of the final loop for L_N on the Nichols chart. The transfer function G derived from L_N is:

$$G(s) = 15.1693\frac{24.8309s + 1}{0.0332s + 1} \tag{5.85}$$

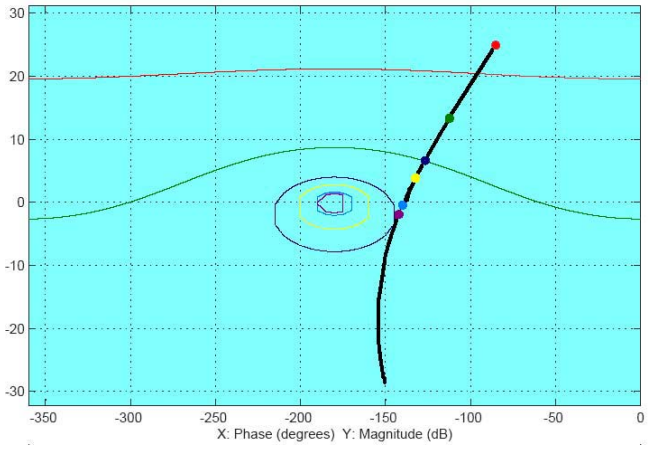

Figure 5.36: Final Loop L_N

A sweep sine signal from 1 to 2 Hz during 20 seconds (see figure 5.37) is applied as disturbance. Absolute displacement at the second floor of the controlled and uncontrolled structure is shown in figure 5.39. It is seen that structural vibration are reduced at all the frequencies range by using the QFT controller.

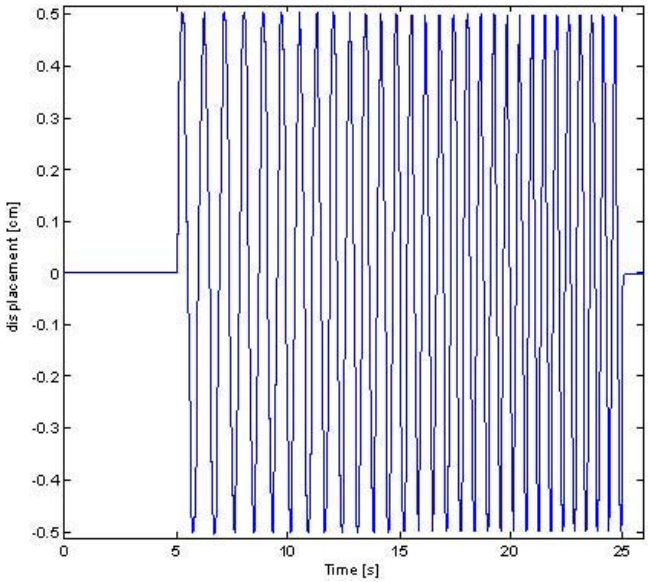

Figure 5.37: Sweep excitation signal

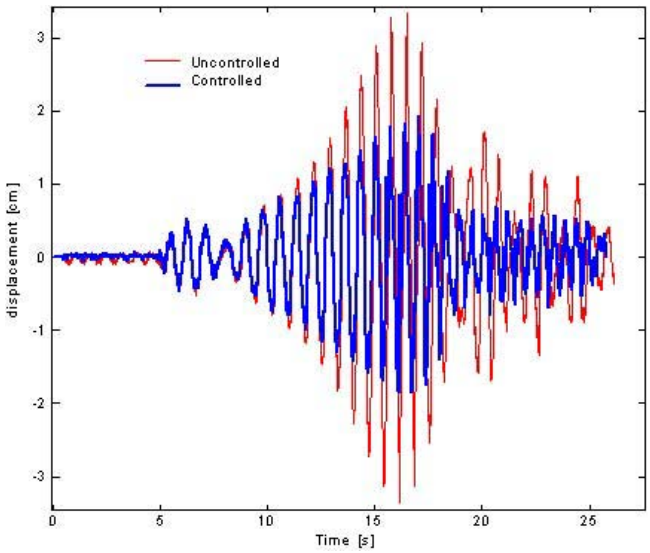

Figure 5.38: Absolute displacement at the second floor

Controller 2

The second controller designed, is based on the Lyapunov stability theory. Consider the next candidate Lyapunov function:

$$V = \frac{1}{2}\boldsymbol{x}^T\boldsymbol{P}\boldsymbol{x} \tag{5.86}$$

Its derivative take the form

$$\dot{V} = -\frac{1}{2}\boldsymbol{x}^T\boldsymbol{Q}\boldsymbol{x} + \boldsymbol{x}^T\boldsymbol{P}\boldsymbol{B}u \tag{5.87}$$

Then, the control law obtained, by minimizing V is:

$$u = -k\boldsymbol{x} = -(\boldsymbol{P}\boldsymbol{B})^T\boldsymbol{x} \tag{5.88}$$

By using the estimated state vector, the final control law is:

$$u = -(\boldsymbol{P}\boldsymbol{B})^T\hat{\boldsymbol{x}} \tag{5.89}$$

The control law (5.88) is implemented with $\boldsymbol{Q}$=diag([5000 0.0001 10 0.0001]).

5.3.2 Experimental Results

A sine sweep signal is applied as ground acceleration. The vibrations for the first and second floor of the structure for uncontrolled and controlled cases are those shown in figure 5.39 and 5.40

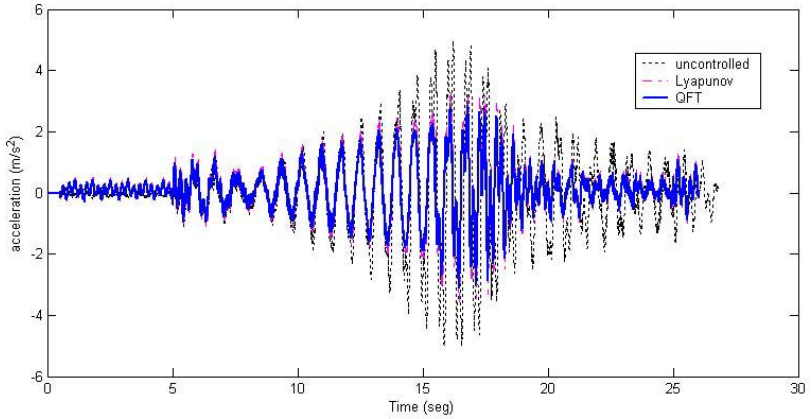

Figure 5.39: Absolute acceleration at the first floor

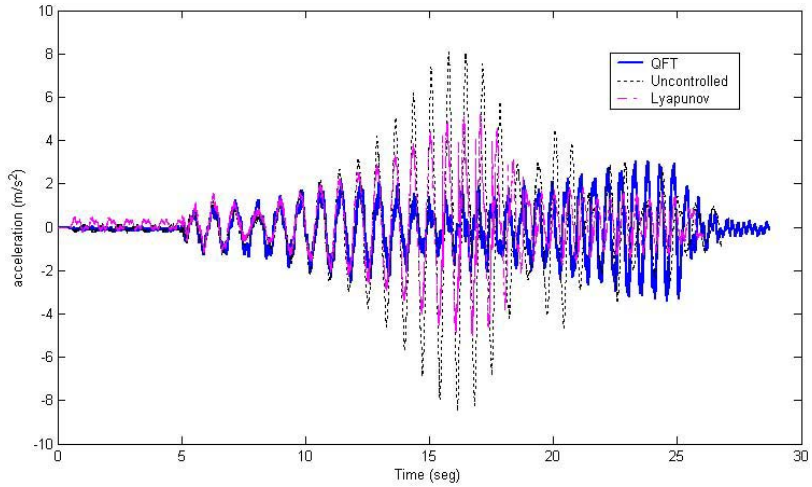

Figure 5.40: Absolute acceleration at the second floor

From the above figures it is observed that both controllers reduce vibrations at the floors 1 and 2, for a ground acceleration reach in frequencies. However, the QFT controller is more effective, because vibration modes of the structure has been taken into account in the controller specifications.

Chapter 6

Conclusions and Future Work

This thesis focuses on the design of robust control laws that can effectively reduce vibrations of structures subjected to unknown disturbances such as earthquakes strong winds or coupled dynamic loads. Parameters of the structure are considered uncertain and measurement of states limited. Actuator dynamics of type hysteresis, time delay and friction force are included in the design.

The main contributions and remarks derived from this thesis are the following:

Many problems presented in the design of structural control laws influence considerably on the control system performance. The consideration of all the problems presented in a structural control system is a difficult task and can be considered as a big challenge in the controller design. In this thesis robust structural control laws have been designed taking into account the most important open structural control problems, presented in most of the structural control systems, such as parametric uncertainty, actuator dynamics, unknown disturbances, dynamic coupling and measurement limitation. Thus, the main contribution of this thesis is the consideration of all the above open structural control problems and the obtention of robust control laws that can effectively improve structural dynamics.

The design of a robust control law for structures with uncertain parameters, unknown disturbances and measurement limitation has been satisfactorily achieved by using the QFT control theory. Numerical and experimental structural models have been used to verify of the control approach. The originality in this design is that by first time a structural control laws is based on QFT control technique. Parametric uncertainty is an significant open structural control problem and here it has been dealt with the additional advantage of designing in the frequency domain. It facilitates defining a desired structural behavior at different excitation frequencies included the resonance frequencies. Another aspect to highlight is that the proposed control approach has been also numerically verified and successfully implemented on experimental prototypes.

The problem of designing control laws for actuator with hysteretic dynamics has been solved by using the Backstepping control technique. The actuators used are semiactive Magnetorheological dampers, whose dynamic behaviour is represented by means of the the hysteretic Bouc-Wen model. The main contribution is that the problem of actuator hysteretic dynamics has been satisfactorily solved by using a control technique recently introduced in structural control. By the first time in the structural control application, experimental studies of Backstepping structural controllers have been successfully done.

Robust structural control laws for structures with unknown disturbances, dynamics coupling, measurement limitation and actuator dynamics (time delay and friction force) have been proposed and satisfactorily verified on numerical models and experimental prototypes. Control laws have been based on Lyapunov stability theory and Sliding Mode Control approach. The main contribution here is that these structural control problems have been solved by using techniques known in structural control, but additionally experimental tests have been realized.

Some future research topics that can be studied in the future are here discussed.

In this thesis different robust control laws that consider open structural control problems have been proposed. However the methodologies used here could be extended to other control areas, since the control problems similar to those studied here can be presented in other systems.

Open structural control problems have been solved by using innovative control techniques such as a Backstepping or QFT. The study of this control techniques could be enhanced to solve other control problems and could be combined with other theories such as Linear Matrices Inequalities approach and Modal Intervals arithmetical theory.

Robust structural control laws proposed in this thesis have been implemented on prototypes scaled to laboratory level. The next step should be the use of experimental prototypes close to full scale.

Bibliography

[1] A. K. Agrawal, J. N. Yang and W. E. Schmitendorf. Hybrid Control of Buildings Using Nonlinear Polynomial Output feedback. *Proceedings of the American Control Conference*. Philadelphia, pp. 2554-2558, June, 1998.

[2] Z. Akbay and HM Aktan. Intelligent energy dissipation systems. *Proceedings of the US National Conference on Earthquake Engineering*. Palm Springs, pp. 427-435, 1990.

[3] L. Bakule and J. Böhm. Robust decentralized H_α control of input delayed interconnected systems. *Smart Structures* NATO Series, Kluwer, Amsterdan, pp. 1-8, 1999.

[4] L. Bakule, F. Paulet-Crainiceanu, J. Rodellar and J. M. Rosell. Decentralized overlapping control design for a cable-stayed bridge benchmark. *Proceedings of the Third World Conference on Structural Control* Vol. 2, John Wiley, pp. 869-874, 2003.

[5] L. Bakule, F. Paulet-Crainiceanu, J. Rodellar and J. M. Rosell. Overlapping Reliable Control for a cable-stayed bridge benchmark. *Proceedings of the 2002 American Control Conference* Vol. 4, IEEE, Piscataway, pp. 3046-3051, 2002.

[6] A. Baños, F. Lamnabhi-Lagarrigue and F. J. Montoya. Advances in the Control of Nonlinear Systems. Lecture Notes in Control and Information Sciences. Springer-Verlag London Limited. pp. 58-132. 2001.

[7] Barbat, A.H., Rodellar, J., Ryan, E.P. and Molinares, N., "Active control of non-linear base-isolated buildings", *Journal of Engineering Mechanics ASCE*, Vol. 121, 676–684, 1995.

[8] Barbat, A.H. and Bozzo, L.M., 1997, "Seismic analysis of base isolated buildings", Arch. Computational Methods in Engineering, 4, 153-192.

[9] G. Bartolini, A. Ferrara and L. Giacomini. A Backstepping Second Order Variable Structure Control Design for a Class of Uncertain Nonlinear Systems. *Proceedings of the 36th Conference on Decision & Control*. San Diego, USA, pp. 4025-4031, December, 1997.

[10] L. Bozzo, X. Cahis and Ll. Torres. Type Energy Dissipator for the Protection of Masonry Infill Walls, *Sixth U.S. National Conference on Earthquake Enginyering*. Seattle, 1998.

[11] X. Cahis, L. Bozzo and Ll. Torres. An innovative elasto-plastic energy dissipator for the structural and non-structural building protection *12th World Conference on Earthquake Engineering*, Auckland, 2000.

[12] X. Cahis, L. Bozzo and Ll. Torres. Experimental Studies of Various Innovative Energy Dissipation Devices. *Eleventh European Conference on Earthquake Enginnering*. París, 1998.

[13] R. E. Christenson. Semiactive Control of Civil Structures for Natural Hazard Mitigation: Analytical and Experimental Studies. *Disertation to obtain the Degree of PhD in University of Notre Dame*. December, 2001. University of Notre Dame, Notre Dame, USA.

[14] Dorka, U.E., 2000, "Testing of algorithms for semiactive control of bridges," Personal communication, Kassel, Germany.

[15] D.J. Dowdell, and S. Cherry. Semiactive Friction Dampers for Seismic Response Control of Structures. *Proceedings of the Fifth US National Conference on Earthquake Engineering*. Vol. 1, pp. 819-828, 1994.

[16] P. Dupont and A. Stokes. Semiactive Control of Friction Dampers. *Proceedings of the 34th Conference on Decision & Control*. New Orleans, USA, pp. 3331-3336, December 1995.

[17] S. J. Dyke. Seismic Protection of a Benchmark Building Using Magnetorheological Dampers. *Proceedings of the 2nd World Conference on Structural Control*. Kyoto, JAPAN, June 29 - July 2, 1998.

[18] S. J. Dyke and B. F. Spencer Jr. A comparison of Semiactive Control Strategies for the MR damper. *Proceedings of the IASTED International Conference, Intelligent Information Systems*. December 8-10, 1997. The Bahamas.

[19] S. J. Dyke and B. F. Spencer Jr. Seismic Response Control using Multiple MR Dampers. *Personal Communication*.

[20] S. J. Dyke, B. F. Spencer Jr., M. K. Sain and J. D. Carlson. Experimental Verification of Semiactive Structural Control Strategies Using Acceleration Feedback. *Proceedings of the 3rd International Conference on Motion and Vibration Control*. Vol 3, pp. 291-296, Chiba, Japan, September 1996

[21] S. J. Dyke, B. F. Spencer Jr., M. K. Sain and J. D. Carlson. Modeling and Control of Magnetorheological Dampers for Seismic Response Reduction. *Smart Materials and Structures*. Vol. 5, pp. 565-575, 1996

[22] S. J. Dyke, B. F. Spencer Jr., M. K. Sain and J. D. Carlson An Experimental Study of MR Dampers for Seismic Protection. *Smart Materials and Structures: Special Issue on Large Civil Structures*. 1997.

[23] S. J. Dyke, B. F. Spencer Jr., M. K. Sain and J. D. Carlson On the efficacy of magnetorheological dampers for seismic response reduction. *Proceedings of DECTC'97. ASME Design Engineering Technical Conferences*. Sacramento, USA. September 14-17, 1997.

[24] S. J. Dyke, F. Yi, S. Frech and J. D. Carlson. Application of Magnetorheological Dampers to Seismically Excited Structures. *Proceedings of the 17th International Modal Analysis Conference*. Kissimmee, USA, Feb. 8 - 11, 1999.

[25] S. J. Dyke, J. M. Caicedo, G. Turan, L. A. Bergman and S. Hague. Benchmark Control Problem for Seismic Response of Cable-Stayed Bridges. *http://wusceel.cive.wustl.edu/quake/*. December 27, 2000

[26] R. C. Ehrgott and S.F. Masri. Structural Control Applications of an Electrorheological Device. *Proceedings on the International Workshop on Structural Control*. USC, pp. 115-129, 1994.

[27] M. Q. Feng, M. Shinozuka and S. Fujii. Friction-Controllable Sliding Isolation System. *Journal of Engineering Mechanics*. ASCE, Vol. 119, No. 9, pp. 1845-1864, 1993.

[28] T. Fujita, M. Shimazaki, H. Yutaka, S. Aizawa, M. Higashino and N. Haniuda. Semiactive Seismic Isolation system using controllable friction damper. *Bulletin of Earthquake Resistant Structure Research Center*. No. 27, pp. 21-31, 1994.

[29] V. Gatulli and F. Romeo. Structural Identifiability Enhancement via Feedback. *Proceedings of the Third World Conference on Structural Control*. Como, Italy, Vol.2, pp. 95-100, 2003.

[30] H. P. Gavin. Control of Seismically Excited Vibration Using Electrorheological Materials and Lyapunov Function. *IEEE Transactions on Control Systems Technology*. Vol. 9, No. 1, pp. 27-36, 2001.

[31] H. P. Gavin, R.D. Hanson and F.E. Filisko, Electrorheological Dampers, Part I: Analysis and Design. *Journal of Appliccated Mechanical*. ASME, vol. 63, no. 3, pp. 669-675, 1996.

[32] H. P. Gavin, R.D. Hanson and F.E. Filisko. Electrorheological Dampers, Part II: Testing and Modeling. *Journal on Applicated Mechanical*. ASME, vol. 63, no. 3, pp. 676-682, 1996.

[33] J. Ghaboussi and A. Joghataie. Active Control of Structures using neural networks. *Journal of Engineering Mechanics*. ASCE, Vol. 121, No. 4, pp. 555-567, 1995.

[34] Giraldo, D., Yoshida, O., Dyke, S.J. and Giacosa, L. 2004, "Control Oriented System Identification Using ERA," Journal of Structural Control and Health Monitoring, (in press)

[35] M Haroun, J. Pires and A. Won. Active orifice control in hybrid liquid dampers. *Proceedings of the First World Conference on Structural Control* . Los Angeles, USA, pp. 69-78, 1994.

[36] T. Hatada and H. A. Smith. Development and Application of Nonlinear Controller Using Variable Damping Devices. *Proceedings of the American Control Conference*. New Mexico, USA, pp. 453-457, June 1997.

[37] M. J. Hochrainer. Tuned Liquid Column Dampers in Structural Control. *European Meeting on Intelligent Structures*. Ischia, September 22-28, 2001.

[38] M. J. Hochrainer. Control of Wind and Earthquake Excited Tall Buildings. *Proceedings of the Third World Conference on Structural Control*. Como, Italy, Vol.3, pp. 63-68, 2003.

[39] J. Holnicki and M. Wiklo. Adaptive Impact Absorvers-The Concept, Design Tools and Applications. *Proceedings of the Third World Conference on Structural Control*. Como, Italy, Vol.3, pp. 69-78, 2003.

[40] G. W. Housner, A. G. Chassiakos, R. E. Skelton and B. F. Spencer Jr. Structural Control: Past, Present and Future. *Journal of Engineering Mechanics, ASCE*. Vol. 123, No. 9, pp. 897-923, 1997.

[41] Ikhouane, F. and Krstic, M., 1998, "Adaptive backstepping with parameter projection: Robustness and asymptotic performance," in Automática, Vol. 34, 49-435.

[42] F. Ikhouane, V. Mañosa, J. Rodellar. Adaptive backstepping control of some uncertain nonlinear systems. Application to Bouc-Wen hysteretic oscillators. *Preprint Departament de Matemàtica Aplicada III, Universitat Politècnica de Catalunya*, N–535, 2003.

[43] F. Ikhouane, V. Mañosa and J. Rodellar. Adaptive backstepping control of some uncertain nonlinear oscillators. *Preprint Departament de Matemàtica Aplicada III (UPC)*, 2003.

[44] F. Ikhouane, V. Mañosa, J. Rodellar. Adaptive backstepping control of a class of hysteretic systems. Preprint *To appear in Proceedings of SPIES conference on SMART STRUCTURES AND MATERIALS (Modelling, signal procesing and control)*. San Diego CA, March 2-4, 2003.

[45] F. Jabbari, W. E. Schmitendorf and J. N. Yang. H-infinity Control for Seismic-Excited Buildings with Acceleration Feedback. *Journal of Engineering Mechanics, ASCE*. 21(9), pp. 994-1002, 1995.

[46] L. M. Jansen and S. J. Dyke. Investigation of Nonlinear Control Strategies for the Implementation of Multiple Magnetorheological Dampers. *http://wusceel.cive.wustl.edu/quake/*. 2001.

[47] L. M. Jansen and S. J. Dyke. Semiactive Control Strategies for MR Dampers: A comparative Study. *Journal of Engineering Mechanics, ASCE*. Vol. 126, No. 8, pp. 795-803, 2002.

[48] S. Kamagata and T. Kobori. Autonomous Adaptive Control of Active Variable Stiffness System for Seismic Ground Motion. *Proceedings of the First World Conference on Structural Control*. Los Angeles, California, pp. TA4:33-42, August, 1994.

[49] T. Kengo and O. Tetsuya. Sliding Mode Control for Seismic Excited Tall Buildings with installed Varying Springs at Boundary of Resistant Structural Components. *Proceedings of the Third World Conference on Structural Control*. Vol. 3, pp. 91-100, 2003.

[50] I. E. Kose, W. E. Schmitendorf, F. Jabbari and J. N. Yang. H-infinity Active Seismic Response Control using Static Output Feedback. *Journal of Engineering Mechanics, ASCE*. 122(7), pp. 651-659, 1996.

[51] J. Kuehn, G. Song, and J. Sun. Experimental Verification of a NON-Protruding Intelligent Stiffener for Bridges (ISB). *Proceedings of the International Post-SMiRT Conference Seminar on Seismic Isolation, Passive Energy, Dissipation and Active Control of Vibrations of Structures*. Cheju, Korea, August 23-25, 1999.

[52] H. N. Kurata, T. Kobori, M. Takahashi and N. Niwa. semiactive Damper System in Large Earthquakes. *Proceedings Second World Conference on Structural Control*, Kyoto, Japan, Vol. 1, pp. 359-366, 1998.

[53] N. Kurata, T. Kobori, M. Takahashi, N. Niwa, and H. Midorikawa. Actual Seismic Response Controlled Building with Semiactive Damper System. *Earthquake Engineering and Structural Dynamics*. Vol. 28, pp. 1427-1447, 1999.

[54] N. Kurata, T. Kobori, M. Takahashi, T. Ishibashi, N. Niwa, J. Tagami and H. Midorikawa. Forced vibration test of a building with semiactive damper system. *Earthquake Engineering and Structures Dynamics*, Vol. 29, pp. 29-645, 2000.

[55] H. Kurino, T. Yamada, J.Tagami and K. Shimizu. Semiactive Structural Control by switching Oil Damper with Built-in Controller. *Proceedings of the Third World Conference on Structural Control*. Vol 3, pp. 91-100, April 7-11, 2003.

[56] H. Kurino and T. Kobori. Semiactive Structural Response Control by Optimizing the Force-deformation Loop of Variable Damper. *Proceedings Second World Conference on Structural Control*, Kyoto, Japan, Vol. 1, pp. 407-416, 1998.

[57] G. Leitmann. Semiactive Control for Vibration Attenuation. *Proceedings of the Second International Conference on Intelligent Materials*. 1994.

[58] G. Leitmann and E. Reithmeier. Semiactive Control of a Vibrating System by Means of Electrorheological Fluids. *Dynamics and Control*. Kluwer Academic Publishers, Boston. Vol 3, pp. 7-33, 2002.

[59] G. Leitmann and E. Reithmeier. An ER-material based control scheme for vibration suppression of dynamical systems with uncertain excitation. *Proceedings of the International Symposium on Mathematical Theory of Networks and Systems*. Regensburg, Germany, pp. 755-760, 1993.

[60] F. Lopez-Almansa, R. Andrade, J. Rodellar, and A. M. Reinhorn. Modal Predictive Control of Structures I: Formulation. *ASCE, Journal of Engineering Mechanics*. Vol. 120, No. 8, pp. 1743-1760, 1994.

[61] N. Luo, M. de la Sen, J. Vehí and J. Rodellar. Adaptive Decentralized Vibration Control of A Cable-Stayed Bridge in the Presence of Seismic Excitation. *Proceedings of the 17th Biennial Conference on Mechanical Vibration and Noise*. Editorial: ASME, Las Vegas, 1999.

[62] N. Luo, J. Rodellar, J. Vehí and M. de la Sen. Composite semiactive control of a class of seismically excited structures. *Journal of the Franklin Institute*. Pergamon, Elsevier Science Ltd., 338, pp 225-240, 2001.

[63] N. Luo, J. Rodellar, M. de la Sen and J. Vehí. Decentralized active control of a class of uncertain cable-stayed flexible structures. *International Journal on Control*. Taylor & Francis, Vol 75, pp. 285-296, 2002.

[64] N. Luo, J. Rodellar, M. de la Sen and J. Vehí. Interval Model Based Robust Control of Uncertain Flexible Structures. *Proceedings of the Third World Conference on Structural Control*. Como, Italy, Vol.2, pp. 89-94, 2003.

[65] N. Luo and J. Rodellar. semiactive Sliding Mode Control of Uncertain Base Isolated Structures. *International Conference on Advanced Problems in Vibration Theory and Applications*. Xian, China, pp. 72-78, 2000.

[66] Mañosa, V., Ikhouane, F. and Rodellar, J., 2004, "Control of uncertain nonlinear systems via adaptive backstepping,' To appear in Journal of Sound and Vibration.

[67] J. M. Martín S. and J. Rodellar. Adaptive Predictive Control: From the Concepts to Plant Optimization. *Prentice Hall International Series in Systems and Control Engineering*. 1996.

[68] F. Marazzi and G. Magonette, 2001. Active and semiactive Control of Structures. *European Meeting on Intelligent Structures*.Ischia, Italy, 22 - 28 September 2001.

[69] S.F. Masri, S. Chavakula and T.K. Caughey. Control of Intelligent Nonlinear Adaptive Structures Under Earthquake Excitation. *Journal on Structural Control*. Vol. 1, No. 1-2, pp. 23-38, December, 1994.

[70] N. H. McClamroch and H. P. Gavin. Closed Loop Structural Control using Electrorheological Dampers. *Proceedings of the American Control Conference*. Seatle, USA, pp. 4173-4177, June 1995.

[71] J. Medanic. Backstepping with Multi-Stage Polar Controllers for MIMO Nonlinear Systems. *Proceedings of the American Control Conference*. San Diego, USA, June 1999.

[72] G. Mei, A. Kareem and J. C. Kantor. Real-Time Model Predictive Control of structures under earthquakes. Proceedings of the Second World Conference on Structural Control Vol. 2, pp. 1585-1594, 1998.

[73] S. Nagarajaiah and D. Mate. Semiactive Control of Continuosly Variable Stiffness System. *Proceedings Second World Conference on Structural Control*, Kyoto, Japan, Vol. 1, pp. 397-406, 1998.

[74] T. Nasu and T. Kobori. A Study of new stiffness-selection method for high rise buildings with the AVS system. *Proceedings of the Third World Conference on Structural Control*. Como, Italy, Vol.3, pp. 915-920, 2003.

[75] A.C. Nerves, R. Krishnan. Active Control Strategies for Tall Civil Structures. *Proceedings of the 1995 IEEE IECON 21st International Conference on Industrial Electronics, Control, and Instrumentation*. Vol. 2, pp. 962 -967, 6-10 Nov 1995.

[76] H. Nishimura and S. Shidomaira. Vibration Isolation Control for A Structure Taking Account of Actuator Saturation. *Proceedings of the Third World Conference on Structural Control*. Como, Italy, Vol.3, pp. 275-282, 2003.

[77] J. Pandya, Z. Akbay, M. Uras and H. Aktan. Experimental implementation of hybrid control. *Proceedings of the Structures Congress XIV*.Illinois, pp. 1172-1179, 1996.

[78] W. Patten, J. Sun, G. Li, J. Kuehn and G. Song. Field Test of an Intelligent Stiffener for Bridges at the I-35 Walnut Creek Bridge *Earthquake Engineering and Structural Dynamics*. Vol. 28, No. 2, pp. 109-126, 1999

[79] W. Patten, J. Sun, G. Li, J. Kuehn and G. Song. Field Test of an Intelligent Stiffener for Bridges at the I-35 Walnut Creek Bridge *Earthquake Engineering and Structural Dynamics*. Vol. 28, No. 2, pp. 109-126, 1999

[80] E. Reithmeier and G. Leitman. Robust Control of Seismic Structures Employing Active Suspension Elements. *Advances in Structural Control*. CIMNE, Barcelona, pp. 87-102, 1998.

[81] F. Ricciardelli, M. Mattei and A. D. Pizzimenti. Effectiveness of Passive and Active Mass Dampers for the Control of the Wind Excited Motion of Tall Buildings. *Proceedings of the Third World Conference on Structural Control*. Como, Italy, Vol.3, pp. 283-290, 2003.

[82] J. Rodellar, A. H. Barbat and J. M. Matin-Sanchez. Predictive Control of Structures. *ASCE, Journal of Engineering Mechanics*. Vol. 113, No. 6, pp. 797-812, 1987.

[83] J. Rodellar, V. Mañosa and C. Monroy. A Robust Tendon Control Scheme for a Class of Cable-Stayed Structures. *Proceedings of the Third World Conference on Structural Control*. Como, Italy, Vol.3, pp. 184-190, 2003.

[84] R. L. Sack and W. Patten. Semiactive hydraulic Structural Control . *Proceedings of the International Workshop on Structural Control*. USC, Honolulu, Hawai, pp. 417-431, 1998.

[85] F. Sadek and B. Mohraz. Semiactive Control Algorithms for Structures with Variable Dampers. *Journal of Engineering Mechanics.* Vol. 124, No. 9. pp. 981-990, September 1998.

[86] M. Sakamoto, T. Kobori, T. Yamada and M. Takahashi. Practical applications of active and hybrid response control systems and their verification by earthquake and strong winds observations *Proceedings of the First World Conference on Structural Control* WP. 2 pp. 90-99, 1994.

[87] B. Samali, K. Kwak and H. Gao. Wind Induced Motion Control of a 76-Story Building by Liquid Dampers. *Second World Conference on Structural Control.* June 28 - July 1, Kyoto, Japan, Vol. 3, pp. 2431-2438, 1998.

[88] W. E. Schmitendorf, F. Jabbari and J. N. Yang. Robust Control Techniques for Buildings Under Earthquake Excitation. *Journal of Earthquake Engineering and Structural Dynamics.* 23(5), pp. 539-552, 1994.

[89] K. Seto and Y. Matsumoto. Vibration Control of Multiple Connected Buildings using Active Controlled Bridges. *Proceedings of the Third World Conference on Structural Control.* Como, Italy, Vol.3, pp. 253-261, 2003.

[90] H. Sira-Ramírez and O. Llanes-Santiago. Adaptive Dynamical Sliding Mode Control via Backstepping. *Proceedings of the 32nd Conference on Decision and Control.* pp. 1422-1427, 1993.

[91] Skinner, R.I., Robinson, W.H. and McVerry, G.H., 1992, An Introduction to Seismic Isolation, John Wiley, Chichester, United Kingdom.

[92] T. T. Soong and B. F. Spencer, Jr. Supplemental Energy Dissipation: State-of-the-Art and State-of-the-Practice. *Engineering Structures*, Vol. 24, No. 3, pp. 243-259, 2002.

[93] Spencer, B.F. Jr., Dyke, S.J. and H.S. Deoskar. 1997, "Benchmark Problems in Structural Control-Part I: Active Mass Driver System," Proceedings of the ASCE Structural Congress. XV, Oregon

[94] B. F. Spencer Jr. and M. K. Sain. Controlling Buildings: A New Frontier in Feedback. *IEEE Control Systems Magazine: Special Issue on Emerging Technologies* Tariq Samad Guest Ed., Vol. 17, No. 6, pp. 19-35, 1997.

[95] B. F. Spencer Jr and T. T. Soong. New Applications and Development of Active, semiactive and Hybrid Control Techniques for Seismic and Non-Seismic Vibration in the USA. *Proceedings of International Post-SMiRT Conference Seminar on Seismic Isolation, Passive Energy Dissipation and Active Control of Vibration of Structures.* Cheju, Korea, August 23-25, 1999.

[96] B.F. Spencer Jr., J.D. Carlson, M.K. Sain and G. Yang. On the Current Status of Magnetorheological Dampers: Seismic Protection of Full-Scale Structures. *Proceedings of the American Control Conference.* Albuquerque, New Mexico, pp. 458-462, 1997.

[97] B.F. Spencer Jr., S. J. Dyke, M.K. Sain and J.D. Carlson. Phenomenological Model of a Magnerorheological Damper. *Journal of Engineering Mechanics.* ASCE, Vol. 123, No. 3, pp. 230-238, 1997.

[98] M. D. Symans and M. C. Constantinou. Seismic Testing of a Building Structure with a Semiactive Fluid Damper Control System. *Earthquake Engineering and Structural Dynamics.* John Wiley & Sons, Ltd., Vol 26, pp. 759-777, 1997.

[99] M. D. Symans and M. C. Constantinou. Semiactive control systems for seismic protection of structures: a state-of-the-art review. *Engineering Structures*. Elsevier, Vol 21, pp. 469-487, 1999.

[100] Y. Tamura, K. Fujii, T. Effectiveness of tuned liquid dampers under wind excitations. *Engineering Structures*. Elsevier, Vol 17, pp. 609-621, 1995.

[101] K. Tanida. Active control of bridge towers during erection. *Proceedings of the Third Colloquium on Vibration Control of Structures*. Part A, pp. 173-184, 1995.

[102] Y. P. Wang, and C. J. Liu. Active Control of Sliding Structures Under Strong earthquakes. *Proceedings of the First World Conference on Structural Control*. FP1, pp. 23-32, 1994.

[103] S-G. Wang. Robust active control for uncertain structural systems with acceleration sensors. *Journal of Structural Control*. Vol 10. No. 1, pp. 59-76, January-March, 2003.

[104] JN. Yang, JC. Wu and Z. Li. Control od seismic excited buildings using active variable stiffness systems. *Engineering Structures*. Vol 18, NO. 8, pp. 589-596, 1996.

[105] J. N. Yang, S. Lin, F. Jabbari and W. E. Schmitendorf. H infinity Control With Peak Response Constraints: Energy Bounded & Peak Bounded Excitations. *Proceedings of the Third World Conference on Structural Control*. Vol 2, pp. 101-106, April 7-11, 2003.

[106] F. Yi and S. J. Dyke. Structural Control Systems: Performances Assesment. *Proceedings of the 2000 American Control Conference*. Chicago, USA, June 28-30, 2000.

[107] F. Yi, S. J. Dyke and S. Frech and J.D. Carlson. Investigation of Magnetorheological Dampers for Earthquake Hazard Mitigation. *Proceedings of the 2nd World Conference on Structural Control*. Kyoto, JAPAN, June 29 - July 2, 1998.

[108] F. Yi, S. J. Dyke, J. M. Caicedo and J. D. Carlson. Experimental Verification of Multiinput Seismic Control Strategies for Smart Dampers. *Journal of Engineering Mechanics*, Vol. 127, No. 11, pp. 1152-1164, November 2001.

[109] Yoshida, O., Dyke, S. J., Giacosa, L. M. and Truman, K. Z. "Experimental verification of torsional response control of asymmetrics buildings," in Earthquake Engineering and Structural Dynamics, John Wiley & Sons. Ltd, 32:2085-2105.

[110] K. Yoshida, S. Kang and T. Kim. LQG Control and H_α Control of Vibration Isolation for Multi-Degree-of-Freedom Systems. *Proceedings of the First World Conference on Structural Control*. Los Angeles, California, Vol. 4, pp. 43-52, August, 1994.

[111] K. Yoshida, S. Yoshida and Y. Takeda. Semiactive Control of Base Isolation using Feedforward Information of Disturbances *Proceedings Second World Conference on Structural Control*, Kyoto, Japan, Vol. 1, pp. 377-386, 1998.

[112] O. Yoshida, S. J. Dyke, L. M. Giacosa and K. Z. Truman. Torsional response control of asymmetric buildings using smart dampers. *15th ASCE Engineering Mechanics Conference*. June 2-5,2002. Columbia University, New York, USA.

Vita

Rodolfo Villamizar Mejía

Education

Ph.D. Information Technologies, Universitat de Girona, 2005
B. S. Electronic Engineering, Universidad Inndustrial de Santander, 2000
B. S. Electrical Engineering, Universidad Industrial de Santander, 1999

Research Stays

Dipartimento di Meccanica Strutturale, Università degli Studi di Pavia, Pavia- Italy. January 12-27, 2004. Title: Robust Control of Civil Engineering Structures using Backstepping Control and Quantitative Feedback Theory.

WUSCEEL Structural Control & Earthquake Engineering Lab, University of Washington in St. Louis, St Louis, USA. June 28 -September 28, 2004. Title: Robust Control of Civil Engineering Structures using Hybrid Control Techniques.

Publications

R. Villamizar, N. Luo, J. Vehí, J. Rodellar. Semiactive Control of Base Isolated Civil Engineering Structures. Automatica, 2005, *In review process.*

R. Villamizar, N. Luo, S. J. Dyke and J. Vehí. Experimental Verification of Backstepping Controllers for Magnetorheological MR Dampers in Structural Control. IEEE Transactions on Control Systems Technology. *In review process.*

R. Villamizar, N. Luo, S. J. Dyke and J. Vehí. QFT based controller for Civil Engineering Structures: Design and Implementation. Journal of Engineering Mechanics. *In review process.*

R. Villamizar, N. Luo, J. Vehí and J. Rodellar. Backstepping Control of Nonlinear Structures with Hysteretic Dynamics. IEE Proceedings-Control Theory and Applications. *In review process.*

R. Villamizar, N. Luo, J. Vehí, J. Rodellar. Active and semiactive QFT control for the structural vibration attenuation MOVIC 2004 -7th International Conference on Motion and Vibration Control, Saint Louis, USA, 2004.

N. Luo, R. Villamizar, J. Vehí, J. Rodellar. Active vibration attenuation in structures with uncertain coupled subsystems and actuator dynamics. ACC 04-American Control Conference, Boston, USA, 2004.

R. Villamizar, N. Luo, J. Vehí and J. Rodellar. Backstepping Control of Nonlinear Structures with Hysteretic Dynamics. Tenth Conference on Nonlinear Vibrations, Stability, and Dynamics of Structures, Blacksburg, VA, USA, Jul 25-29, 2004.

N. Luo, R. Villamizar, J. Vehí. Quantitative Feedback Theory (QFT): application to structural control. China-Japan-US Symposium on Health Monitoring and Control of Structures, Dalian, China, 2004.

Rodellar, J. Luo, N. Villamizar, R. Garcia, J. Dorka, U. Semi-Active Control of Bridges. 3rd European Conference on Structural Control, Vienna, Austria, 2004.

R. Villamizar, N. Luo, J. Vehí, J. Rodellar. Semiactive structural control by means of MR dampers and using backstepping control. MOVIC 2004-7th International Conference on Motion and Vibration Control, Sant Louis, USA, 2004.

N. Luo, R. Villamizar, J. Vehí, J. Rodellar.Vibration attenuation of uncertain structures by using Quantitative Feedback Theory. European Conference on Structural Control, Vienna, Austria, 2004.

N. Luo, J. Rodellar, R. Villamizar. Robust control law for a friction-based semiactive controller of a two-span bridge. SPIEs 10th Annual International Symposium on Smart Structures and Materials, San Diego, USA, February 04, 2003.

R. Villamizar, N. Luo, J.Vehi and J. Rodellar. Semiactive control of base isolated structures with actuator dynamics. European Control Conference ECC 2003, University of Cambridge, UK, September 04, 2003.

Rodolfo Villamizar, Ningsu Luo, Josep Vehi and José Rodellar. Semiactive sliding mode control of uncertain base isolated structures with actuator dynamics. AMAS/ECOMAS/STC Workshop on Smart Materials and Structures, Jadwisin, Poland, September 05, 2003.

N. Luo, R. Villamizar, J. Vehí, J. Rodellar, V. Mañosa. Sliding mode control of structures with uncertain coupled subsystems and actuator dynamics. European Control Conference, Cambridge, U.K., 2003.

J. Vehí, N. Luo, R. Villamizar. Health monitoring of cable-stayed bridges via modal intervals techniques. 1st European Workshop on Structural Health Monitoring, Cachan, France, July, 2002.

J. Vehí, R. Villamizar, N. Luo. Interval arithmetic applied to health monitoring of cable-stayed structures. IV Jornadas de ARCA, Vilanova, June, 2002.

J. Vehí, N. Luo, R. Villamizar. Modal Intervals Based health monitoring of cable-stayed bridge structures. 3rd World Conference on Structural Control. Commo, Italy, April, 2002.